# TESIS DOCTORAL

# Use of the advanced numerical simulation techniques for the study and improvement of steel-profiles manufacturing processes

**Alpha Verónica Pernía Espinoza**

UNIVERSIDAD DE LA RIOJA

# TESIS DOCTORAL

# Use of the advanced numerical simulation techniques for the study and improvement of steel-profiles manufacturing processes

**Alpha Verónica Pernía Espinoza**

Universidad de La Rioja
Servicio de Publicaciones
2008

Esta tesis doctoral, dirigida por el doctor D. Joaquín Ordieres Meré, fue leída el 8 de junio de 2007, y obtuvo la calificación de Sobresaliente Cum Laude.



Edita: Universidad de La Rioja
Servicio de Publicaciones

ISBN 978-84-691-7225-4

**UNIVERSIDAD DE LA RIOJA**
**DEPARTAMENTO DE INGENIERÍA MECÁNICA**


**DOCTORAL THESIS**
(TESIS DOCTORAL)

# USE OF ADVANCED NUMERICAL SIMULATION TECHNIQUES FOR THE STUDY AND IMPROVEMENT OF STEEL-PROFILES MANUFACTURING PROCESSES

(USO DE TÉCNICAS AVANZADAS DE SIMULACIÓN NUMÉRICA PARA EL ESTUDIO Y MEJORA DE PROCESOS DE FABRICACIÓN DE PERFILES DE ACERO)

**ALPHA VERÓNICA PERNÍA ESPINOZA**

**UNIVERSIDAD DE LA RIOJA**
**DEPARTAMENTO DE INGENIERÍA MECÁNICA**


# DOCTORAL THESIS
(TESIS DOCTORAL)

# USE OF ADVANCED NUMERICAL SIMULATION TECHNIQUES FOR THE STUDY AND IMPROVEMENT OF STEEL-PROFILES MANUFACTURING PROCESSES

(USO DE TÉCNICAS AVANZADAS DE SIMULACIÓN NUMÉRICA PARA EL ESTUDIO Y MEJORA DE PROCESOS DE FABRICACIÓN DE PERFILES DE ACERO)

**AUTHOR**
(AUTOR)
**ALPHA VERÓNICA PERNÍA ESPINOZA**

**ADVISOR**
(DIRECTOR)
**DR. JOAQUÍN BIENVENIDO ORDIERES MERÉ**

**MEMORIA PRESENTADA EN EL DEPARTAMENTO DE INGENIERÍA MECÁNICA DE LA UNIVERSIDAD DE LA RIOJA POR ALPHA V. PERNÍA ESPINOZA PARA OPTAR AL GRADO DE DOCTOR EUROPAEUS POR LA UNIVERSIDAD DE LA RIOJA**

**JUNE 2007**
(JUNIO 2007)

The author would like to thank the European Community and specially the Research Fund for Coal and Steel (RFCS) for the financial support of the projects RFS-CR-03012 (TESTRA), RFS-CR-04043, RFS-CR-04023 and the research stay (type III) at BFI (RFS-P3-04160). Furthermore, the author is in gratitude with the Spanish 'Dirección General de Investigación' of the 'Ministerio de Ciencia y Tecnología' for the support of the projects DPI2004-07264-C02-01 and DPI2006-03060. Finally, the author wants to thank the Government of La Rioja for its support through the 2º Plan Riojano de I+D+I.





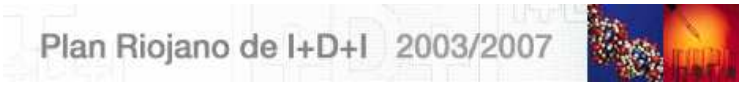


**ACKNOWLEDGMENTS**

I would like to start this acknowledgement saying 'thank you' to my family and friends, especially to my parents Chana and Elvecio, for their encouragement, love, education and the possibilities they have created for me. Also, I would like to thank Mari Carmen and Eduardo for their love and support since I am in Spain and particularly during the development of this dissertation.

I whish to express my gratitude to the Universidad de La Rioja. Especially I would like to thank the partnership and support of the members of the Mechanical and Electrical Engineering Departments.

I would like to gratefully acknowledge the support of my advisor Joaquín Ordieres who has taught me a lot not only on this research topic but about research and life in general.

This research also benefited tremendously from the partners of the UR-EDMANS research group. Thank you for your friendship and support over the years.

I would also like to thank to the ABAQUS® and FLUENT® technical service for answering in an excellent way all my uncertainties.

I want to thank to the European Community and specially the Research Fund for Coal and Steel (RFCS) for make possible the developed of the project TESTRA (RFS-CR-03012). This project was the origin of the present dissertation.

I owe special thanks to BFI, PTG and VA, as project partners, for the extraordinary collaboration on collecting experimental data and solving any doubts. Particularly, I want to give my gratitude to Mr. Eicke, Mr. Haasler from PTG and Dr. Eisenkolb from VA.

I am deeply indebted with Dr. Maag of BFI. Thank your for your patience and dedication in the discussion of these research topic and for taking care of me during my stay at BFI (Düsseldorf). Thanks also for the partnership and support of Mr. Haverkamp, Dr. Gorgels and the rest of the Department of Metal Forming Technology.

I have not enough words to thank my husband for his support during this time. Javi thank you for sharing with me the good and bad moments. For cheer me up in the difficulties and also for your advises and knowledge in this research work. Thank you for the time I have borrowed from you and from our daughter Verónica. It is to you two, Javi and Verónica, that I dedicate this dissertation.

*To Javi and Verónica*

*To Chana and Elvecio, Gerardo and Leo*

*To Mari Carmen and Eduardo*

# INDEX (ÍNDICE)


## 1. CHAPTER 1. INTRODUCTION (CAPÍTULO 1. INTRODUCCIÓN)..... 3

**1.1 PROBLEM STATEMENT (DESCRIPCIÓN DEL PROBLEMA)** ..... **4**

1.1.1 Production of steel profiles (La producción de perfiles de acero) ..... 4

1.1.2 Residual stresses (Las tensiones residuales) ..... 5

1.1.3 Consequences of residual stresses (Consecuencias de las tensiones residuales) ..... 7

1.1.4 Cooling process (El proceso de enfriamiento) ..... 9

1.1.5 Straightening process (El proceso de enderezamiento) ..... 9

1.1.6 Profiles and steels studied (Perfiles y aceros estudiados) ..... 10

**1.2 DELIMITATION OF SCOPE (OBJETIVOS)** ..... **12**

**1.3 FINITE ELEMENT MODELING. THE COMMERCIAL SOFTWARE USED: FLUENT® AND ABAQUS® (MODELADO POR ELEMENTOS FINITOS. SOFTWARE COMERCIAL USADO: FLUENT® Y ABAQUS®** ..... **12**

**1.4 DOCUMENT OUTLINE (ESTRUCTURA DEL DOCUMENTO)** ..... **14**

**1.5 LIST OF SYMBOLS (LISTA DE SÍMBOLOS)** ..... **14**

**1.6 LIST OF ACRONYMS (LISTA DE ACRÓNIMOS)** ..... **15**

## 2. CHAPTER 2. STATE OF THE ART (CAPÍTULO 2. ESTADO DEL ARTE)..... 19

**2.1 STATE OF THE ART ON THE COOLING PROCESS MODELLING (ESTADO DEL ARTE DEL MODELADO DEL PROCESO DE ENFRIAMIENTO)** ..... **19**

**2.2 STATE OF THE ART ON THE STRAIGHTENING PROCESS MODELLING (ESTADO DEL ARTE DEL MODELADO DEL PROCESO DE ENDEREZAMIENTO)** ..... **21**

## 3. CHAPTER 3. THE COOLING PROCESS. (CAPÍTULO 3. EL PROCESO DE ENFRIAMIENTO)..... 27

**3.1 COOLING PROCESS MODELING (MODELADO DEL PROCESO DE ENFRIAMIENTO)** ..... **27**

3.1.1 Introduction (Introducción) ..... 27

3.1.2 Cooling process modeling for the 'H' profile (Modelado del proceso de enfriamiento del perfil 'H') ..... 29

*3.1.2.1 Description of the problem (Descripción del problema)* ..... *29*

*3.1.2.2 Measurements and Observations at PTG cooling bed (Mediciones y observaciones en la mesa de enfriamiento de PTG)* ..... *30*

*3.1.2.3 Experimental values: Beam's surface temperature at the ingoing roller table, during cooling on the cooling bed, and at the outgoing roller table; residual stresses after cooling (Valores experimentales: temperaturas de enfriamiento de superficie de la viga en la mesa de entrada, en la mesa de enfriamiento y en la mesa de salida; tensiones residuales después del enfriamiento)* ..... *37*

*3.1.2.4 FE-thermal model for the 'H' profile cooling process (Modelo térmico de EF para el proceso de enfriamiento del perfil 'H')* ..... *44*

*3.1.2.5 FE-stress/displacement model of the 'H' profile cooling process (Modelo de tensión/desplazamiento del proceso de enfriamiento del perfil 'H')* ..... *53*

3.1.3 Cooling process modeling for the grooved rail (Modelado del proceso de enfriamiento del rail ranurado)....60
*3.1.3.1 Description of the problem (Descripción del problema)....60*
*3.1.3.2 Experimental values: Rail's surface temperature during cooling on the cooling bed; Residual stresses after cooling process (Valores experimentales. Temperatura superficial del rail durante el enfriamiento y en la mesa de enfriamiento)....62*
*3.1.3.3 FE-thermal model for the groved rail's cooling process in standing position (Modelo EF térmico del rail durante el enfriamiento en posición vertical)....64*
*3.1.3.4 FE-stress/displacement model of the rail's cooling process in standing position (Modelo EF de tensiones/desplazamientos del rail durante el enfriamiento en posición vertical)....67*
*3.1.3.5 FE-thermal and stress/displacement model of the rail's cooling process in lie-down position (Modelo EF térmico y de tensión/desplazamiento del rail durante el enfriamiento en posición inclinada)....74*
*3.1.3.6 Comparison of residual stresses values for the rail's cooling in standing position and in lie down position (Comparación de los valores de tensiones residuales del enfriamiento del rail en las posiciones vertical e inclinada)....78*

**3.2 CONVERSION CODE TO COMMUNICATE FLUENT® RESULTS TO ABAQUS® (CÓDIGO DE CONVERSIÓN PARA EXPORTAR LOS RESULTADOS DE FLUENT® A ABAQUS®)....82**

**3.3 CONCLUSIONS (CONCLUSIONES)....85**

## 4. CHAPTER 4. THE STRAIGHTENING PROCESS (CAPÍTULO 4. EL PROCESO DE ENDEREZAMIENTO)....89

**4.1 STRAIGHTENING PROCESS MODELING (MODELIZADO DEL PROCESO DE ENDEREZAMIENTO)....89**

4.1.1 Introduction (Introducción)....89
4.1.2 Straightening process modeling for the 'I' profile (Modelado del proceso de enderezamiento del perfil 'I')....91
*4.1.2.1 Description of the problem (Descripción del problema)....91*
*4.1.2.2 Experimental stresses values (Valores de tensiones experimentales)....92*
*4.1.2.3 FE-stress/displacement model (Modelo EF de tensión/desplazamiento)....92*

**4.2 CONCLUSIONS (CONCLUSIONES)....105**

## 5. CHAPTER 5. COUPLING THE COOLING AND THE STRAIGHTENING PROCESSES (CAPÍTULO 5. ACOPLAMIENTO DE LOS PROCESOS DE ENFRIAMIENTO Y ENDEREZAMIENTO)....109

**5.1 COUPLING THE COOLING AND THE STRAIGHTENING PROCESSES (ACOPLAMIENTO DE LOS PROCESOS DE ENFRIAMIENTO Y ENDEREZAMIENTO)....109**

**5.2 STRAIGHTENING PROCESS MODELING FOR THE 'H' PROFILE INCLUDING COUPLING WITH PREVIOUS COOLING PROCESS. (MODELADO DEL PROCESO DE ENDEREZAMIENTO PARA EL PERFIL 'H' INCLUYENDO EL ENFRIAMIENTO PREVIO)....111**

5.2.1 Description of the problem (Descripción del problema)....111
5.2.2 FE-thermal-stress/displacement model (Modelo EF térmico y de tensión/desplazamiento)....111
5.2.3 Results (Resultados)....113
5.2.4 Conclusions (Conclusiones)....118

**5.3 STRAIGHTENING PROCESS MODELING FOR THE GROOVED RAIL INCLUDING COUPLING WITH PREVIOUS COOLING PROCESS (MODELADO DEL PROCESO DE**

**ENDEREZAMIENTO PARA EL RAIL RANURADO INCLUYENDO EL ENFRIAMIENTO PREVIO) ..... 119**
5.3.1 Description of the problem (Descrición del problema) ..... 119
5.3.2 FE-thermal-stress/displacement model (Modelo EF térmico y de tensión/desplazamiento) ..... 119
5.3.3 Results (Resultados) ..... 121
**5.4 CONCLUSIONS (CONCLUSIONES) ..... 123**

## 6. CHAPTER 6. METHODOLOGY FOR STRAIGHTENING PROCESS IMPROVEMENT BASED ON GENETIC ALGORITHMS (CAPÍTULO 6. METODOLOGÍA PARA LA MEJORA DEL PROCESO DE ENDEREZAMIENTO BASADO EN ALGORITMOS GENÉTICOS) ..... 127

**6.1 A BRIEF INTRODUCTION TO GENETIC ALGORITHMS (UNA BREVE INTRODUCCIÓN A LOS ALGORITMOS GENÉTICOS) ..... 127**
**6.2 APPROACH FOR AN AUTOMATIC STRAIGHTENING PROCESS IMPROVEMENT USING GENETIC ALGORITHM (PROPUESTA PARA LA MEJORA AUTOMÁTICA DEL PROCESO DE ENDEREZAMIENTO USANDO ALGORITMOS GENÉTICOS) ..... 128**
6.2.1 Methodology (Metodología) ..... 128
6.2.2 Results (Resultados) ..... 133
**6.3 AN ON-LINE-TOOL TO MONITOR THE OPTIMIZATION PROCESS (HERRAMIENTA ON-LINE PARA LA MONITORIZACIÓN DEL PROCESO DE OPTIMIZACIÓN) ..... 136**
**6.4 CONCLUSIONS (CONCLUSIONES) ..... 137**

## 7. CHAPTER 7. CONCLUSIONS AND FURTHER RESEARCHES LINES (CAPÍTULO 7. CONCLUSIONES Y LÍNEAS DE INVESTIGACIÓN FUTURAS) .... 141

**7.1 CONCLUSIONS (CONCLUSIONES) ..... 141**
**7.2 FURTHER RESEARCH LINES (LÍNEAS DE INVESTIGACIÓN FUTURAS) ..... 143**

## 8. REFERENCES (REFERENCIAS) ..... 145

# RESUMEN DEL CAPÍTULO 1

## INTRODUCCIÓN

Hoy en día el producir perfiles de acero de calidad ha adquirido mayor importancia debido no sólo a las mayores demandas de los clientes relativas al acabado y la seguridad, sino también al crecimiento del mercado mundial por la inclusión de países asiáticos (China e India) que actúan tanto como productores como compradores. La Comunidad Europea está al corriente de tales necesidades y en consecuencia ha creado numerosos programas de investigación relacionados con el tema, apoyando de esta manera la consolidación de las empresas de acero europeas.

Este trabajo es producto del proyecto europeo titulado TESTRA (*Temperature and Straightness in Sections and Rail Straightening Processes,* RFS-CR-03012), donde se ha estudiado la relación existente entre la temperatura y curvatura de perfiles de acero en los procesos de enfriamiento y enderezamiento con respecto a las tensiones residuales y curvatura final de los mismos. A nivel experimental, el estudio se ha realizado en vigas del tipo 'I' y 'H' y en el rail ranurado Ri60. El proyecto ha contado con la participación de institutos de investigación y de empresas productoras de perfiles de acero. Gracias a la participación de estas empresas (PTG y VA) y al valioso trabajo del instituto de investigación BFI, ha sido posible tener a disposición datos y resultados experimentales de vital importancia para la calibración y validación de los modelos creados con elementos finitos (EF).

El objetivo principal de este trabajo ha sido el modelado y simulación, mediante EF, de dos procesos secuenciales muy importantes en la fabricación de perfiles de acero: el *enfriamiento* y el *enderezamiento*. En particular, este trabajo se ha centrado en el análisis de las tensiones residuales desarrolladas en estos dos procesos con el objetivo de aportar conocimiento útil y estrategias que ayuden a atenuar las mismas.

Se denominan tensiones residuales a las tensiones que quedan atrapadas en un objeto cuando no se aplica ninguna carga externa. Numerosos estudios teóricos y prácticos han destacado la influencia de las tensiones residuales en las características en servicio de los perfiles de acero (reducción de la capacidad de carga de las vigas estructurales y propagación de grietas en raíles de trenes, por mencionar algunos de los efectos). A través del modelado de estos procesos mediante EF se pretende contar con una herramienta flexible de análisis de la formación de dichas tensiones residuales, alternativa a la obtención de estas tensiones de forma experimental pues, ésta resulta complicada y con un consumo de tiempo apreciable.

Los procesos estudiados (enfriamiento y enderezamiento) son comunes a la mayoría de las industrias dedicadas a la fabricación de productos largos de acero. Después del laminado en caliente, los perfiles son depositados en la mesa de enfriamiento hasta que alcanzan la temperatura adecuada para ser enderezados. Los rodillos que componen el proceso de enderezamiento se encargan de doblar el perfil de forma cíclica para que alcance el régimen plástico en varias instantes durante el proceso. Es común asumir que las tensiones residuales aparecen por primera vez en el enfriamiento de los perfiles. Posteriormente, el proceso de enderezamiento reduce y homogeniza estas tensiones.

Además del análisis de los procesos mencionados mediante el modelado por EF, se ha planteado una metodología basada en algoritmos genéticos para mejorar el proceso de enderezamiento. A través de esta metodología se pretende encontrar los valores de la deflexión de los rodillos más adecuados que garanticen unas tensiones residuales mínimas y una curvatura final del perfil también mínima.

Finalmente es de destacar que el software empleado para el modelado y simulación por EF de los procesos ha sido ABAQUS® y FLUENT®, aunque también se han desarrollado diferentes herramientas software propias para solucionar algunas dificultades, optimizar procesos, exportar formatos y comprobar la metodología de mejora propuesta (la basada en algoritmos genéticos).

CHAPTER 1

# INTRODUCTION

Nowadays, the importance of producing steel profiles of high quality is more and more significant. The reasons are not only that clients are more demanding in product's finishing and safety characteristic, but also the steel market is growing faster since the incorporation of Asian industries, acting as both buyer and makers. Therefore, the steel companies invest on better production machinery and in employees' training to improve the quality standard, and they are also aware that the investment on R&D and innovation is decisive to survive. The European Community is sensitive to these needs and as a consequence several research programmes have been created. One of these programmes is the Research Fund for Coal and Steel (RFCS) in which a research and technological development (RTD) project named TESTRA (RFS-CR-03012) was developed. TESTRA stands for Temperature and Straightness in Section and Rail Straightening Processes and it is the project that has given birth to this doctoral thesis.

This work was focused on the modeling and simulation through Finite Elements (FE) analysis of two main sequential and coupled production processes, common to most of the manufacturing of long steel products. These processes were the *cooling process* and the *straightening process*. The long products studied here were 'I' and 'H' beams and the grooved rails. It have been verified by theoretical and practical researches that residual stresses affect the final performance of sections and rails (column buckling and fracture propagation, to mention some effects). The main objective was to study the residual stresses development during these processes, as these stresses appears first at the end of the cooling (growing up from the thermal stresses) and subsequently they are modified during the straightening process.

The methodology to attain this task was first to listen the problematic from the steel makers and then study the state of the art related to the topic investigated. After this first contact, the study of the processes directly on real facilities was achieved. Furthermore, it was possible a deeper study of the processes through the pilot plant constructed by BFI that recreates the analysed processes. Thanks to the excellent work accomplished by the leader of the project, BFI, and the priceless collaboration of the steel companies involved in the project (PTG and VA), was possible to obtain valuable experimental results to compare with the simulations and to make possible the calibration of the FE models. These experimental data was kindly disclosed by the enterprises for the development of this dissertation.

The modelling and simulations of these processes through FE tools was considered important as the study of the residual stresses formation and their measurement are complicated to perform not only in laboratories but much more during normal production in real plants. Most of the common mechanical measurement methods in stress analysis (as sectioning, hole drilling, trepanning, etc.) enable the measurement of released strains to be made by strain gauges. The residual stresses are then calculated involving the use of the elastic module. Some non-destructive method as X-ray diffraction only measures strain in terms of lattice parameter changes at the surface of the product. In contrast to X-rays neutrons can penetrate the material more easily allowing the measurement of residual stresses farther in the surface, however neutron diffraction is a rather expensive method as a nuclear reactor is necessary to provide the neutrons and the investigation of the specimen's interior is still limited (Orringer et al., 1992-vol. I; Kalker et al., 1993; Schleinzer G., 2000). All these methods are very time consuming and have disadvantages as they only offers general information about the stress distribution in the studied product and most of them are surface sensitive. The advances on computer science have allowed to increas processing and storage computers capacity and thus the development of powerfull simulation softwares. The new finite-element-analysis (FEA) tools have provided an alternative to the understanding of processes, combining experimental results with computer simulations.

## 1.1 PROBLEM STATEMENT

### 1.1.1 PRODUCTION OF STEEL PROFILES

The manufacturing process of the steel long products studied in this work (and followed by most of mills) is sketched in the next figure.

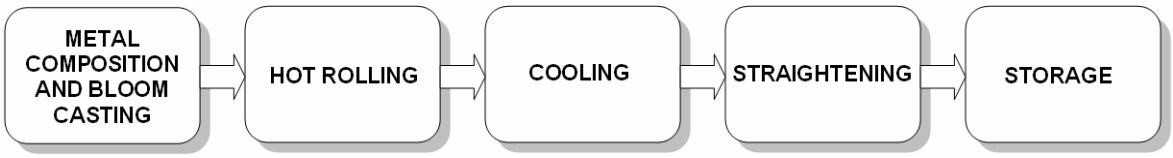


*Figure 1. Manufacturing of steel profiles.*

Metal composition is first achieved according to the steel grade desired. Then the liquid steel is cast into semi finished products as blooms or slabs. The blooms are reheated to make metal malleable and are then formed to finished products (as beams or rails) by hot rolling. After this process, the beams or rails have still high temperature (around 1000ºC) and are therefore sent to a cooling bed where they stay until they reach the desired lower temperature. During the cooling process, because of the unsymmetrical cross section of the products, thermal stresses develop with the consequent distortion of the profiles. Given that there are specific costumer's requirements in the product to fulfil, including straightness,

surface flatness improvement and residual stresses tolerances (Kalker et al., 1993), another process is required: the straightening process. This can be achieved through different techniques: roller straightening; gag-pressing; stretch straightening, etc. Nevertheless, the roller straightening is the most common method used for long products, as it is fast, allows continuous operation and its basic principle is rather simple (Schleinzer G., 2000).

One legacy left by this manufacturing route is the presence of residual stresses caused by thermal and mechanic deformation. Knowledge of their magnitude and distribution within the product is important with regard to subsequent performance (Kalker et al., 1993).

Of all these steps the *cooling process* is the first stage of the manufacturing process in which the residual stresses start to appear. Afterwards, at the straightening process, the distortion coming from the cooling is homogenized and decreased by the plastic deformation. Therefore, according to their importance on the residual stresses generation, the *cooling process* and the *straightening process* are being deeply studied throughout this work.

### 1.1.2 RESIDUAL STRESSES

Since the middle of the 19$^{th}$ century it has been known that stresses exist in structure members or even in solitary material, without being under loads (Meier, 1936; Horger et al., 1943; Alpsten, 1967).

As a concept, residual stresses are those stresses that are locked in an object without the application of any service or external loads. But let us see a very simple example formulated by Orringer (1993) that illustrate this concept and set the problematic on determining experimentally the magnitudes and distribution of residual stresses.

The example is based on a nut retaining a sleeve surrounding a bolt. The text and figure are mainly taken from (Orringer et al., 1993). Figure 2 shows the system.

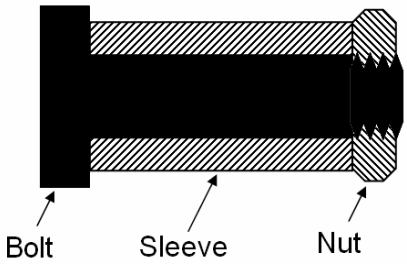


*Figure 2. Mechanical assembly example to illustrate residual stress concept.*

Tightening the nut causes the tension of the bolt's shank and compresses the sleeve. The tension and compression persist after the external nut-tightening torque has been removed,

as long as the position of the nut is not disturbed. Also, since no external forces are acting on the assembly, the total tensile force (which is the product of the tension and the bolt's shank cross section area) is exactly counter-balanced by the total compressive force (which is the product of the compression and the sleeve cross section area). Persistence and self-equilibrium are the two defining characteristics of a residual stress field.

Now assume that we are given the assembly with no information about the thread pitch, friction coefficient or the tightening torque. What can be done to estimate the residual stress magnitude? On one hand, we might apply a strain gauge to the outside surface of the sleeve and measure the change in strain when the nut is removed. An equal strain of opposite sign would represent the state before removing the nut. On the other hand, we might leave the nut tight and expose the sleeve surface to X-rays to determine the strain indicated by the atomic lattice spacing. Applying Hook's law in either case would then provide a direct estimate of the residual compression, at least in the sense of an average value over the part of the sleeve surface where the measurement was made. We might assume further that the residual stresses are uniformly distributes in both the sleeve and bolt's shank, and if the cross section areas were know, we could then apply the self-equilibrium principle to infer the residual tension magnitude in the bolt.

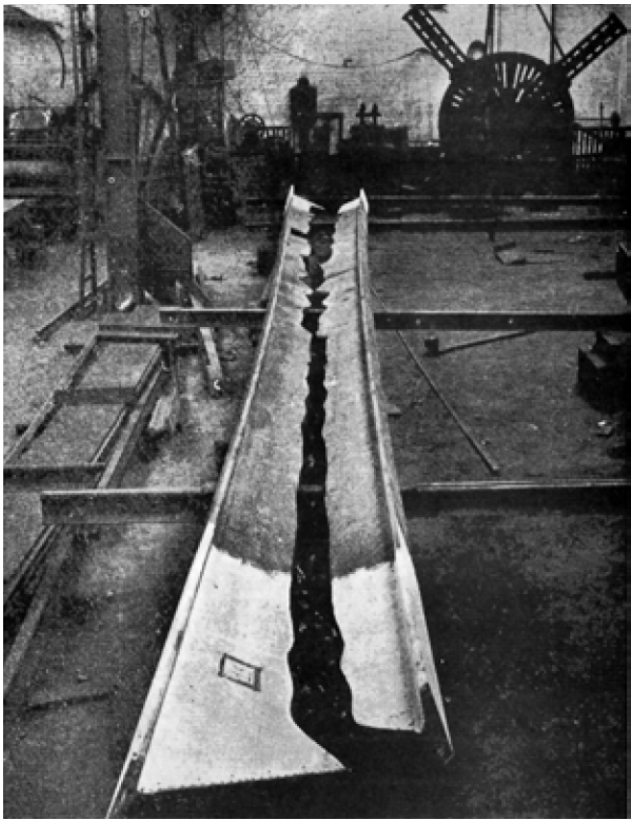

*Figure 3. Effects of residual stresses in structural profiles. Taken from (Osgood and Campus, 1954).*

The above speculations illustrate the following limitations of experimental and analytical methods for estimating residual stresses: destructive measurements require confidence that total relief is achieved; both kinds of measurements are localized and, strictly speaking, represent only average strains. Experimentally determined stresses are, therefore, also localized, averaged and inferred based on the assumption that relief obeys Hook's law. The principle of self-equilibrating forces is a powerful tool for analysis, but cannot be applied without making assumptions about the distribution of stresses in a continuum. These limitations may seem trivial for the bolt example, but they pose great challenges in practical situations (Schleinzer G., 2000; Kalker et al., 1993)

### 1.1.3 CONSEQUENCES OF RESIDUAL STRESSES

Researchers have proved that residual stresses produce significant effect on the carry capacity of steel **beam** columns into a structure (Osgood and Campus 1954; Strating and Vos, 1973; Fukumoto, et al., 1976; European Conv., 1976; Szalai, 2003, Nikitin, 2007). Figure 3 show a beam collapsed by its web because of the effect of residual stresses.

Therefore, engineering have paid special attention to the consideration and modeling of residual stresses in the comprehensive research into column buckling. It is a fact that columns containing residual stresses stars to soften (materially) earlier due to the additional stresses and cause the decrease in the ultimate load. Figure 4 shows the load vs. displacement path for a geometrically imperfect beam column with and without residual stresses (Szalai and Papp, 2005).

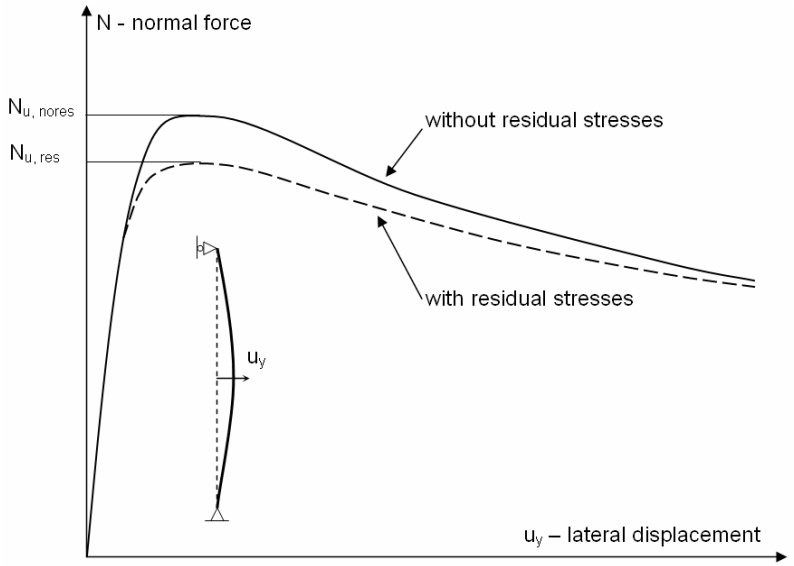


*Figure 4. Effect of residual stresses on the ultimate normal force of column (illustrative purposes only).*

On the other hand, in 1980s-1990s the problem of reducing residual stresses in **rails** arose among almost all rail-producing firms of the world (Nedorezov et al., 1999). Residual

stress was judged to be a secondary variable in the first theoretical investigations of detail fracture propagation (Besuner, 1978). However, later correlation of full scale tests, stress measurements and rail failure reports with a similar model showed that residual axial tension in the rail head has a strong effect on detailed fracture propagation life (Orringer et al., 1988). Figure 5, taken from Kalker et al. (1993), presents the influence of some variables on detail fracture safe life (as logical, the values depicted in the figure depend upon the conditions considerer, which are not discussed here; therefore the figure is given for illustrative purpose only).

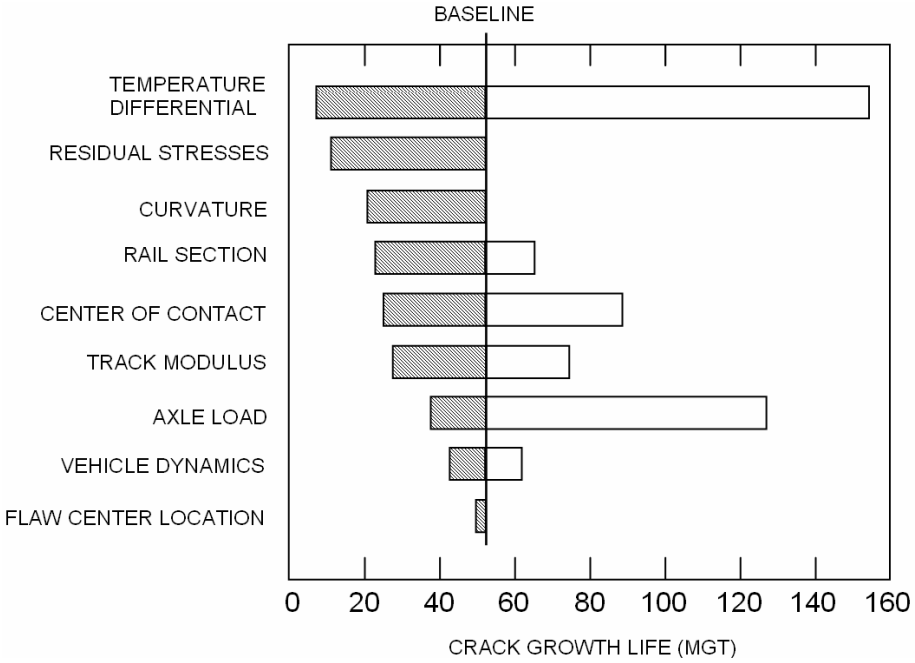


*Figure 5. Relative effects of several factors on crack growth life of detail fractures (illustrative purposes only).*

According to this picture, the difference between continuously welded rail stress free temperature and the actual temperature (that is the temperature differential) and the rail residual stresses produce the mayor effects on crack growth life of fractures.

It has been verified for many authors that residual stresses influence mechanical properties of structural material and, as a consequence, facilitate the propagation of cracks (Orringer et al., 1992-vol. I, vol. II; Kalker et al., 1993; Orringer et al., 1996; Rongbin et al., 1998; Ringsberg and Lindbäck, 2003; Cannon, 2003; Maximov et al., 2006). Residual stresses can cause plastic deformation around the contact surface rail-wheel and modify the stress field near the running line and internally in the railhead (Webster et al., 1992) causing railways failures.

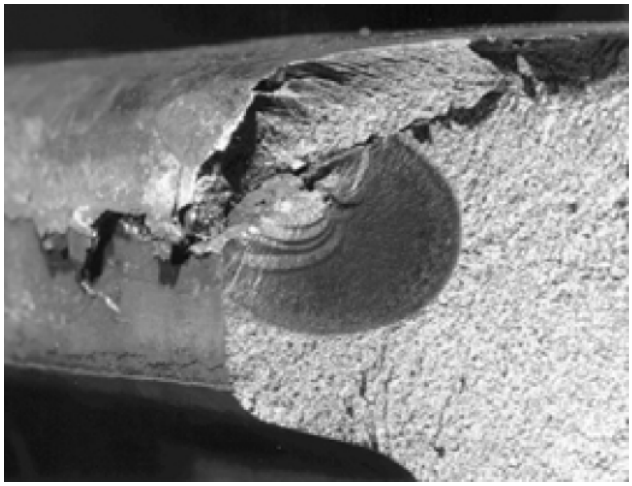

*Figure 6. Shelling and detail fracture. Taken from (Cannon, 2003).*

### 1.1.4 COOLING PROCESS

As said before, this is the first stage on the manufacturing process where the residual stresses start to appear. The main reason because residual stresses develop at the cooling stage is thermal stresses. The profiles have constant cross-sectional geometries but different parts of the cross-section have different thickness. Such asymmetries lead to non-uniform cooling and the development of thermal stresses, which may be higher than the yield stress of the material at high temperatures. The situation leads to bending of the rail or beam and the development of residual stresses.

The idea was to model and to simulate thought FE techniques the cooling of the beams and rails in its correspondent cooling bed. Each profile studied in this work (the 'H' beam and the grooved rail) is produced by a different company, and as it will be seen further on in the document, each company has its particular production characteristics.

### 1.1.5 STRAIGHTENING PROCESS

To solve the problem of improper curvatures and to achieve the quality standards regarding mechanical properties, surface flatness and running surface contour (on the case of rails) and residual stresses, the long product (beam or rail) is moved forward to the straightener machine(s). At this stage, the long product is submitted to cyclic bending (up and down) to reach plastic deformations. An example of a roller straightening machine is depicted in Figure 7.

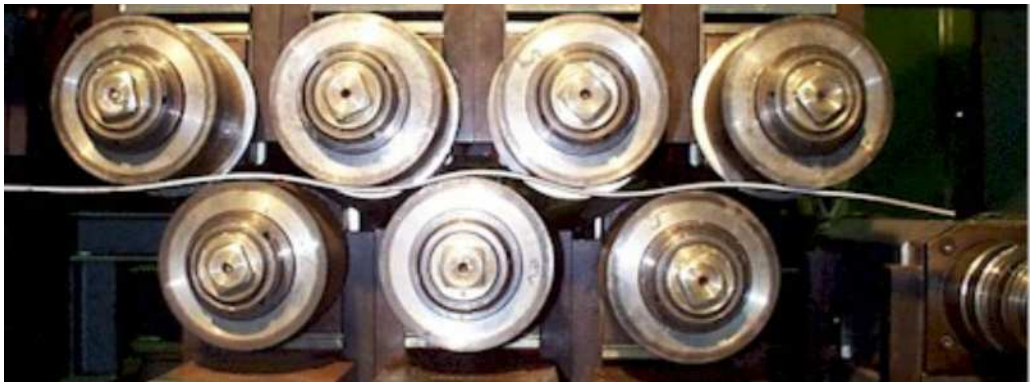

*Figure 7. A straightener machine example.*

In some cases the section is straightened about only one axis (primary or secondary straightening axis, regarding the axis along the width or the height of the section, respectively). Nevertheless, some products need to be cyclically bended about the two axes. In the case of the beams, they are straightened about only the secondary straightening axis. However, in the case of the rails, the straightening is applied about the two axes: first about the primary axis and successively about the secondary axis.

To attain the correct results the rollers have to be set at the right distances to give the balance between roll crush, straightness and residual stresses, which is a difficult task. Up to now the set up of the roller deflexions has been a matter of trial and error, largely influenced by the operator's skills and expertise.

The study of the straightener process has become a very important matter as it is the final deformation process of the manufacturing route which determines the residual stress pattern.

### 1.1.6 PROFILES AND STEELS STUDIED

The profiles and steels grades studied on this work were the following:

- **IPE 100 made of S235 steel**: This section was studied because it is the one used at BFI's pilot plant *HMS* (where the cooling and straightener are carried out in a smaller scale). Its dimensions are displayed in Figure 8. The S235 steel grade was the one used for the researches at the PTG's plant.

- **HEM 500 made of S235 steel**: This is one of the section produced at the real plant (PTG). The experimental values regarding the cooling and the straightening process were taken on this section. The dimensions of the HEM500 are presented in Figure 8.

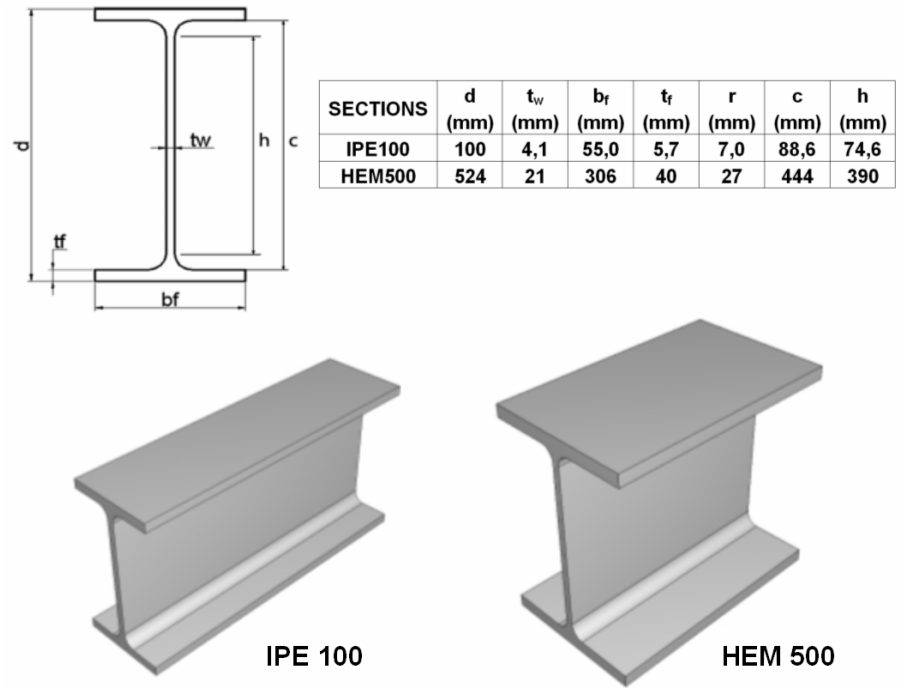


| SECTIONS | d (mm) | $t_w$ (mm) | $b_f$ (mm) | $t_f$ (mm) | r (mm) | c (mm) | h (mm) |
|---|---|---|---|---|---|---|---|
| IPE100 | 100 | 4,1 | 55,0 | 5,7 | 7,0 | 88,6 | 74,6 |
| HEM500 | 524 | 21 | 306 | 40 | 27 | 444 | 390 |

*Figure 8. Dimension of the beam profiles studied*

- **Ri60 made of EN200 steel**: This is one of the grooved rails produced in the rail's production plant (VA) and studied in the project. Experimental results of both processes, cooling and straightening, were taken on this type of rail. Its dimensions are displayed in Figure 9.

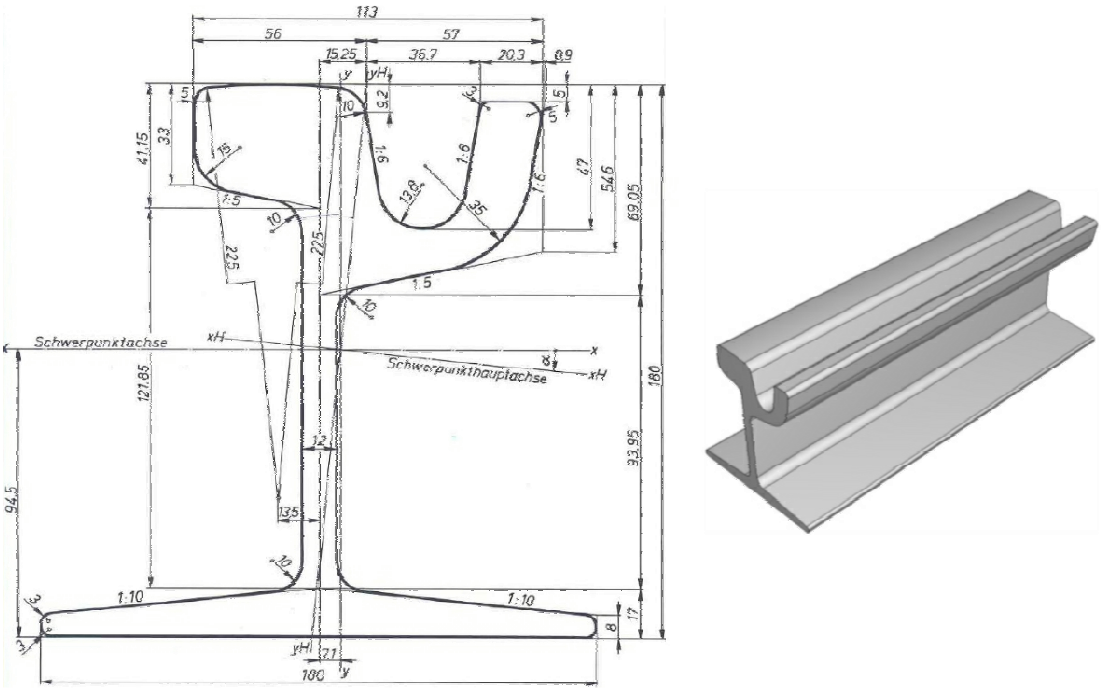


*Figure 9. Dimension of rail Ri60.*

## 1.2 DELIMITATION OF SCOPE

The main objectives of this Thesis were:

1. Study of the cooling process and the straightener process: This involved a state of the art study; observation of the processes on the real plants (PTG and VA); knowledge acquisition from the experts; measurements of the environmental conditions (for the cooling processes); and the study of the processes on the BFI's pilot plant.

2. Development of realistic finite element models of the studied processes: that included a selection of the suitable FE software; searching for the mechanical and thermal properties of the studied steel grades; investigation of the plastic behavior of these steels under cyclic loads throughout the straightening process; modeling of each process based on realistic observations and experimental measurements.

3. Calibration and integration of the processes: which consists in the simulation and pre-calibration of each process separately; development of a tool for the coupling of both processes (the results of the cooling process as the input of the straightening process); calibration of the two processes together.

4. Analysis of the residual stresses and bending development during the cooling process and during the subsequent straightening process.

5. Improvements on the straightening process: development of a methodology based on genetic algorithms designed to find the suitable roller's deflexion in order to reduce the residual stresses values and improve the straightness of the sections.

## 1.3 FINITE ELEMENT MODELING. THE COMMERCIAL SOFTWARE USED: FLUENT® AND ABAQUS®

Both problems studied, the cooling process and the straightening process, involved thermal and stress/displacement analysis:

- During the cooling process the thermal distribution and evolution depend on the surroundings conditions, thermal properties and geometries. On the other hand, the stress/displacement response mainly depends on the thermal distribution and the mechanical properties (which also depend on the current temperature).

- In the straightening process, the stress/displacement distribution depends primarily on the profile's input temperature, the straightener configuration (rollers' positions), and the mechanical properties at the current temperature. The cooling of the profile during the straightener is not quite relevant as the temperatures are low and the duration of the process is short.

Considering these facts, the software selection was based on bibliographic research, comparative tests and the previous experiences on FE simulations. Finally, the software chosen were ABAQUS® and FLUENT®.

ABAQUS® is a powerful tool that has the capability for coupled and uncoupled mechanical and thermal analysis. Therefore, at the beginning ABAQUS® was chosen to model both, the cooling process and the straightening process. Nevertheless, some limitation were found on the software when pretending a realistic thermal modeling of the cooling process (see bellow). As an alternative, FLUENT® was tested and approved to model and simulate the thermal response of the profiles during the cooling process.

In the case of the cooling process, the type of thermo-mechanical problem studied is such that the thermal evolution of the problem affects the stress response, but the temperature field does not depend on the stress evolution. Consequently, the temperature history can be calculated in a decoupled thermal analysis and, afterwards, introduced as a predefined field in the stress/displacement analysis. As said before, ABAQUS® has this capability but is quite limited when pretending to define some thermal properties. Instead FLUENT® is used worldwide for robust simulation, visualization and analysis of fluid flow and heat transfer, with a wide capability for defining the thermodynamic characteristics of the processes. As a result more realistic thermal models could be accomplished using FLUENT®. It was possible to calculate the thermal variables of interest from a relatively simple problem definition: geometries, materials' thermal properties, boundary conditions, operating conditions, radiation model, etc.). In ABAQUS® all these characteristics definitions would represent a more complex task, as it would be necessary to define the radiation cavities, the view factors, and the coefficient of heat transfer on the profiles surfaces and, as it is known, this is not an easy matter, especially in the case of the grooved rail.

The straightening process was modelled and simulated with ABAQUS®, using the 'Explicit' integration approach in a coupled thermal and stress analysis. ABAQUS/Explicit is especially recommended for contact problems (as for the roller-profile contact). Also, is computationally efficient for the analysis of large models with relatively short dynamic response (the straightener speed is relatively low) and uses a consistent large-deformation theory. In addition, ABAQUS/Explicit has some tools that provide numerical efficiency. In

particular, and as far as the inertial forces were not relevant in this problem, the strategy take advantage of the 'mass scaling' tool, which increases the material density in order to allow a time step bigger than those granted by the numerical stability calculus, decreasing the computing time.

## 1.4 DOCUMENT OUTLINE

The document is divided into seven chapters and outlined as follow. Chapter 2 reviews the work of other authors on the experimental and theoretical study of the cooling and straightening processes, oriented to the residual stresses formation. Chapter 3 focuses on the development and simulation of the FE models for the cooling processes analysed in this thesis: one for the 'H' beams and one for the grooved rails. In Chapter 4, the modeling of the pilot plant straightening process (BFI's *HSM*) for the IPE100 beams is presented. The suited ABAQUS® simulation controls and plastic model are studied to obtain satisfactory results as well as efficient computational times. The coupling procedure of the previous models (cooling-straightening) is worked on Chapter 5. Chapter 6 presents a new methodology, based on genetic algorithm, suggested to improve the straightening process, in order to reduce the residual stresses and final bending. The conclusions and contributions of the investigation and the proposed future research works are reported on Chapter 7.

## 1.5 LIST OF SYMBOLS

| | |
|---|---|
| $c$ | specific heat [J/kg ºC] |
| $E$ | Young's modulus [Pa] |
| $e_m$ | emissivity |
| $g$ | acceleration due to gravity (9,81 m/s$^2$) |
| $k$ | thermal conductivity [W/m ºC] |
| $S$ | stress [Pa] |
| $S$-$B$ | Stefan-Boltzmann constant (5.67e-8 W/m$^2$K$^4$) |
| $U$ | displacement |
| $\alpha$ | coefficient of linear thermal expansion [ºC$^{-1}$] |
| $\alpha_k$ | Backstress tensor |
| $\rho$ | density [Kg/m$^3$] |
| $\sigma_y$ | yield stress [Pa] |
| $v$ | Poisson's ratio |

## 1.6 LIST OF ACRONYMS

| | |
|---|---|
| *BFI* | Betriebsforschungsinstitut (VDEh-Institut für Angewandte Forschung GmbH) |
| *EN* | European Norm |
| *FE* | Finite Element |
| *HSM* | Hot Straightening Machine |
| *MGT* | Million Gross Tons |
| *PTG* | Peiner Träger GmbH |
| *UR* | Universidad de La Rioja |
| *VA* | Voestalpine Stahl Donawitz GmbH & Co KG. |

# RESUMEN DEL CAPÍTULO 2

## ESTADO DEL ARTE

*Estado del arte del modelado del proceso de enfriamiento*

Los trabajos iniciales sobre el estudio de las tensiones residuales durante el proceso de enfriamiento de productos laminados en caliente han sido en su mayoría experimentales. El método experimental más empleado es el de seccionado, ayudado por galgas extensiométricas para medir las deformaciones después del corte de las secciones. Se destaca el trabajo de Siebert (1973), quien presentó en su disertación una gran cantidad de experimentos de enfriamiento de perfiles 'I', buscando la relación entre las tensiones residuales y las diferentes posiciones de dichos perfiles y las tasas de enfriamiento. Su mayor contribución ha sido la gran cantidad de datos experimentales proporcionados. Desafortunadamente no desarrolló una conclusión general de su investigación. De las investigaciones teóricas destaca el trabajo de Yoshida (1984a) quien desarrolló un método numérico en dos dimensiones para predecir las temperaturas y tensiones térmicas. Más adelante, en (Yoshida, 1984b), utiliza su método para proponer algunas estrategias de enfriamiento. Su mayor aportación fue el concluir que para reducir las tensiones residuales se deben aplicar estrategias al inicio del enfriamiento que homogenicen la diferencia de temperatura entre las diferentes partes del perfil (alma y alas). Kusakabe and Mihara (1980) concuerdan con esta afirmación. Tanto los estudios experimentales como los teóricos coinciden en que el patrón de las tensiones residuales al final del enfriamiento de perfiles en 'I' es el siguiente: tracción en el centro de las alas y en la raíz y contracción en el centro del alma y bordes de las alas.

Los primeros estudios para modelar el proceso de enfriamiento por elementos finitos (EF) (Zienkiewicz et al., 1969; Argyris et al., 1971; Comini et al., 1974; Abouaf et al., 1983; Marcelin et al., 1986) se basaron en modelo ideales en dos dimensiones, asumiendo el pandeo del perfil según una circunferencia perfecta. Desafortunadamente el contraste de estos estudios con valores experimentales no fue muy claro. El estudio contemporáneo más destacado es el realizado por Basu et al. (2004) quienes desarrollaron un modelo del enfriamiento de un raíl UIC con resultados bastante próximos a la realidad. Sin embargo, se asumió una curvatura circular perfecta, lo cual no siempre es verdad. Además el coeficiente de película fue calculado inicialmente a partir de unas condiciones ideales y después su valor fue modificado a lo largo del proceso para cumplir con la tasa de enfriamiento real. Es importante destacar que todos los trabajos encontrados se centran en el modelado del rail UIC, el cual posee una sección transversal simétrica. El rail ranurado estudiado en este trabajo representa un reto mayor al no poseer simetría con respecto a ningún plano.

*Estado del arte del modelado del proceso de enderezamiento*

Alpsten (1970) fue uno de los primeros en estudiar experimentalmente la influencia que tienen la deflexión de los rodillos en las tensiones residuales obtenidas después del proceso de enderezamiento. De nuevo, se empleo el método de seccionado para obtener los valores de las tensiones residuales. Destaca en el artículo la mención del autor sobre la causa por la que sus resultados experimentales no coinciden con los resultados teóricos u otros resultados experimentales. Razona que esto pudo ser debido a la diferencia en las condiciones iniciales del proceso (temperatura y curvatura) tomadas en cuenta en cada caso.

En numerosos estudios teóricos y experimentales relativos a las tensiones residuales en el rail después del proceso de enderezamiento (Kolmogorov et al., 1987; Szelazek, 1992; Urishama and Sugino, 1992; Wineman and McClintock, 1992; Hodgson, 1993) se llega a la conclusión de que el patrón general tiene forma de 'C': tracción en la cabeza y pie del rail y contracción en el alma del rail. Sin embargo, en la superficie del rail no se llega a ninguna conclusión definitiva por existir contradicciones entre los diferentes estudios.

En el modelado del proceso de enderezamiento mediante EF destaca el trabajo de Schleinzer and Fischer (2001) donde se realiza un modelo en 3D aplicando *Chaboche* para simular el comportamiento plástico del acero. Sin embargo, las condiciones iniciales provenientes del proceso de enfriamiento no fueron consideradas. Es decir, un rail sin tensiones residuales y sin curvatura fue el introducido en la máquina de enderezamiento. Esto último es lo generalmente asumido en la literatura consultada.

CHAPTER 2

# STATE OF THE ART

## 2.1 STATE OF THE ART ON THE COOLING PROCESS MODELLING

Measuring and modeling thermal stress developed during continuous cooling of hot-rolled products has received significant attention in the last decades, as is in this stage were the residual stresses formation begins. Nevertheless, while extensive studies on long product behaviour during straightening process have been reported, very few references about the behaviour of these products during the cooling process can be found.

Most of the initial researches were experimental (Meier, 1936; Horger et al., 1943; Alpsten, 1967), with verifications based on very simplified theoretical models. Siebert (1973) in his dissertation made a big amount of cooling experiments over I-shaped beams in order to know the influence of cooling positions and rates on the final stress distribution. The main measurement method used was the sectioning with the help of strain-gauges to measure the released strains. As can be seen in his work, the research was very time consuming and the measurement method had a great scatter band. His main contribution was the great amount of experimental data provided. Besides, and unfortunately, he did not make a general conclusion of his research. Yoshida (1984a) developed a numerical method for the prediction of temperature and thermal stress during cooling of hot-rolled H-beams, taking phase transformation into account. The method was based on a simplification of the heat transfer variables using a two dimensional model for the temperature and a one dimensional model for the stresses (observing only the longitudinal stresses). He investigated the influence of finishing temperature (after hot-rolling) and cross-sectional size on the residual stresses and web-bucking. The main conclusions were that the larger the thickness ratio of flange to web ($t_f/t_w$) is the larger the stresses are and, also, that the larger the difference in finishing temperature between web and flange is the larger the stresses are. These results agree with the experimental results. Afterwards, Yoshida (1984b) used his numerical method to propose strategies to reduce the residual stresses on hot-rolled H-beams. All suggestions were based on reduce the difference between the web and flange finishing temperature at the beginning of the cooling process. Nevertheless, the suggestions with better results were not viable to implement inside the industrial facilities. Kusakabe and Mihara (1980) proposed and tested other strategies, based on forced cooling on certain points of the flange. However, as before, the feasibility of these proposals in the industrial field was not evaluated.

All these references agree in the residual stress pattern after the cooling process of 'I' and 'H' beams: tension stresses on flange center and at the connection of the web and flange (root), and pressure at the tips of the flange and web center (see Figure 10).

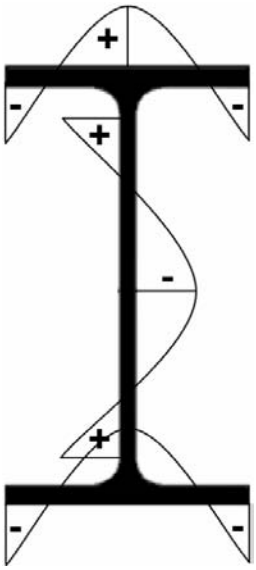


*Figure 10. Residual stress distribution inside 'I' and 'H' beams after cooling process.*

Abouaf et al. (1983) and Marcelin et al. (1986) were the first to analyse the residual stresses in hot-rolled complex beams using a finite element method. Their work was preceded by those of Zienkiewicz et al. (1969), Argyris et al. (1971), Comini et al. (1974) who study the thermal stresses formation using a finite element approach but in a more general context. These early studies were based on two-dimensional thermoelastic finite element idealizations, and the bending effect was introduced in a general plane-strain formulation assuming circular curvature along the beam. However, the verifications of the methods with experimental values were not clear. Moreover, some of the assumptions, such as symmetrical cooling along the beam, and cooling in ideal still air are not borne out in reality. Fisher et al. (1991, 1992) studied the residual stress distribution in rails during cooling taking into account the friction with the supports. They concluded that the assumption that the measured residual stresses are constant over the whole length except a small end part in the range of approximately two beams heights is not valid. They also pointed out that frictional forces between the rail and supports have some influence on the residual stress state but are not decisive in the final distribution. Ringsberg and Lindbäck (2003) arrived to a stress distribution on a rail after cooling based on a two dimensional finite element model, but with a poor validation against experimental results. In contrast, Basu et al. (2004) elaborated a finite element model of the rail's cooling, with results approximated to the reality. The problem was investigated in a three-dimensional model of the rail and as a decoupled thermo-mechanical transient problem, using ANSYS® for both, the thermal and the structural analysis. They also considered the influence of the surrounding rails on the cooling bed. Nevertheless, the bending of the rail was assumed to

be in the form of a circular arc, which is not always true. Also, the film heat transfer coefficient was calculated for ideal conditions and modified throughout the process to achieve the real cooling rate. Boyadjiev et al. (2004a,b) used a plane-strain FE analysis for the computational prediction of deflection and residual stress in the cooling of hot-rolled beams. The analysis was based on the generalized plane-strain model of Abouaf et al. (1983). They include the contact with the supporting table and the effect of the weight of the beam. The main contribution was to represent the coefficient of thermal expansion of the beam as a function of temperature, cooling rate and kinetics of phase transformation. The agreement between the simulation results and experimental measurements regarding the model of the rail's cooling was not clear. Szalai and Papp (2005) went one step further and proposed a new residual stress distribution on unstraightened I-shaped beams considering the beam's buckling. The work was focused on the evaluation of this new distribution on the steel beam columns stability. They concluded that their proposal corrects the errors on the LTB (lateral-torsional buckling) problems, because of the presence of torsion in the equilibrium equations.

It is important to point out that all references found, related to the residual stresses formation during rail's cooling, were developed studied symmetrical cross-section rails (UIC-profile rails), as they are typical profiles for main railroad lines. The grooved rails, like the one studied in this work, represents a greater challenge because of its lack of symmetric about any axis.

## 2.2 STATE OF THE ART ON THE STRAIGHTENING PROCESS MODELLING

As was said in Chapter 1, the biggest contribution to the final residual stresses distribution in long products comes from the straightening process. Comprehensive efforts have been carried out for the understanding and improvement of this important manufacturing process.

Most of the literature found about straightening processes refers to rails and only a few to beams. Once more the references are oriented to investigate the rail's straightening process focuses on the symmetrical cross-section rails (UIC-profile).

Already in the 70's a number of solid experimental tests were developed by Alpsten (1970) to study the influence of some straightening parameters (as the roller's deflexion) on the H-beam's residual stresses and mechanical properties. He made all tests using beams at the same input temperature. Residual stresses were measured with the sectioning method and mechanical extensometers. The author stated that some of the results did not agree with the theoretical and experimental results available till that moment, but he argued that this could

be caused by the differences on cooling conditions of the beams compared. This underline the importance of consider the initial conditions in the profiles inherited from the cooling process.

On the other hand, in 1987 the European Rail Research Institute (ERRI) carried out a broad study of stresses in roller straightener machines (ERRI, 1987). The sectioning method was again the one researchers used for this propose. It was established that the longitudinal residual stress pattern in the rail's cross section was C-shaped, with tensile stresses in the head and foot and compressive stresses in the web (Figure 11). This research verified the result obtained by Fastenrath in 1977. The same results can be found in several references (Kolmogorov et al., 1987; Szelazek, 1992; Urishama and Sugino, 1992; Wineman and McClintock, 1992; Hodgson, 1993). Later, in 1993, Webster et al. reported similar results applying another measurement method, the non-destructive technique 'neutron diffraction'. There were some differences near the head surface between both results. The longitudinal tensile stresses dropped from a maximum just beneath the surface to a lower value at the surface. These results were included in a new ERRI report (ERRI, 1993) with a warning mentioning that the results near the rail surface must be interpreted with caution due to the extrapolation of the data. In 1994, Hauk and Kockelmann reported residual stresses results with different measurement methods, increasing the uncertainties at the rails surface. For example, the X-ray diffraction measurements showed a very steep stress gradient from compressive stresses at the surface to tensile stresses near the surface. Also high speed drilling and ring core methods were applied. Even though it is difficult to compare results from different experimental methods (as each of them characterize the stresses in a different way), in a general point of view, these researches did not arrive to a final residual stresses profile near the surfaces areas. Therefore, from the experimental point of view, the rail's general cross section stress pattern seems to be clear: a C-shaped stress distribution, while near the surface the uncertainties remain.

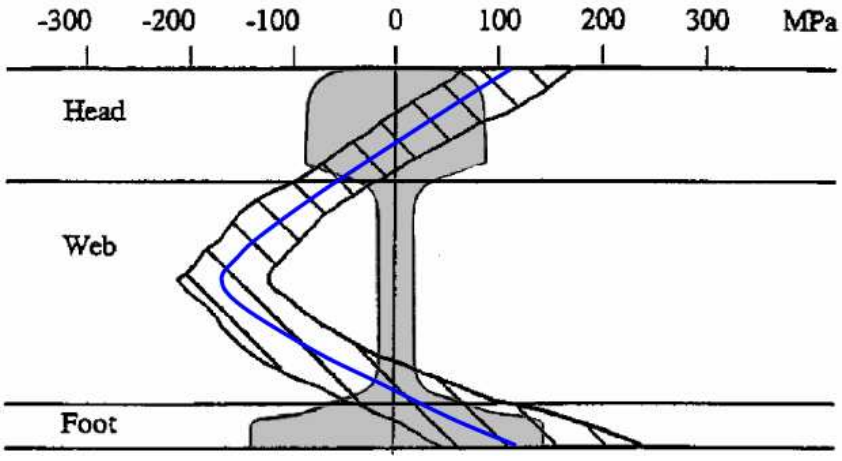


*Figure 11.Longitudinal residual stresses pattern on straightened rails measured with destructive method (Hodgson, 1993).*

The first attempts to model the effect of the straightening process in steel profiles using FE were carried out by Brünig (1989). Although he used an enhanced plasticity model, the finite element definition was too poor that only stress average values along the cross section were obtained. In his research he concluded that the contact pressure at the rollers only has a minor effect on the final residual stress pattern. Guericke et al. (1994) simulated the contact pressure of the rollers with an overlay of Hertz-type contact pressure. They applied it to a 2D FE model of the rail. The analytically determined contact pressure was used to predict the yield stress on the material. Their results were in agreement with the experimental measurements. Later on, Naumann (1998) proposed a 3D FE model with a coarse mesh and using a linear kinematic hardening plasticity model. For this purpose he used the package ABAQUS®. He concluded the opposite stated by Brünig: the rollers contact pressure is decisive for the residual stress pattern. However, he did not publish residual stress values from his research. Rongbin et al. (1998) studied the principle of forming the residual stresses in the straightening process using ANSYS®. They proposed a pattern with tensile stresses on the rail base center. Finstermann et al. (1998), presented a 3D FE simulation, using ABAQUS®, which combines the straightening mechanic for the rail as a uniaxial infinite beam with the actual 3D contact of the upper and lower rollers. They stated that in the contact roller-rail area compressive longitudinal residual stresses appear on the surface, and that a very steep gradient of these stresses can be observed (Figure 12). These results are in agreement with X-ray and neutron diffraction experimental investigations.

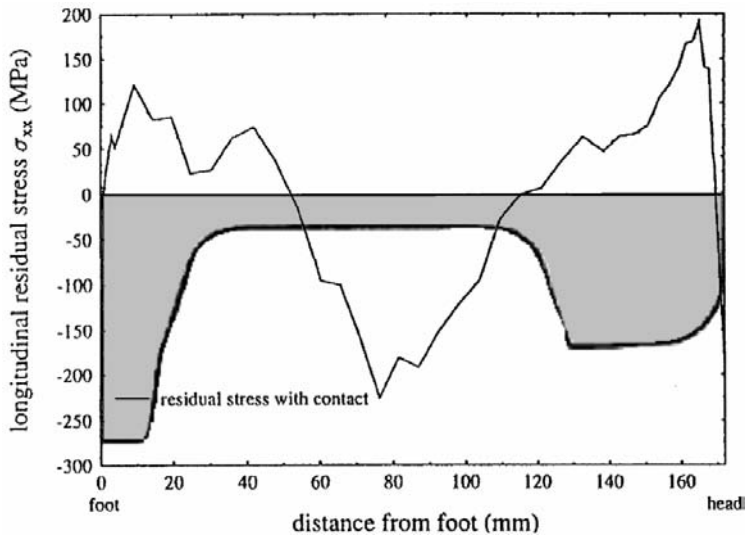


*Figure 12. Longitudinal residual stresses by Finstermann et al. (1998).*

In (Schleinzer and Fischer, 2001) the authors resume and improve the results showed in (Schleinzer, 2000). A two step 3D FEM was applied using ABAQUS® as the FE software. The most important fact was that they applied a Chaboche's multiple component non-linear kinematic hardening model to account for the plastic behavior of rail steel. Their results are in harmony with experimental investigation. However, a stress free rail was

straightened, not considering the influence of the previous cooling process. Further on, Srimani et al. (2005), modelled the rail straightening process using ANSYS®. The analysis focused on the evaluation of the straightness of a finished rail for a specific set of straightening machine's parameters. The article provided guidance for the minimum length of the rail to be cut, in order to achieve the end straightness within acceptable limits. Nevertheless, the initial conditions for the straightening process were again a stress free state.

All the references mentioned before, related to the FE modeling and simulation of the straightening process, worked with a previous stress-free profile, i.e. they had not taken into account the residual stresses generated in the earlier manufacturing stage, the cooling process. Also, they have not considered the input temperature of the product in the straightening process, which has an influence in the straightening process.

# RESUMEN DEL CAPÍTULO 3

## EL PROCESO DE ENFRIAMIENTO

En este capítulo se describen los procesos de enfriamiento modelados. Ambos procesos son básicamente muy parecidos: el perfil llega del proceso de laminado en caliente con altas temperaturas y es depositado en la mesa de enfriamiento en una posición específica. Una vez allí, las partes móviles de la mesa transportan el perfil desde la entrada hasta la salida de la mesa mientras éste se enfría hasta alcanzar una temperatura adecuada para pasar el siguiente proceso, el de enderezamiento. Sin embargo, las mesas de enfriamiento modeladas se diferencian en las condiciones ambientales que las rodean. El enfriamiento del rail se realiza en una mesa de enfriamiento que se encuentra dentro de las instalaciones de la planta, mientras que la mesa de enfriamiento para los perfiles 'H' está ubicada a la intemperie. Esto hace que cada proceso se modele de forma diferente.

Para el modelado del enfriamiento de la viga en 'H' fue necesario recopilar información sobre las condiciones ambientales in situ. Para ello se diseño un programa de mediciones de las condiciones ambientales coordinado con las mediciones de la temperatura superficial de la viga a la entrada, durante y a la salida del proceso de enfriamiento (desarrolladas por BFI y PTG). Además, gracias a BFI, fue posible obtener las tensiones residuales experimentales de un perfil 'H' después del enfriamiento (antes de ser enderezado). Con toda esta información (cedida amablemente por PTG y BFI) fue posible modelar, calibrar y validar los modelos desarrollados.

También para el modelado del enfriamiento del rail, se contó con información cedida por VA sobre las condiciones del viento, que al estar dentro de las instalaciones se caracterizaba por tener una magnitud conocida y una dirección definida. Además, VA generó gran cantidad de valores experimentales para el proyecto europeo relacionados con la temperatura durante el enfriamiento y las tensiones residuales posteriores del enfriamiento. Generosamente, VA ha permitido el uso de estos valores en esta disertación.

El proceso de enfriamiento fue analizado como un proceso termo-mecánico desacoplado. Esto fue posible porque en este caso la evolución de las temperaturas afectaba el desarrollo de las tensiones, pero la evolución de las tensiones no afectaba la temperatura. Por lo tanto, el modelado se desarrolló en dos partes: un modelo térmico creado en FLUENT® y un modelo de tensión/desplazamiento desarrollado en ABAQUS®.

El uso de FLUENT® permitió modelar el proceso de enfriamiento de una forma realista. Se modeló el enfriamiento por conducción, convección y radiación especificando básicamente las geometrías, las condiciones de contorno y las propiedades del acero de

cada perfil. A partir de estos parámetros, FLUENT® fue capaz de calcular las temperaturas de los perfiles a lo largo del tiempo, la transferencias de calor, el coeficiente de película y otras variables de interés. Es decir, no fue necesario introducir el coeficiente de película ni los factores de forma, que es lo que comúnmente se hace en las referencias bibliográficas consultadas.

Después de obtener la historia de la temperatura en el perfil, se introdujo este resultado en del modelo de tensión/desplazamiento desarrollado en ABAQUS®, en la forma de un campo predeterminado. De esta forma se obtuvieron las tensiones y deformaciones del perfil durante el proceso de enfriamiento. Sin embargo, para comunicar los resultados del FLUENT® al ABAQUS® fue necesario crear un programa de conversión de los resultados. El programa fue desarrollado usando software libre y presentó un buen manejo de la memoria y excelente eficiencia computacional.

Los modelos desarrollados en este capítulo fueron verificados usando los valores experimentales disponibles. Estos modelos fueron la base para modelar el proceso aguas abajo (el proceso de enderezamiento) de una forma realista, ya que las condiciones iniciales de este modelo (relativas a la temperatura, tensiones residuales y curvatura) fueron el resultado del modelo de enfriamiento.

CHAPTER 3

# THE COOLING PROCESS

The first part of the chapter is focused on the modeling and simulations of the cooling process for the 'H' profile. Exhaustive experimental data was available to tune this model. The weather measurement required to establish realistic boundary conditions for the thermal model are also outlined. These measurements were important as the cooling bed for this profile was located outdoors.

Further on, the FE model developed for the cooling of grooved rail is presents. Two possible cooling configurations are modelled: cooling in standing and in lie down position. The residual stresses along the rail are compared.

The models presented in this chapter were the base for the simulation of the models presented in chapter 5 (*coupling the cooling and the straightening processes*) as in the actual production line the initial conditions for the straightening process are the temperature and stress/displacement final results coming from the cooling process.

## 3.1 COOLING PROCESS MODELING

### 3.1.1 INTRODUCTION

Basically both cooling processes, the one for the 'H' profile and the one for the grooved rail, are the same: the profile comes from the hot rolling mill at high temperatures over the ingoing roller table to the cooling bed where is placed in a certain position. Once there the profile is moved along the cooling bed helped with the walking beams till it reaches an appropriated lower temperature to be sent to the next process, the straightening. Nevertheless, each cooling bed presents its own special features: location (indoors or outdoors), cooling times, profiles' configuration and position, input and output temperature, etc.

Another common assumption for both cooling processes modeling is that the profile goes out from the last rolling mill with no stresses' state because of the high temperatures (around 1000ºC) (Marcelin et al., 1986). Afterwards, depending on the cross section shape and thickness, the profile starts to cools down at different rates and is when thermal stresses appear. At the beginning of this cooling process the temperatures in the profile are

very high and the thermal stresses could be higher than the yield stress of the material. These conditions allow plastic deformations with the consequent bending and development of residual stresses.

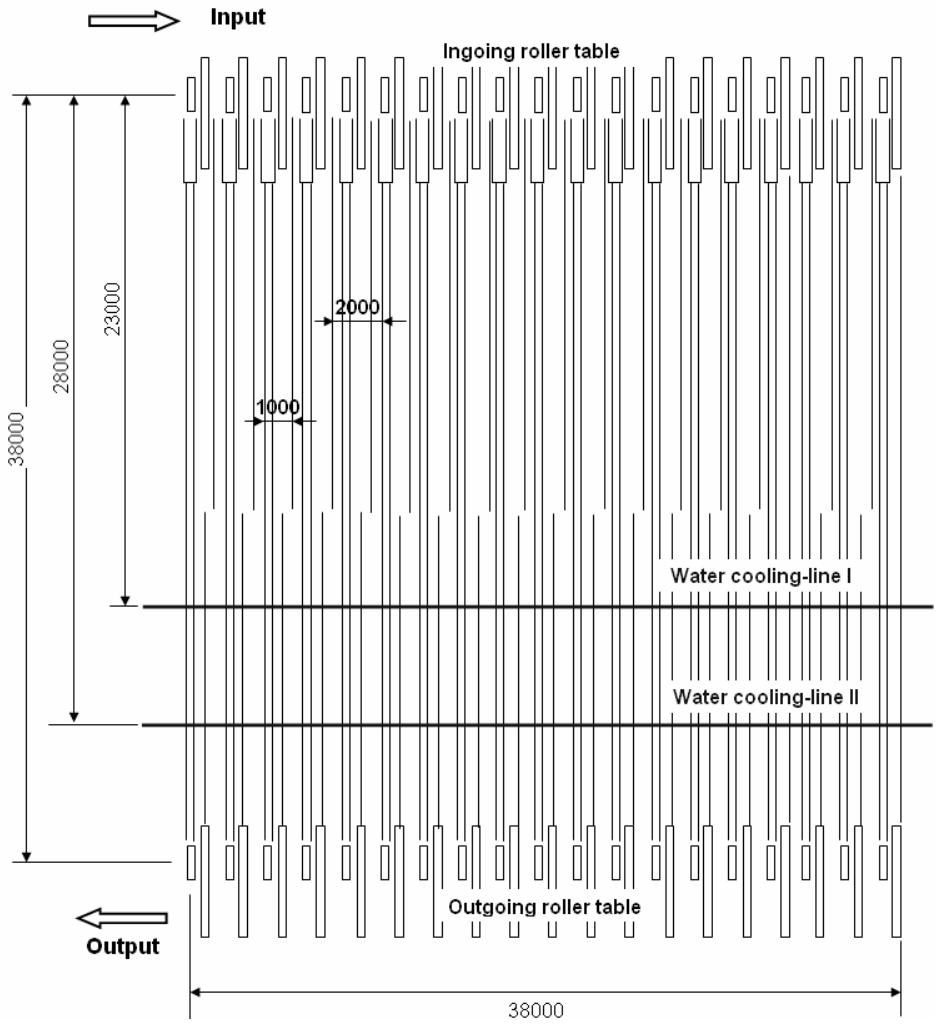


*Figure 13. Sketch of the cooling bed used for the 'H' profiles.*

The cooling process has been analysed as decoupled thermo-mechanical problem, as the stress/deformation field in the profile depends on its temperature history, but the temperature history can be found without the knowledge of the stress/deformation response (Basu et al., 2004). Therefore, the transient thermal analysis of the problem was developed first, using the powerful computational fluid dynamics (CFD) software FLUENT®. Afterwards, the temperature results were introduced into the stress/displacement model created in ABAQUS® (specifically using ABAQUS/Standard), in order to calculate the profile's stress field and deformations. This procedure is called *sequentially coupled thermal-stress analysis*. Nevertheless, in doing so, we faced the need to communicate FLUENT® and ABAQUS®. For this propose a 'results-conversion code' was developed using free software. The description of this code is also presented further on in this chapter.

## 3.1.2 COOLING PROCESS MODELING FOR THE 'H' PROFILE

### 3.1.2.1 DESCRIPTION OF THE PROBLEM

The cooling bed analysed for the 'H' profiles (PTG's cooling bed) was a framework of equally spaced carbon steel beams parallel to each other, some of them fixed and some of them moveable used to transport the beams along the cooling bed. A sketch of the cooling bed studied is presented in Figure 13.

The rolled beam at high temperatures arrives to the cooling bed input through the ingoing roller table in 'H' position. A manipulation system turns the beam and locates it in the cooling bed in 'I' position. The beams are separated a certain distance to avoid a domino effect in a possible equilibrium missing of a beam. The beams cools down while they are moved all at the same time along the cooling bed, helped by the walking beams toward the output, where each beam is transported by the outgoing roller table to the straightener machine.

As can be seen in Figure 13, the PTG's cooling bed count with an accelerated cooling system composed by two water lines. The company cools down the beam in two ways: with and without the water system, depending on the production rates and product size. If the beams are too hot to be straightened, the accelerated cooling system is activated. Although, the accelerated system is an interesting characteristic of this cooling bed, it is not considered in this work. The cooling process was study only as a consequence of convection and radiation to the ambient.

An important fact regarding this cooling bed is that it is located outdoors, at a temperature that could change from -15ºC to 35ºC depending on the season.

A picture of the studied cooling bed is presented in Figure 14.

*Figure 14. PTG's cooling bed. Picture courtesy of BFI.*

The following table resumes the main dimensions and time parameters of this cooling bed.

*Table 1. PTG's cooling bed parameters.*

| PARAMETER | VALUE | UNIT |
|---|---|---|
| Total length | 38000 | mm |
| Total width | 38000 | mm |
| Distance between fixed beams | 1000 | mm |
| Distance between walking beams | 2000 | mm |
| Input temperature | 750-850 | ºC |
| Output temperature | 20-120 | ºC |
| Cooling total time | 46-90 | min |
| Step width | 750 | mm |
| Time between two steps (idle time) | 97 | s |

### 3.1.2.2 MEASUREMENTS AND OBSERVATIONS AT PTG COOLING BED

In order to get an idea of the weather conditions over the cooling bed in term of temperature, wind speed and relative humidity, while the beams are cooled down, the UR and BFI research teams design a measurement program to get these parameters at the PTG cooling bed. At the same time BFI research team carried out measurement of the beam's surface temperature at the ingoing rolling table and surface temperature and straightness at the outgoing roller table. The observation and measurement of the cooling process at PTG helped to achieve a realistic thermal model of the process. The values obtained were necessary to set the boundary conditions of the thermal finite element model and to calibrate it after some simulation trials.

## *MEASUREMENT EQUIPMENT*

The main equipment used for the measurements was:

- Control Unit and Data Logger TESTO® 454/350: With this unit was possible to control automatically the initial and final time of the measurement, sample speed and also to store the data.


*Figure 15. TESTO® Control Unit 454/350.*

- 3-function probes TESTO® (0635 9340): We used two probes to measure the wind speed, the temperature, and the relative humidity (RH) above the cooling bed.

*Figure 16. TESTO® 3-function probe.*

It was necessary to implement a cover to make them able to measure the wind speed in the main directions: east-west; north-south.

*Figure 17. TESTO® 3-function probes with a cover to measure unidirectional wind speed.*

- Anemometer TESTO® (0635 1540): to measure the down to up wind.

*Figure 18. TESTO® Anemometer.*

## MEASUREMENT SCHEMA

To the measurements trials PTG used both half parts of the cooling bed (38 m wide) locating the studied beams (18.1 m long) in each half of it. For space reason, the ambient measurements were taken on the Easter side of the cooling bed, following a beam at the time while it cools down, using for this aim a crane. The following figure shows the two path followed by the equipment on the crane to get the values.

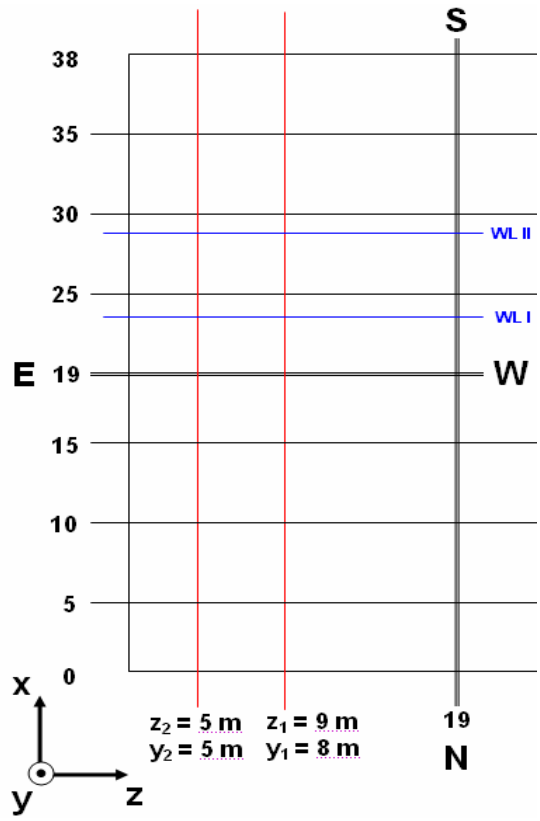


*Figure 19. Plane view of the two path followed in the measurement: ($x_1$,$y_1$=8m,$z_1$=9m) and ($x_2$,$y_2$=5m,$z_2$=5m).*

The original idea was to take the measurements quite near above the studied beam (around two meters), but the equipment available was not resistant enough to get that near (in the sense of the maximum operation temperature). However, we could get some values and important observation to have a better understanding and a feeling about the conditions on the cooling bed.

The two path followed were: Path 1($x_1$,$y_1$=8m,$z_1$=9m), which was located in around the middle of the studied beam (z=9m); and Path 2($x_2$,$y_2$=5m,$z_2$=5m), which was nearer in height to the studied beam (y=5m). The water cooling lines were turned off during the measurements on the first path and *on* during the second path. Each path took about 1.50 hours and 1 hour respectively to achieve. The difference in time was caused to a production stop during the first path.

The measurement equipment was installed on a cage as shown in the figure.


*Figure 20. Crane's cage with measurement equipment.*

Then the cage was hanged in a crane and moved in such a way that the equipment followed a beam as it moved along the cooling bed on the correspondent path.

*Figure 21. Crane with measurement equipment during the first path. Picture courtesy of PTG.*

## MEASURED VALUES

After getting the values it was necessary to process the data in order to get the right wind direction and to remove outliers point from the measurements. The next figures show the

values obtained on the second path ($x_2$,$y_2$=5m,$z_2$=5m). The observations for the first path were similar.

The temperature during the cooling time in a height of 5m (Path 2) is showed in Figure 22.

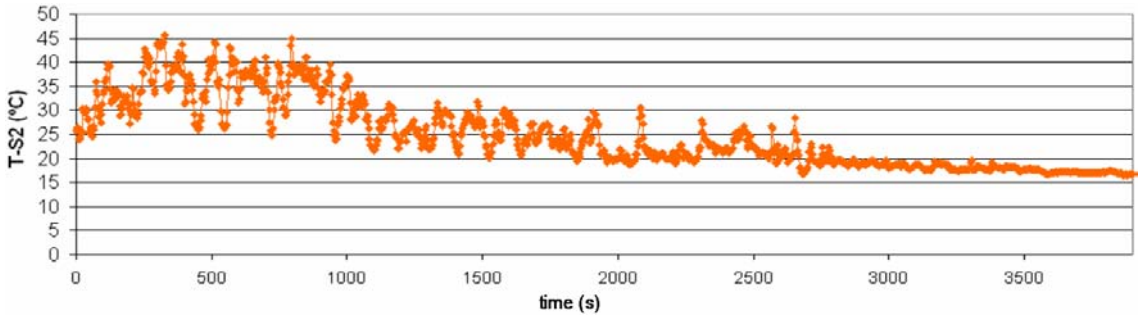


*Figure 22. Temperature values from the second path ($x_2$,$y_2$=5m,$z_2$=5m).*

As logical, at the beginning of the cooling process the temperature was higher, with a maximum of 45.7ºC, than at the end, with a minimum of 15.9ºC.

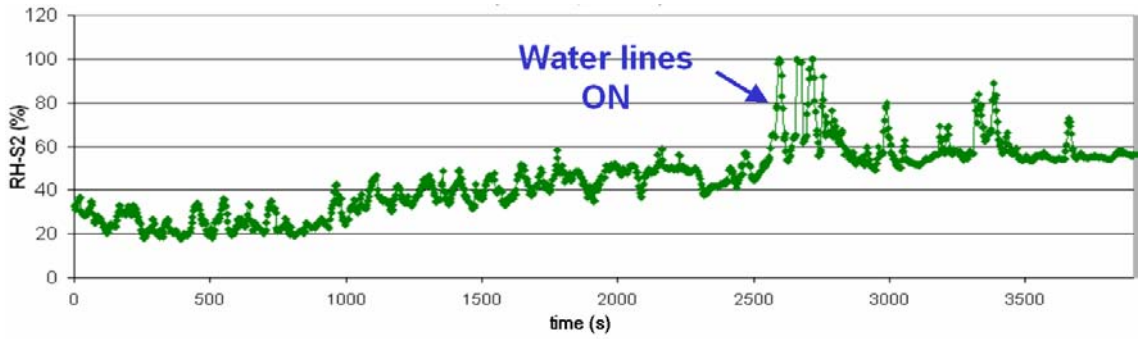


*Figure 23. Relative Humidity values from the second path ($x_2$,$y_2$=5m,$z_2$=5m).*

The relative humidity (Figure 23) increases as the beam get near the water lines. Before the zone of the water lines the RH% has an average of 35.4%.

The modulus and direction of the wind speed during the measurement are shown in the next figures.

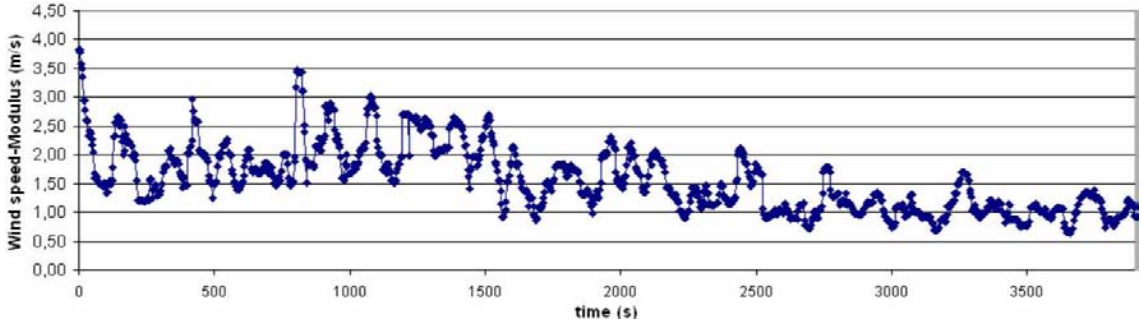


*Figure 24. Wind Speed modulus during the second path ($x_2$,$y_2$=5m,$z_2$=5m).*

The maximum and minimum wind speed registered was 3.8 m/s and 0.6 m/s respectively. This show the variability of the wind during the cooling period.

A schema of the cooling bed orientation is presented in Figure 25-a. The wind speed direction is represented by an argument from 0º to ±180º as in the Figure 25-b.

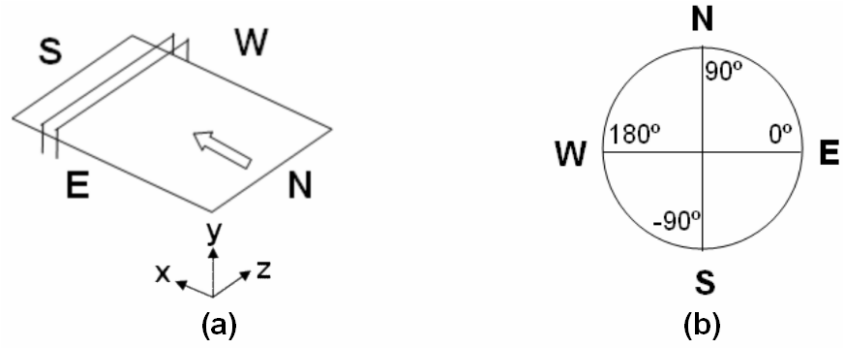


*Figure 25. Orientation of the Cooling Bed (a) and representation of the wind speed direction in argument from 0º to ±180º (b).*

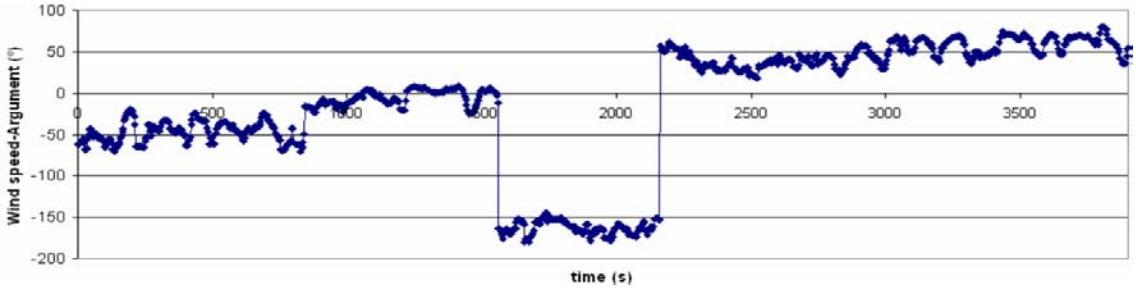


*Figure 26. Wind Speed direction represented by arguments from 0º to ±180º.*

We could observe that during the measurements the wind was very variable and came from all directions.

## MAIN OBSERVATIONS AND CONCLUSIONS

The next table presents a resume of the measured values.

*Table 2. Resume of measured values for second path: Temperature (T), Relative Humidity (RH) and Wind Speed magnitude (WS)*

| In total time | T (ºC) | RH (%) | WS (m/s) |
|---|---|---|---|
| Max | 43.52 | 80.63 | 3.83 |
| Min | 15.92 | 12.34 | 0.62 |
| Average | 23.60 | 39.80 | 1.57 |

After the measurements and observations carried out we could set the following facts:

- The weather conditions are strongly variable during the cooling period: the wind came from different directions, with magnitudes between 3.8 m/s and 0.6 m/s.

- The time for cooling the beams is also variable. It depends on the production rates.

- The beams arrive on the ingoing roller table in H position, as can be seen in Figure 27.


*Figure 27. Input part of the cooling bed studied for the H profiles. Picture courtesy of PTG.*

This situation makes the beam's zone faced down to maintain a higher temperature than the outer zone at the beginning of the cooling process.

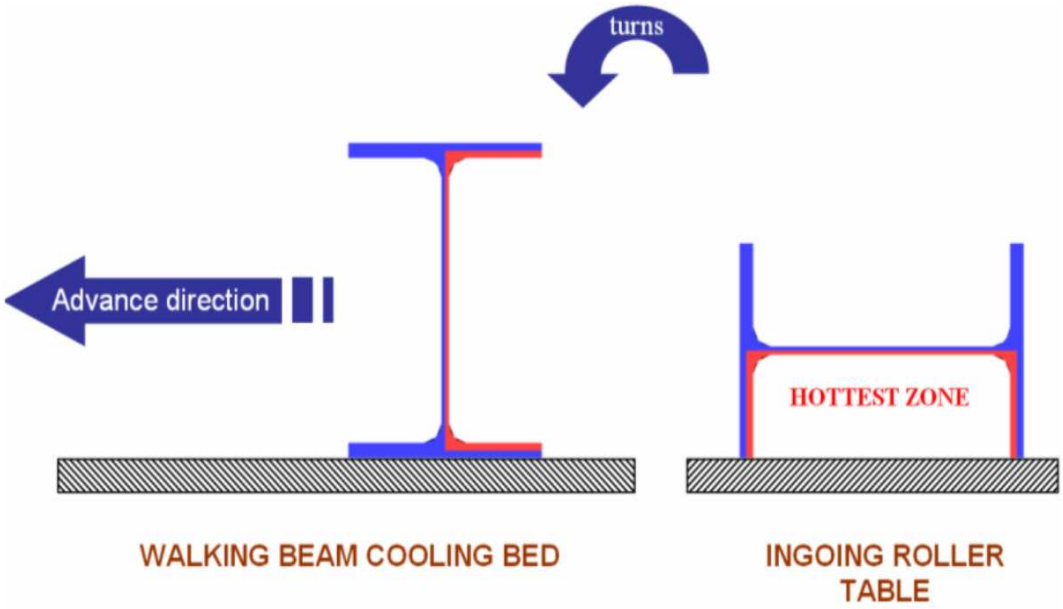


*Figure 28. General scheme of the initial stage of the walking beam cooling bed.*

The beam's surface temperatures at the ingoing roller table were measured by BFI. Therefore, the initial temperature differences were available for the modeling of the cooling process.

- The beam's bending starts before the water system influence. It is caused by the non symmetry initial temperature conditions around the beam (Figure 28). It also depends on the beam's length.

### 3.1.2.3 EXPERIMENTAL VALUES: BEAM'S SURFACE TEMPERATURE AT THE INGOING ROLLER TABLE, DURING COOLING ON THE COOLING BED, AND AT THE OUTGOING ROLLER TABLE; RESIDUAL STRESSES AFTER COOLING..

The beam's surface temperature at the ingoing and outgoing roller tables was carefully measured by BFI's research team using three linear infrared cameras installed on a C-hook-structure as shown in Figure 29 and Figure 30.

As explained in previous section, at the cooling bed input (or 'hot side') the beam was transported in 'H' position. Therefore, in this case (Figure 29), the camera 1 measured the surface temperature of the web faced up, camera 3 the web faced down and camera 2 one flange surface temperature (the so called 'south flange'). This made possible to know the initial temperature differences between the two sides of the beam.

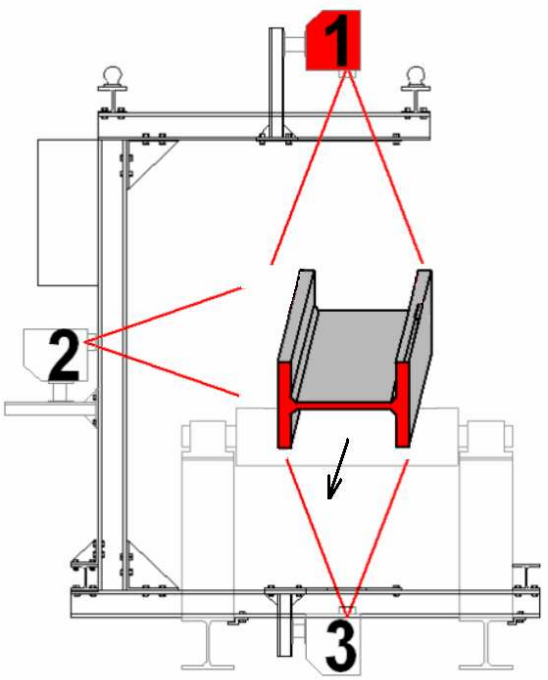


*Figure 29. Configuration of the linear infrared cameras on the C-hook at the ingoing roller table or 'hot side' of the cooling bed. Figure courtesy of BFI.*

The configuration displayed next is the one used at the cooling bed output (or 'cold side'). In this case, the cameras measured the two flange and one web surface temperatures.

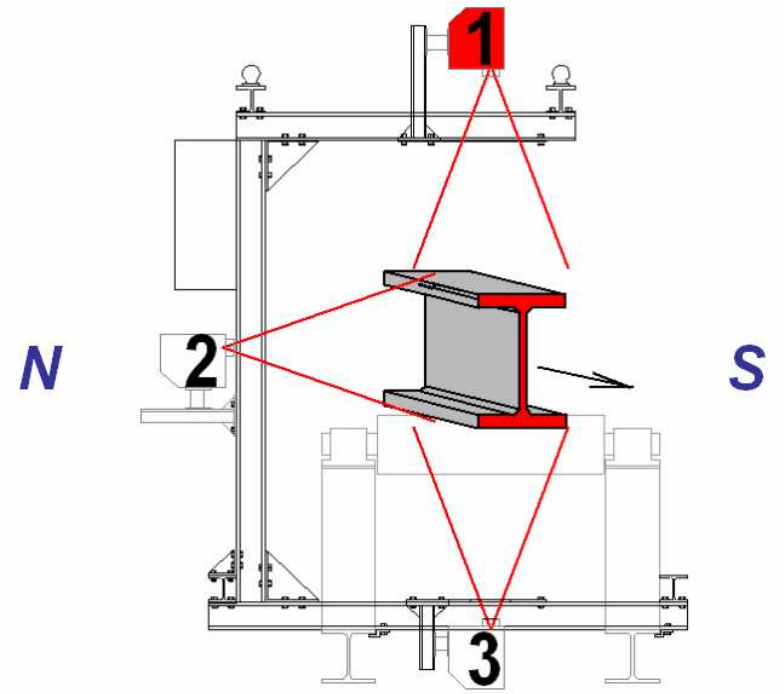


*Figure 30. Configuration of the linear infrared cameras on the C-hook at the outgoing roller table or 'cold side' of the cooling bed. Figure courtesy of BFI.*

Beside this measurements, the temperature evolution for some interesting surface points (including the upper flange center) during the cooling process on the cooling bed, was measured by PTG's collaborators using a manual infrared pyrometer.

In addition, the residual stresses after the cooling process were provided by BFI for a similar beam. The values were measured using the sectioning method.

### *EXPERIMENTAL TEMPERATURE VALUES AT THE INGOING ROLLER TABLE*

The three linear cameras at the C-hook could measure the input surface temperature for several HEM500 beams. The surface temperature resulted for one of the beam measured (section 175) is displayed in Figure 31.

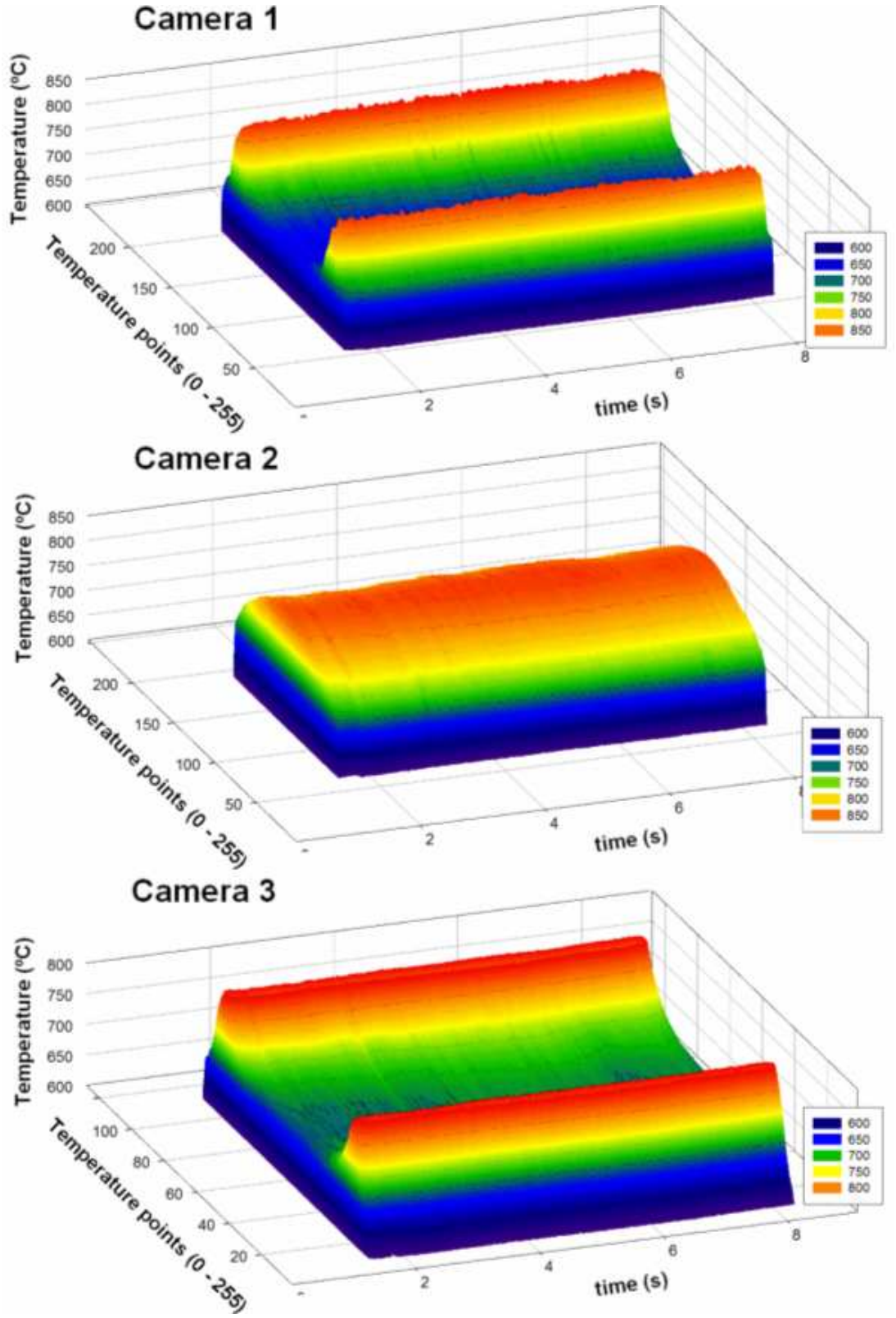


*Figure 31. Three dimensional surface temperature of the HEM500 section nº 175 at the cooling bed ingoing roller table (hot side). Data obtained by the BFI's three infrared cameras on C-hook structure. Figure courtesy of BFI.*

In these graphics one can observe how the highest surface temperatures are located on the beam's roots (camera 1 and 3 graphics) and flange center (camera 2 graphic).

For several trials at the 'hot side', the average temperature difference between the two web surface side's centers was 16.8 ºC.

## EXPERIMENTAL TEMPERATURE VALUES DURING COOLING PROCESS

For the same set of beams, measurements of the flange center surface temperatures, at 500 mm from the end of the section, during cooling along the cooling bed were carried out. The average of several trials is displayed in Figure 32.

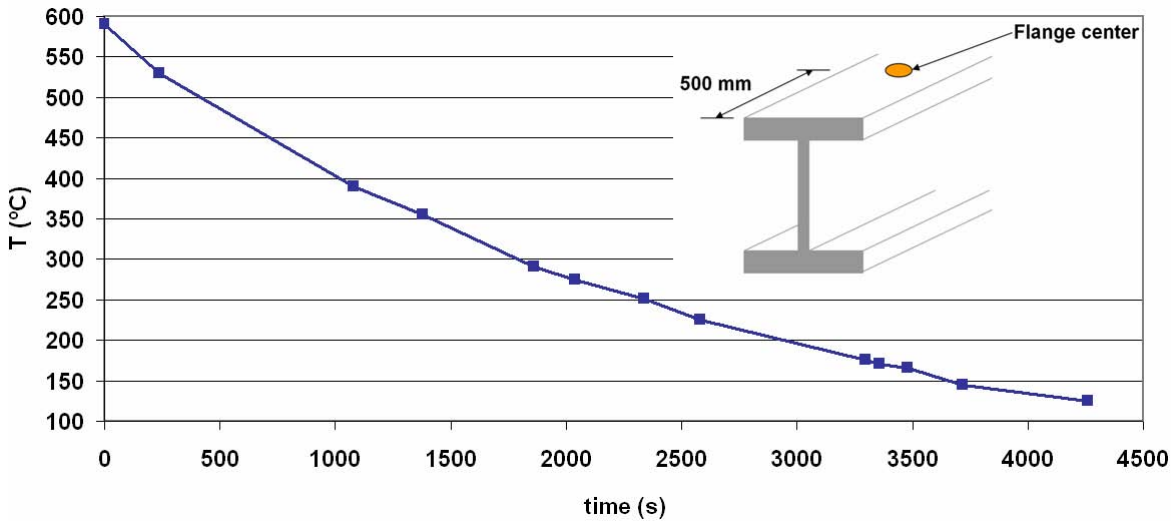


*Figure 32. Average of flange center surface temperature for several HEM500 beams' cooled on the cooling bed. Data courtesy of PTG.*

As the values were taken manually with an infrared pyrometer, there were some inevitable deviations. The important fact was that the tendency of the cooling rate of these types of beams along the cooling bed could be set.

## EXPERIMENTAL TEMPERATURE VALUES AT THE OUTGOING ROLLER TABLE

The same sections were measured by BFI system at the cooling bed output ('cold side'). The 3D surface temperature results for the section nº175 are showed in Figure 33.

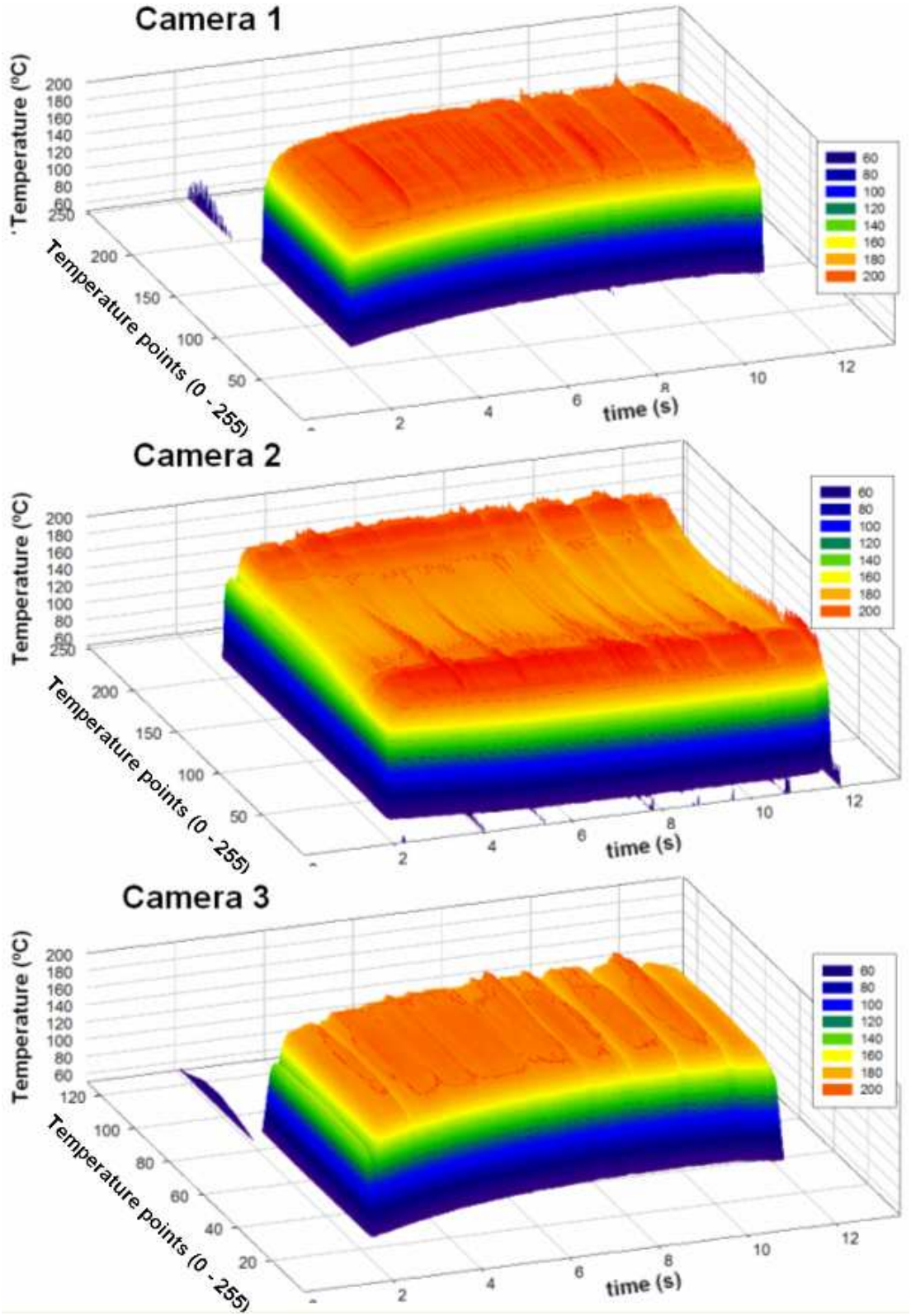


*Figure 33. Three dimensional surface temperature of the HEM500 section nº 175 at the cooling bed outgoing roller table (hot side). Data obtained by the BFI's three infrared cameras on C-hook structure. Figure courtesy of BFI.*

In this case the temperatures were more homogeneous. The cuts on these graphics, used to compare with the simulated result, are presented in Figure 34. These surface temperatures were taken for a cross-section near the center of the studied beam.

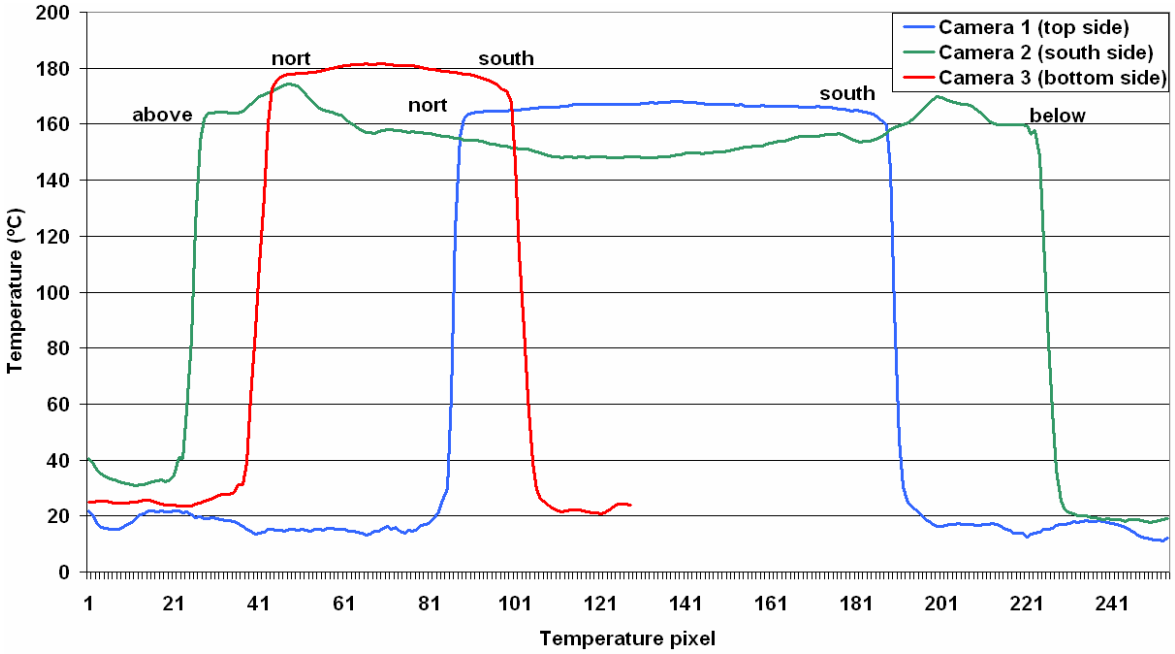


*Figure 34. Temperature values from camera 1, 2 and 3 for a location near the center of the beam at the cooling bed output (cold side). Figure courtesy of BFI.*

Some interesting values to compare with the simulations — like the temperature difference between the flange center and its edge ($\Delta T_F$) and the web-root and the web's center ($\Delta T_W$) — are presented in the next table.

*Table 3. Experimental surface temperatures and the differences (ΔT) at the end of the cooling process..*

| Camera | Points for ΔT | Values (ºC) | ΔT (ºC) |
|---|---|---|---|
| 1 | $T_{Flange's\ Center} - T_{Flange's\ Edge}$ | 168.1 – 164.2 | 3.9 |
| 2 | $T_{Root} - T_{Web's\ Center}$ | 170.5 – 148.5 | 22 |
| 3 | $T_{Flange's\ Center} - T_{Flange's\ Edge}$ | 182.0 – 177.7 | 4.3 |

## EXPERIMENTAL RESIDUAL STRESSES VALUES AFTER COOLING PROCESS

BFI kindly provided the experimental residual stresses results for a similar profile, the HEB500 ($d$ = 500 mm, $b_f$ = 300 mm), after the cooling process. These longitudinal residual stresses were measured using the sectioning method and are displayed in Figure 35 and Figure 36.

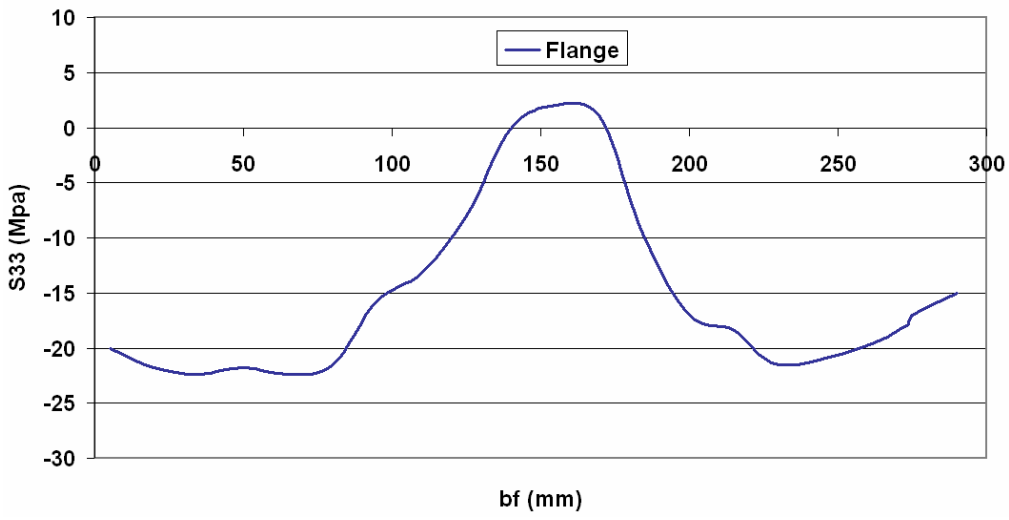


*Figure 35. Flange experimental longitudinal residual stresses for a HEB500 beam, measured using the sectioning method. Data courtesy of BFI..*

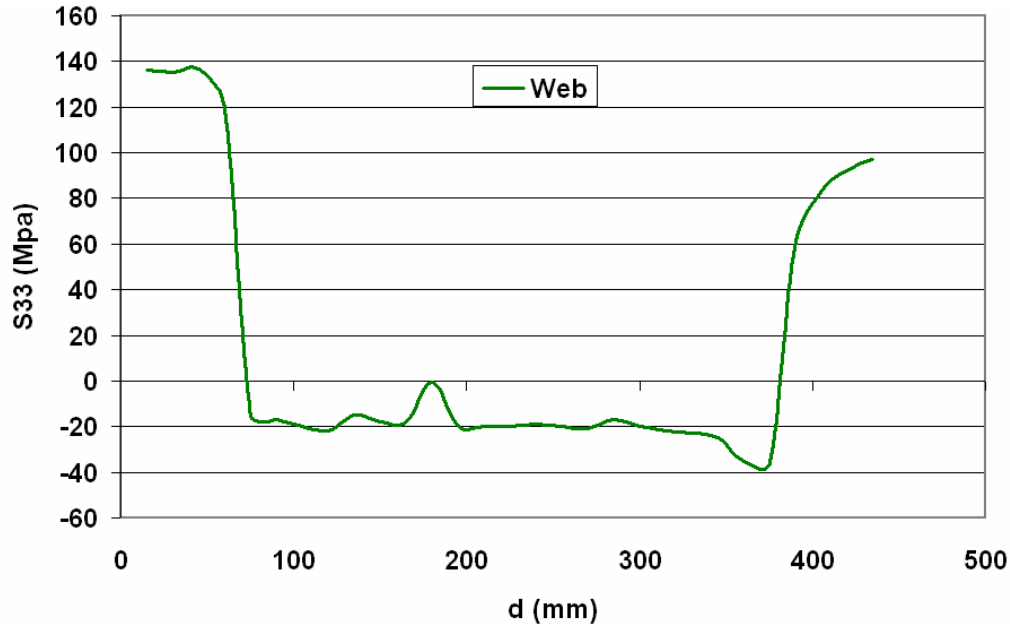


*Figure 36. Web experimental longitudinal residual stresses for a HEB500 beam, measured using the sectioning method. Data courtesy of PTG.*

### 3.1.2.4 FE-THERMAL MODEL FOR THE 'H' PROFILE COOLING PROCESS

From the measured values and observations at PTG plant a thermal model was designed using the software FLUENT®. It included the following characteristics:

a) The cooling of the beam was simulated by means of the heat transfer achieved by conduction inside the beam and convection and radiation to the surrounding fluid

(moved air). The influence of heat transfer by conduction between the beam and the cooling bed's supports was considered not relevant in this study.

b) The model incorporates the influence of the surrounding beams on the cooling of the studied beam. During the cooling, a beam is subject to the heat from the beams located at both sides. To represent this fact the model includes lateral symmetry planes.

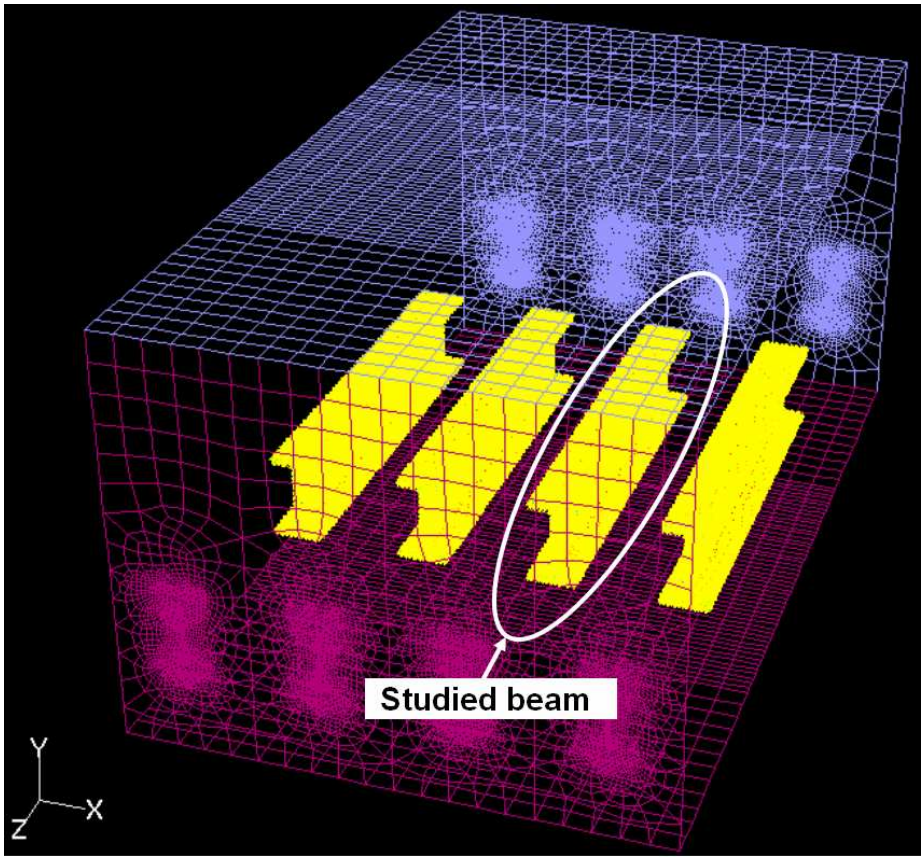


*Figure 37. Thermal model view activating the symmetry planes.*

c) The model allows the change of the boundary conditions related to the wind speed magnitude and direction, based on the measurements and observations at the PTG cooling bed.

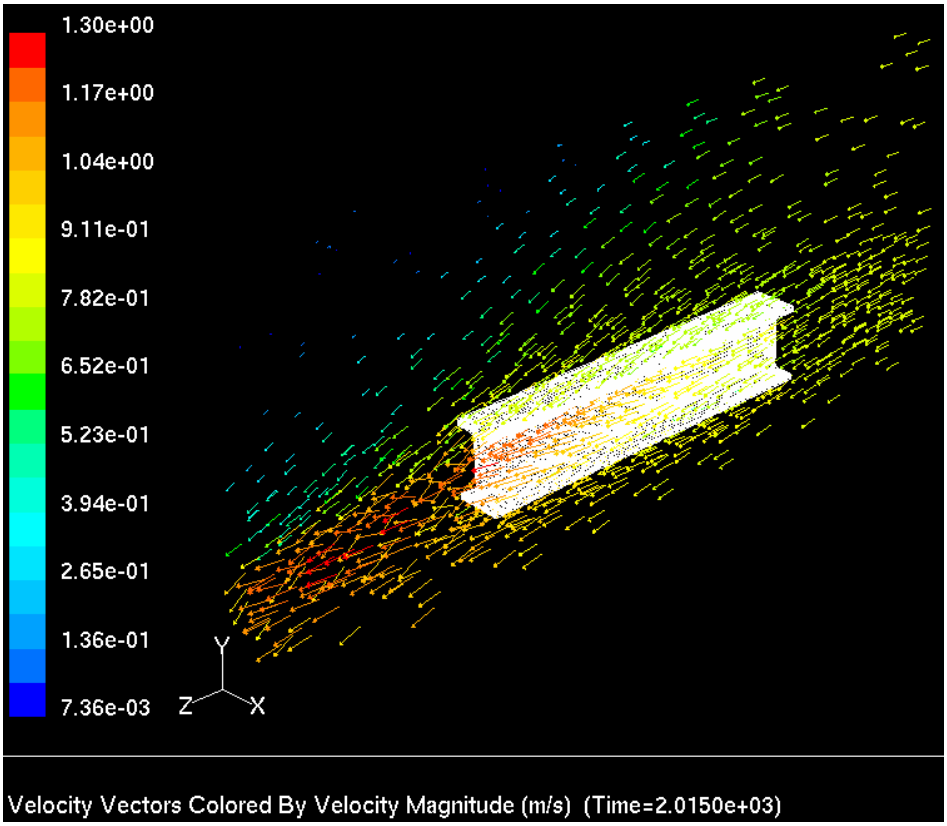


*Figure 38. Velocity Vectors (from west to east) in m/s, at time 2015 s*

d) Initially, the HEM500 beam simulated was 2.5 m length, long enough to avoid the border effects and to perceive the bending of the beam. Also, not too long to achieve an acceptable computational time. The meshing was based on 3D hexahedral elements. A plane view of the mesh is presented in Figure 39. The element length in the *Z* direction was 50 mm.

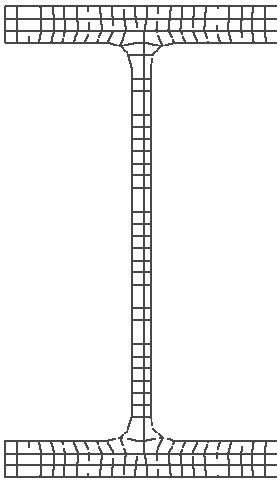

*Figure 39. Mesh of the HEM500 beam.*

e) To simulate the beam's non symmetric initial temperature (at the beginning of the cooling bed), the mesh was divided in such a way (Figure 40) that a different temperature could be set at the red zone (initial hottest zone) and at the blue zone (outer zone). The approach was as follow: At the beginning of the cooling process (simulating the stage after the last rolling mill) a homogenous temperature was set in the beam (1000 ºC). Almost immediately after (10 s) a boundary condition set a temperature difference of 20ºC in both beam sides: 950ºC to the hottest zone and 930ºC to the outer zone. These values were obtained by calibration of the model to get an agreement with the experimental trials. And after that the beam was free to cool down, simulating the cooling process in 'I' position (with surrounding beams) at the cooling bed.

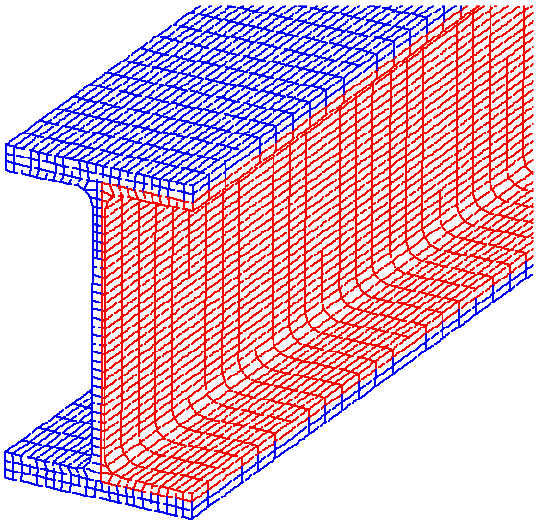

*Figure 40. Beam's mesh: outer zone in blue and inner zone in red, in order to simulate the non symmetrical initial condition.*

f) The material thermal properties used for the studied steel, the S235, are presented in Table 4.

*Table 4. Thermal properties for steel S235.*

| ºC | *k* (W/mºC) | *c* (J/kg ºC) |
|---|---|---|
| 20 | 56.9 | 461 |
| 100 | 56.4 | 479 |
| 200 | 53.5 | 499 |
| 300 | 49.4 | 517 |
| 400 | 45.2 | 536 |
| 500 | 41.3 | 558 |
| 600 | 37.6 | 587 |
| 700 | 33 | 625 |
| 800 | 26.5 | 674 |
| 900 | 21 | 738 |
| 1000 | 15 | 818 |

This information was found in data base www.stahldat.de and in reference (Rohloff and Neuschütz, 1990) for the rage from 20 to 600ºC. For the range form 700 to 1000ºC there was no information available, so the values were interpolated. The emissivity was set in 0.85.

## RESULTS OF THE THERMAL MODEL SIMULATION

### COMPARISON OF EXPERIMENTAL AND SIMULATED VALUES AT THE BEGINNING OF THE COOLING PROCESS

The temperature evolution in time at the first period of the cooling, for both sides of the web center are presented in Figure 41.

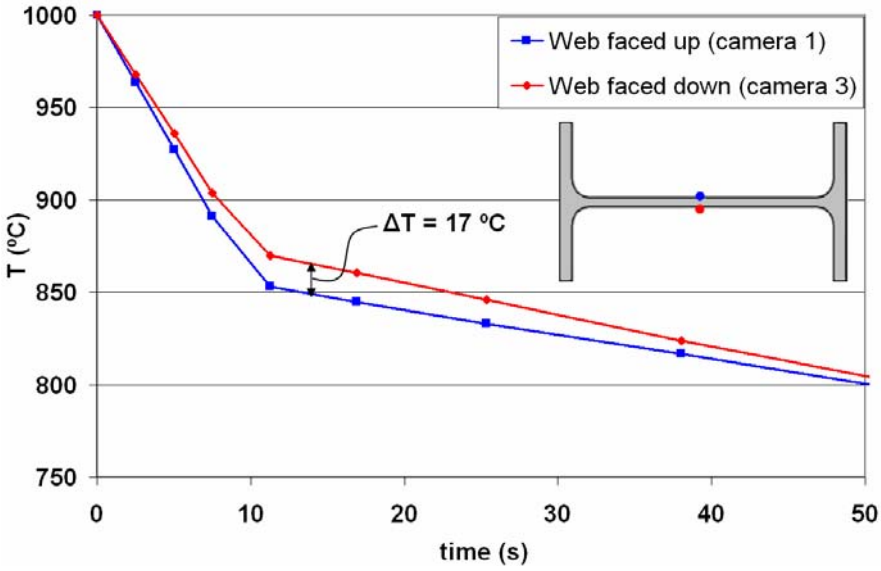


*Figure 41. Surface temperature values from FE-thermal model simulation for both sides of the web surface center, at the beginning of the cooling process.*

In the figure, the initial conditions for the cooling in the cooling bed can be observed. At the beginning, a uniform temperature of 1000ºC was set in the beam (simulating the last rolling mill beam's temperature). Then, the beam cooled down non symmetrically, simulating the conditions at the ingoing roller table, where the beam was set in 'H' position. A maximum temperature difference of 17 ºC at the web center surfaces (the one faced up and the one faced down) was obtained. This is a value very close to the experimental one, 16.8 ºC. Afterward, the temperatures tended to homogenized. The unsymmetrical initial temperatures can be also verified in the temperature contour plot of the beam's center cross section displayed in Figure 42.

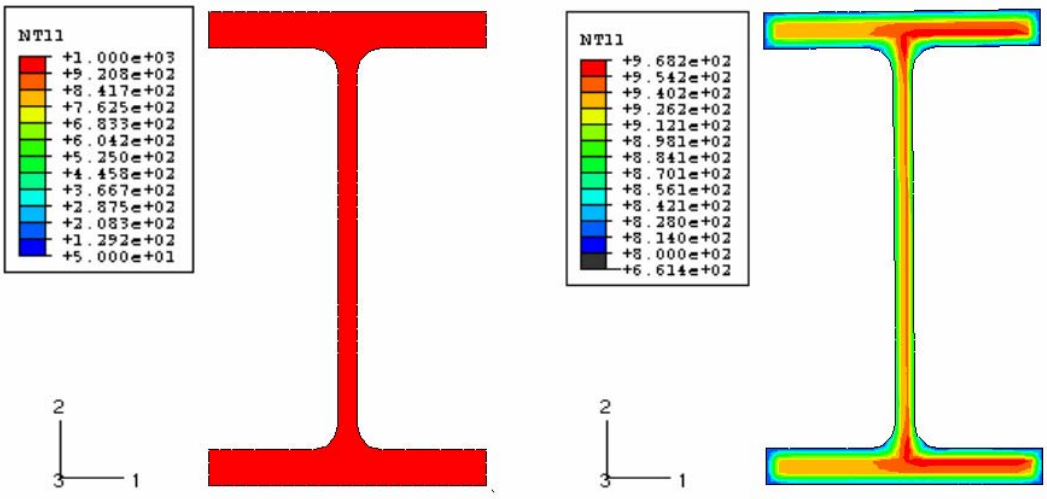


a. Temperature contour plot at time 0 s b. Temperature contour plot at time 11 s

*Figure 42. Temperature contour plot of the beam's center cross section at several times: a. time=0 s and b. time=11s.*

In Figure 42.b is clearly showed the non uniform initial temperature.

After this first stage, the beam cooled down in a more uniform way as it moved forward over the cooling bed.

## COMPARISON OF EXPERIMENTAL AND SIMULATED VALUES DURING THE COOLING PROCESS AT THE COOLING BED

Once on the cooling bed, the beam is set in 'I' position and stay like this and surrounded by other beams until the end of the cooling process. The cooling rates of the beam's flange center obtained in both, the simulation of the FE-thermal model and the experimental trials (Figure 32), are displayed in Figure 43.

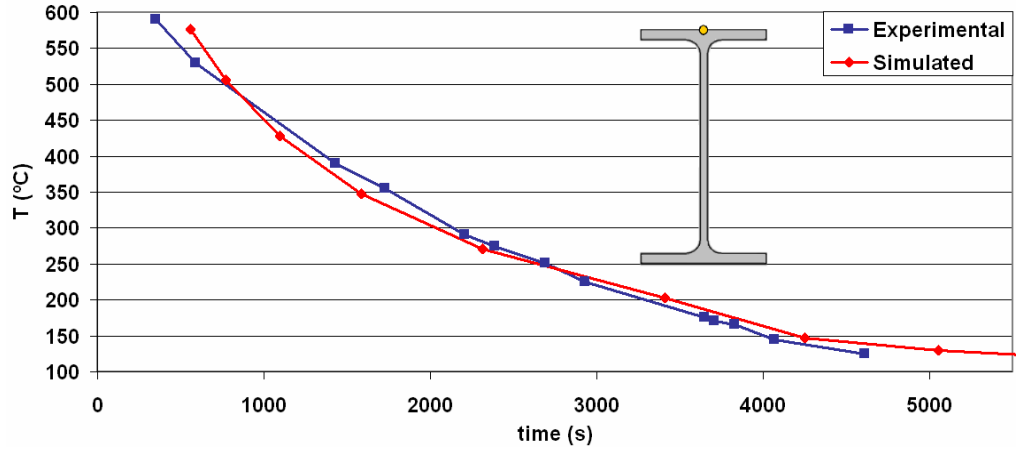


*Figure 43.Temperature history for the flange center surface: simulated and experimental values.*

The figure shows an agreement between the experimental and the simulated cooling rate values.

## COMPARISON OF EXPERIMENTAL AND SIMULATED VALUES AT THE END OF THE COOLING PROCESS

A general view of the final temperature contour plot for the HEM500 beam studied is displayed in Figure 44 (this figure was obtained directly from FLUENT®, which uses as temperature unit the Kelvin (K). Therefore, the scale presented corresponds to a range from 149 ºC to 186 ºC). Axis X, Y and Z correspond to 1, 2 and 3 respectively.

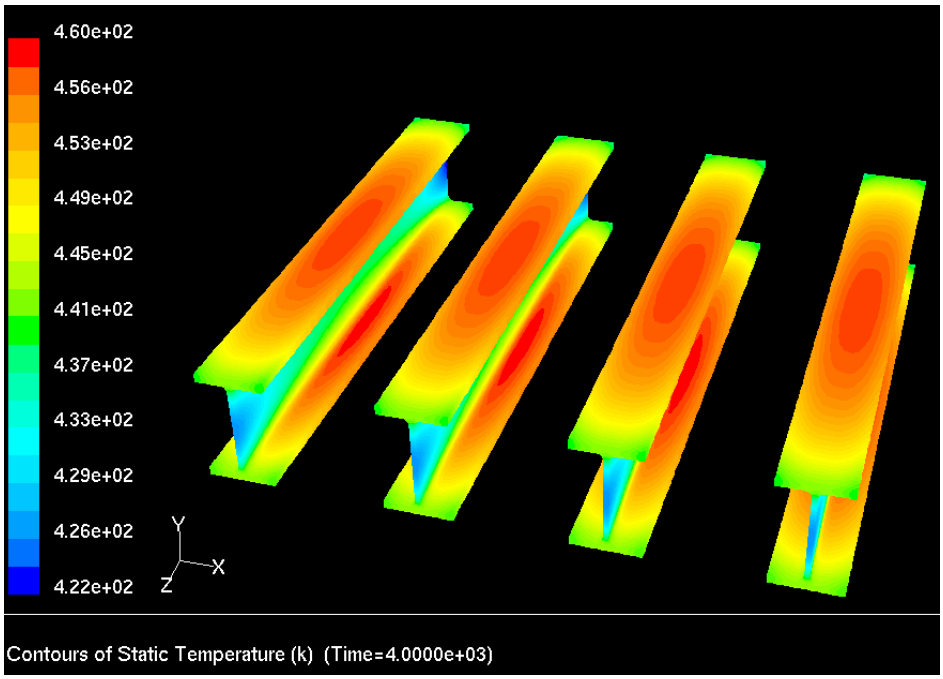


*Figure 44. Surface temperature contour plot at final time (4000 s ≈ 67 minutes). The scale is in Kelvin and corresponds to a range from 149 ºC to 186 ºC.*

As expected, the hottest surface temperatures were at the beam's center and specifically at the flange center and root area.

What happens inside the beam is presented in Figure 45, where the temperature contour plot of the beam's center cross section (at final time) is displayed.

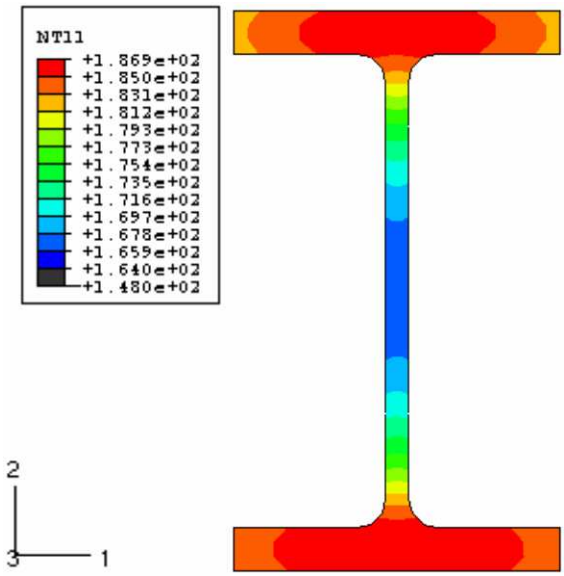


*Figure 45. Temperature contour plot of the beam's center cross section at final time.*

It can be seen that the heat flows from the flange center to the flange edges and root. The reason is the wide flange of this type of profile (HEM500). As the wind affects the beam's part more exposed (upper flange and web), the higher temperatures were located at the lower flange center, with a value of 186.4 ºC. The web's center presented the lowest temperature, 166.8 ºC.

In the next figures the surface temperature of both, flanges and web, are presented in order to compare with the experimental value of Figure 34. The 'temperature points' reported on the graphics are the one showed in Figure 46.

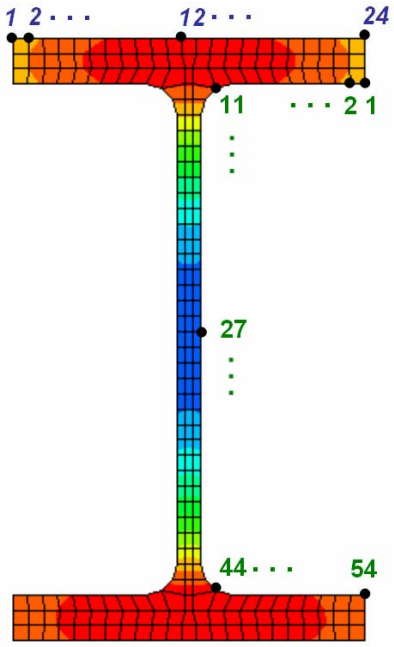


*Figure 46. 'Temperature points' for temperature values of Figure 47 and Figure 48.*

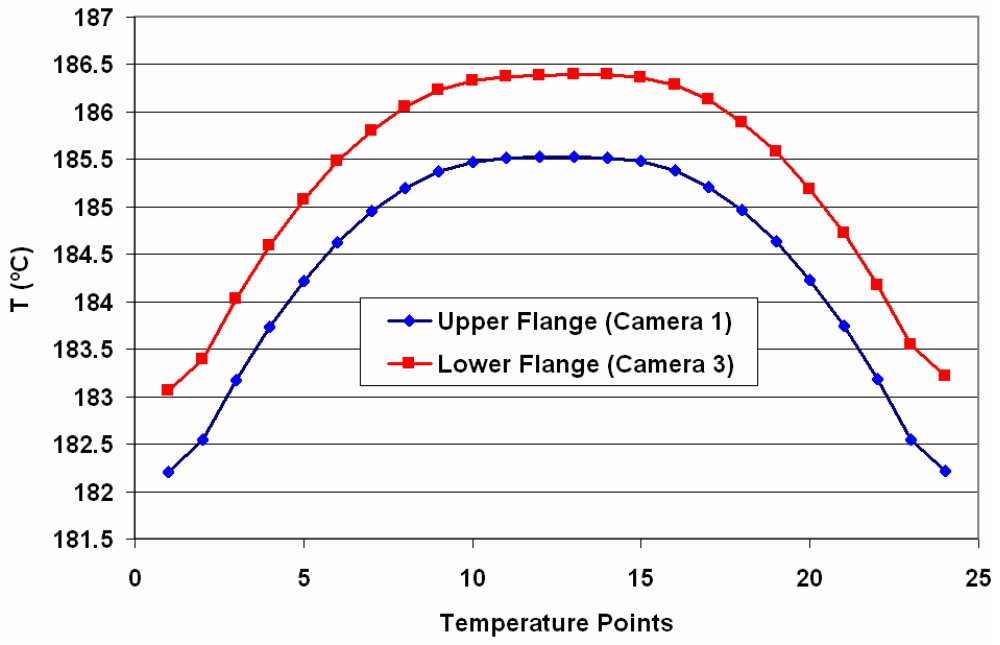


*Figure 47. Surface temperature on upper and lower flange, at final time (4000 s).*

Again is visible that the lower flange surface presented higher temperature than the upper one, as in the real case.

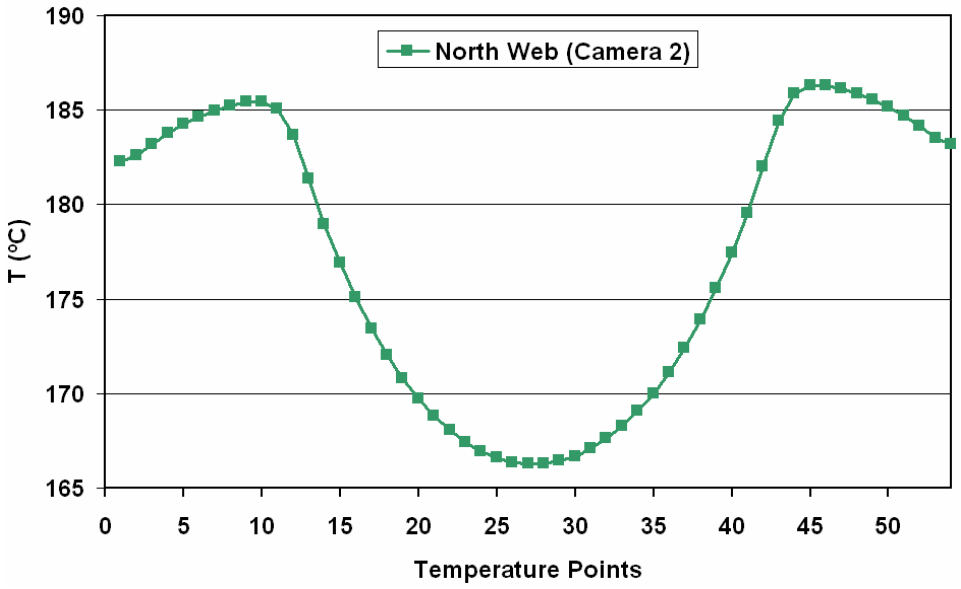


*Figure 48. Surface Temperature of north web, at final time (4000 s).*

Comparing Figure 47 and Figure 48 with the experimental curves on Figure 34, a similar behavior is observed. The maximums in Figure 47 are in points 12, the flange's centers, with 185.5 ºC on upper flange and 186.5 ºC on lower flange. And in Figure 48, the maximums are located on points 11 (with 185.5 ºC) and 44 (with 186.3 ºC), which are

points near the beam's roots. The minimum, 166.3 ºC, is located at the web's center (point 27). The shapes of the curves were also observed on the experimental curves.

In addition, to compare the simulated results with the experimental values, next table present the main temperature differences calculated in the same way as for Table 3.

*Table 5. Simulated surface temperatures and the difference values (ΔT) at the end of the cooling process.*

| "Camera" | Points for $\Delta T$ | Values (ºC) | $\Delta T$ (ºC) |
|---|---|---|---|
| 1 | $T_{Flange's\ Center}$ - $T_{Flange's\ Edge}$ | 185.5 – 182.2 | 3.4 |
| 2 | $T_{Root}$ -$T_{Web's\ Center}$ | 186.3 -166.3 | 20 |
| 3 | $T_{Flange's\ Center}$ - $T_{Flange's\ Edge}$ | 186.5 -183 | 3.5 |

The temperature differences obtained from the simulated results were similar to the experimental values with errors of 12%, 9% and 18% respectively. The temperature difference at the lower flange should be higher but the value was acceptable taking into account the variability of the weather conditions.

As a result of all comparisons with experimental values, the FE-thermal model developed was considered adequate.

Once the temperature results from FE-thermal model were obtained, a conversion of their format was necessary in order to introduce them to the FE-stress/displacement model created in ABAQUS®. Section 3.2 presents the main characteristics of the conversion code developed to accomplish this task.

### 3.1.2.5 FE-STRESS/DISPLACEMENT MODEL OF THE 'H' PROFILE COOLING PROCESS

The FE-stress/displacement model was designed using the software ABAQUS®, specifically using the ABQ/Standard modulo. The model presented the following characteristics:

a) The model included the gravity forces: 9.81 m/s$^2$.

b) The beam laid on a plane table with friction. The friction value was set on 0.07, as an approximation for the support bars friction presented in the cooling bed.

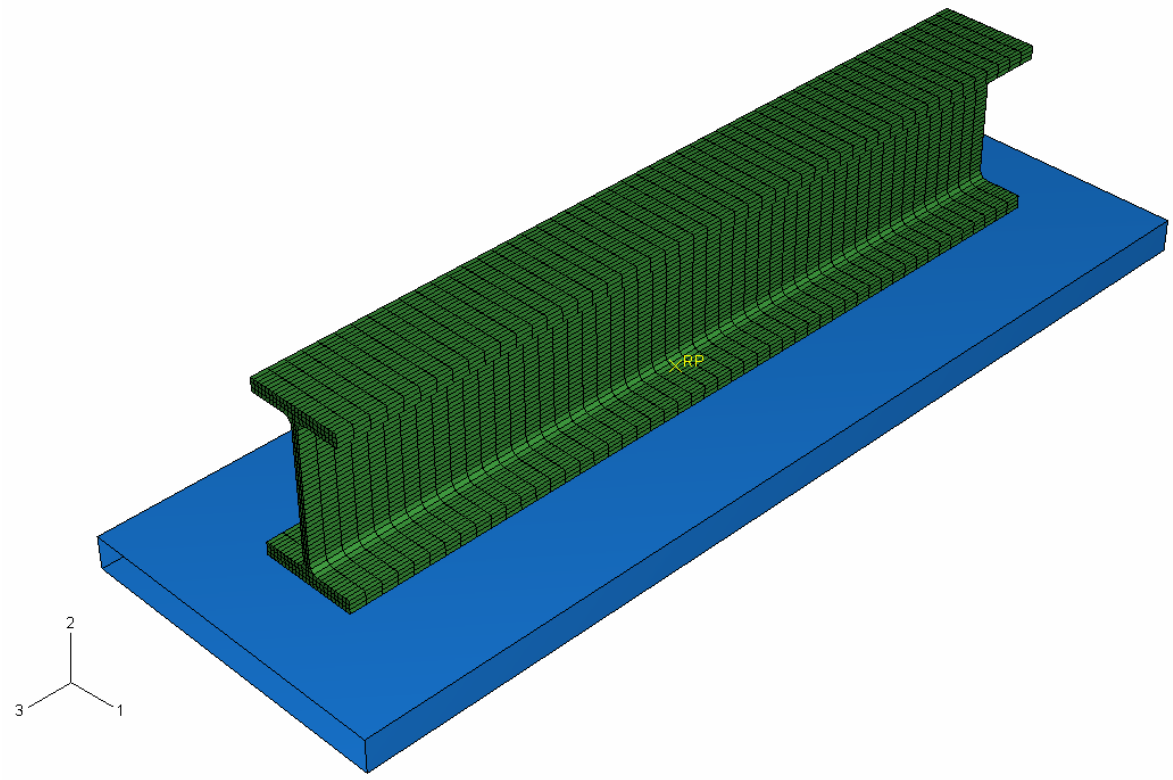


*Figure 49. FE-stress/displacement model created in ABAQUS® for the 'H' profile cooling process.*

c) The material properties used for the studied steel, the S235, regarding the elastic behaviour and thermal expansion are resumed in Table 6.

*Table 6. Mechanical properties for steel S235. Elastic behaviour and thermal expansion coefficient.*

| ºC | ***E*(GPa)** | **v** | ***α*(e-5/ºC)** |
|---|---|---|---|
| 20 | 212 | 0.28 | 1.19 |
| 100 | 207 | 0.28 | 1.25 |
| 200 | 199 | 0.28 | 1.30 |
| 300 | 192 | 0.28 | 1.36 |
| 400 | 184 | 0.28 | 1.41 |
| 500 | 175 | 0.28 | 1.45 |
| 600 | 164 | 0.28 | 1.49 |
| 700 | 150 | 0.28 | 1.52 |
| 800 | 134 | 0.28 | 1.55 |
| 900 | 115 | 0.28 | 1.58 |
| 1000 | 93 | 0.28 | 1.60 |

As said before, there was no information available for the range form 700 to 1000ºC, so the values were interpolated.

The values from the yield stress-strain curve were provided by PTG for the range from 20 to 200ºC. The values for the range from 800ºC to 1000ºC were found at reference (Rohloff and Neuschütz, 1990) for similar steels. To find the values between these rages the curves were interpolated, trying to follow the tendencies. Next table presents the values for the plastic model, obtained for the tension test.

*Table 7. Yield stress vs. Plastic strain for S235 steel grade*

| | Yield stress (GPa) | | | | | |
|---|---|---|---|---|---|---|
| **Plastic Strain** | **20ºC** | **200ºC** | **400ºC** | **600ºC** | **800ºC** | **1000ºC** |
| 0 | 250 | 330 | 250 | 330 | 85 | 45 |
| 0.1 | 589 | 470 | 589 | 470 | 132 | 78 |
| 0.2 | 670 | 580 | 680 | 580 | 165 | 94 |
| 0.3 | 711 | 660 | 731 | 665 | 175 | 100 |
| 0.4 | 732 | 705 | 762 | 715 | 185 | 104 |

d) The mesh of the profile for the stress/displacement model was the same as for the thermal model. It was made in this way to facilitate the job of the conversion code (Section 3.2) that converts the result from FLUENT® format to ABAQUS® format.

## *RESULTS OF THE STRESS/DISPLACEMENT MODEL SIMULATION*

The longitudinal stress and displacement evolution during several times of the cooling process are presented in the figures below. For a more complete view of the evolution, the temperature contour plot was also included.

The displacement in the XZ-plane (or 1-3 plane) can be seen at the top of the figures (the contour plot is referred to the longitudinal stresses, S33). On the lower left side the temperature of the center cross-section in displayed. Finally, the longitudinal stress (S33) of the same cross-section is showed on the lower right side.

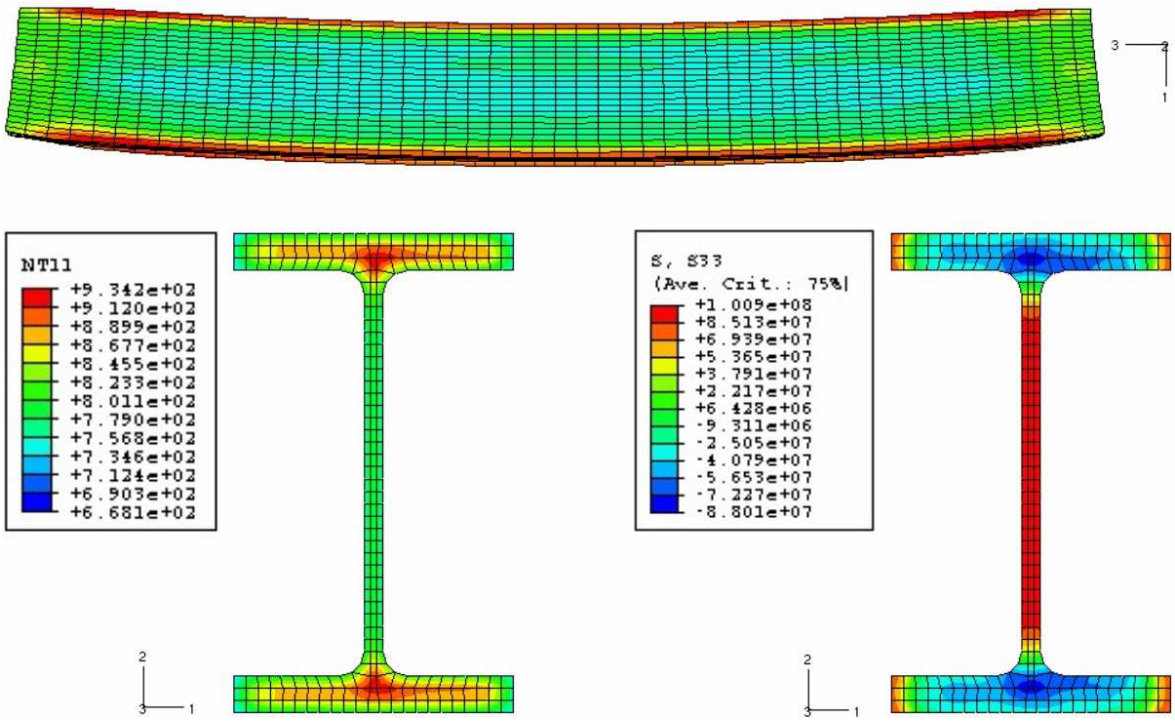


*Figure 50. Stress (S33 in Pa), displacement behavior and temperature (NT11 in ºC) at the beginning of the cooling process on the cooling bed (time = 76 s).*

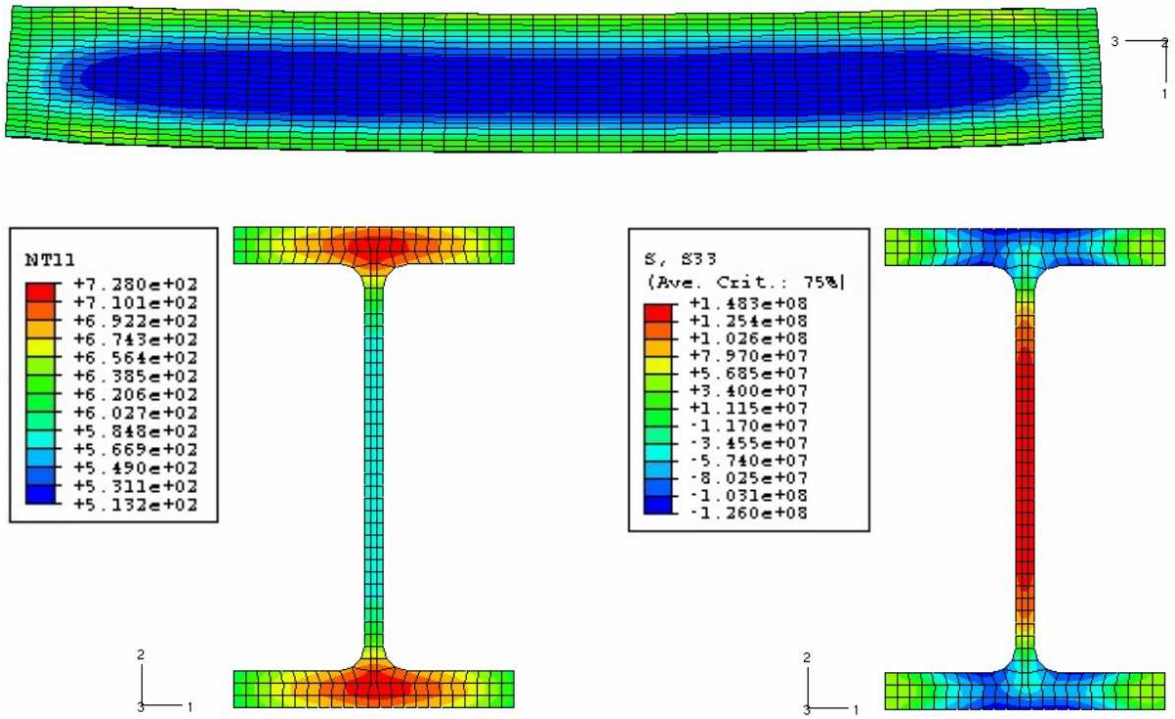


*Figure 51. Stress (S33 in Pa), displacement behavior and temperature (NT11 in ºC) at time 316 s.*

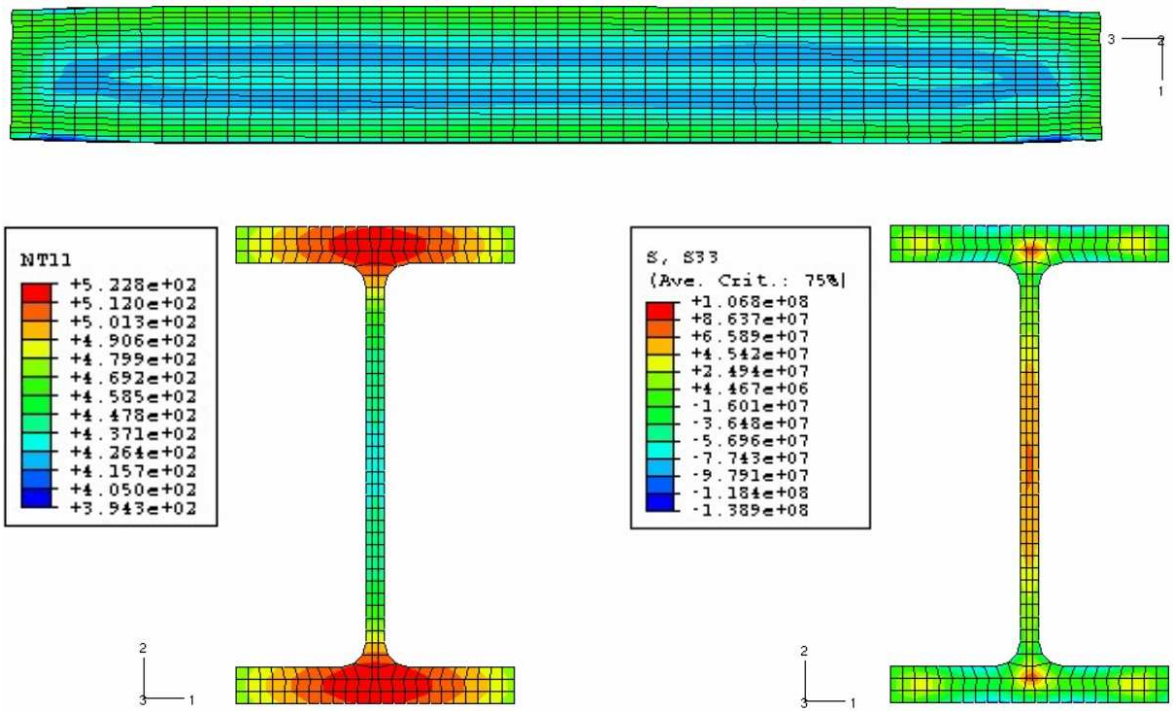


*Figure 52. Stress (S33 in Pa), displacement behavior and temperature (NT11 in ºC) at time 773 s.*

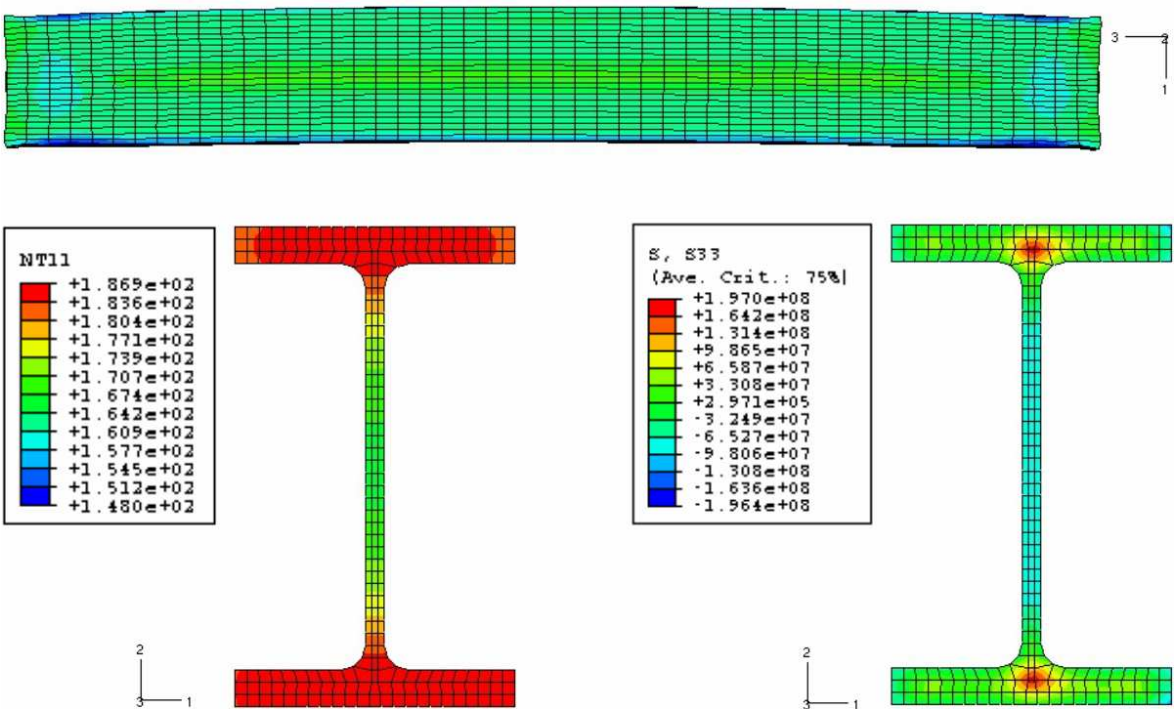


*Figure 53. Stress (S33 in Pa), displacement behavior and temperature (NT11 in ºC) at the end of the cooling process (time 4000 s).*

From these figures the following conclusions could be set:

a. During the whole cooling process, the longitudinal stress (S33) changed signs from compression (-) to tension (+) in the beam's root, and from tension (+) to compression (-) at the beam's web and flanges-tips.

b. At the beginning of the cooling process the parts of the beam that had larger external surface, as the web and flange-tips, cooled down and shrank faster that the parts that had more material inside, as the root. Therefore the web and flange-tips parts tended to pull the beam's root, and, as a reaction, the root contracted (Figure 50 y Figure 51). In points where the stresses reached the yielding stress (which is low for high temperatures, as can be seen in Table 7), plastic deformation developed.

c. The non-symmetry on the temperature at the beginning of the process (Figure 50) was caused by the non uniform initial temperature.

d. Because of the non uniform temperature at the beginning of the process, the 'outer-cooler' part of the beam cooled down first than the 'inner-hotter' part. This caused the initial bending of the beam to the 'south-side' of PTG's cooling bed (Figure 50 y Figure 51). In the real case, at PTG's cooling bed, this bending is not noticed with naked eye maybe because at the beginning of the cooling the beam remains in 'H' position for a while before is turned to the 'I' position, and in this case the gravity forces of these longer beams can be counteracting the initial bending mentioned.

e. At the final stage of the cooling process (Figure 52 y Figure 53), the web and flange-tips reached a more uniform temperature and was the root that started to cool down with a higher rate. This caused the opposite reaction than before: pressure stresses in the web and flange-tips, and tensile stresses in the root. The greatest residual stresses were located in the root center (tension) and in the web center (compression).

f. This can also explain the beam's bending. The initially 'outer-cooler' part of the beam reached, near the ending time, a more uniform temperature and was the initially 'inner-hotter' part that started to cools down in a faster way, causing the bending to the 'north-side' of PTG's cooling bed, which is the final bending observed in real cases (Figure 53).

### COMPARISON OF EXPERIMENTAL AND SIMULATED RESIDUAL STRESSES VALUES

The longitudinal residual stresses, at the end of the cooling process are presented in Figure 54. They are displayed in the way they would be measured through the sectioning method: the average of the set of elements' stresses values along the *flange* and the average of the set of elements' stresses values along the *web*.

These stress behavior and curvatures are in accordance with the literature (Szalai and Papp, 2005; Prime, 1999; Totten, 2002; Young, 1972). In these references, the maximum tensile value is located at the flange center and the maximum compressive value is located at the web center, similar to the simulation results.

The shape of the curves, of the simulated results and the experimental measurement, for both, the flange (not considering the flange tips) and the web are very similar. We can observe the same 'Mexican-hat' shape in the residual stresses at the flange (comparing Figure 54 and Figure 35), and the middle-plane and high-extremes shape at the web (in Figure 54 and Figure 36). Even though these experimental values are not in agreement with the general location of the tensile and compressive maximums set in the literature, the common residual stresses behavior (shape of the curves) for these type of beam ($t_f > t_w$, i.e. the flange wider than the web) after cooling process can be taken as the right one.

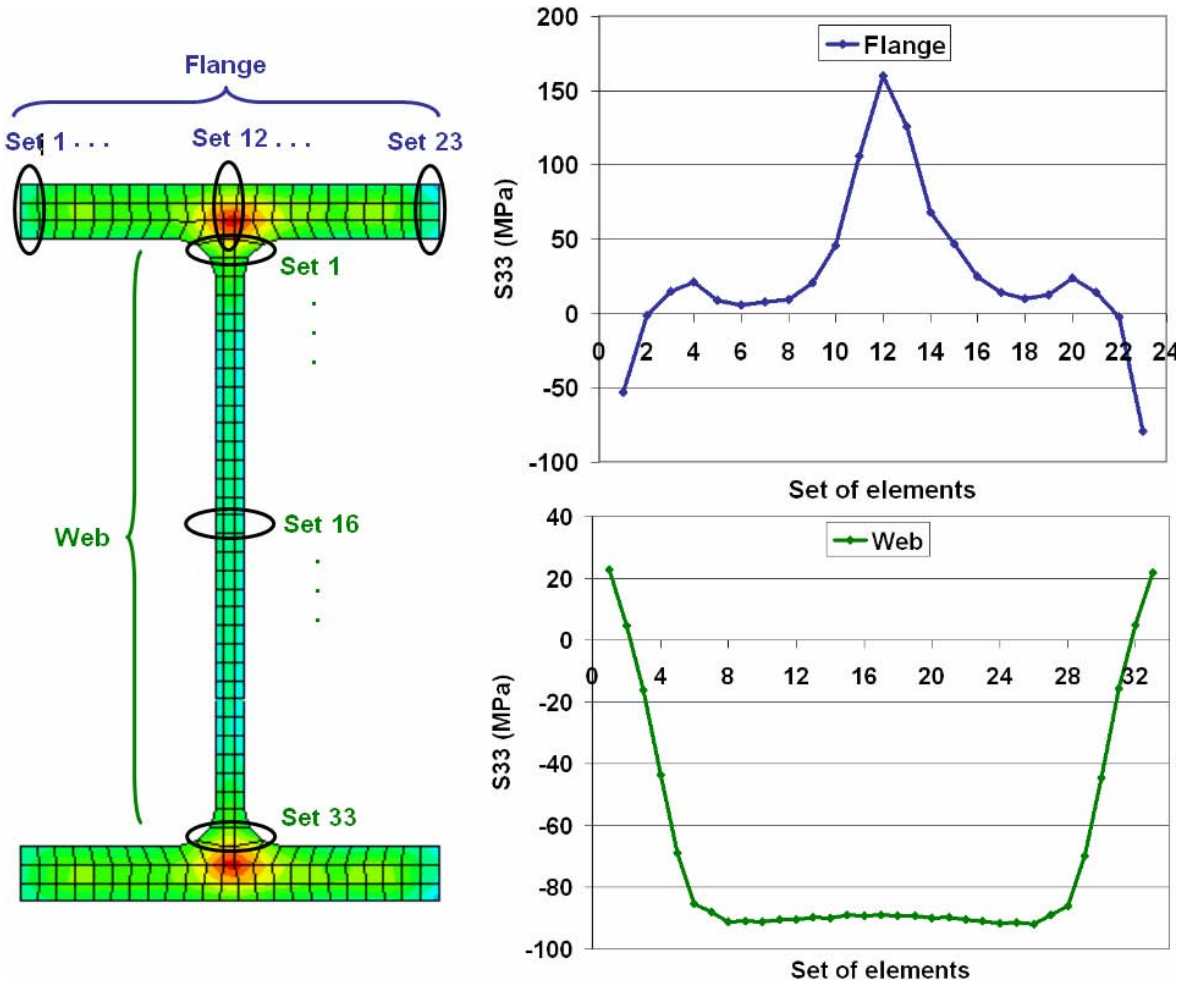


*Figure 54. Longitudinal residual stresses (S33) of the HEM500 beam after cooling process.*

## 3.1.3 COOLING PROCESS MODELING FOR THE GROOVED RAIL

### 3.1.3.1 DESCRIPTION OF THE PROBLEM

The cooling bed used to cool down the grooved rails was structurally similar to the previous cooling bed for the "H" profiles, but larger in extension, with dimensions 125 m length by 20 m width.

In general, the cooling process is also similar. The rails are set by the ingoing roller table in the cooling bed input, and through the walking beams they are transferred to the output as they cool down during the journey. Then, they are set on the outgoing roller table, which leads them to the straightener machines. The rails studied were cooled only by air until they reached the appropriate temperature for the straightening.

A picture of the cooling bed modelled is displayed in Figure 55.

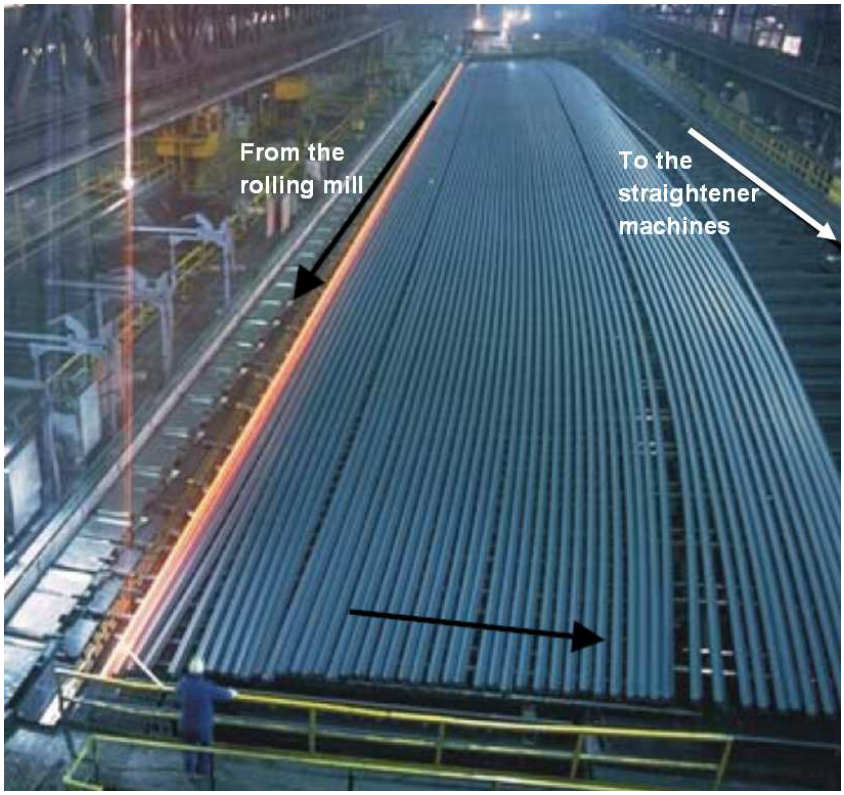


*Figure 55. Cooling bed studied for the rails. Picture courtesy of VA.*

The main difference between this cooling bed and the previous one was its location. The studied cooling bed was located indoors and, according to the layout, the air flows in one principal direction. Figure 56 shows a general description including the main wind

direction, named in the enterprise 'St. Peter-Leoben', according to the location of those cities.

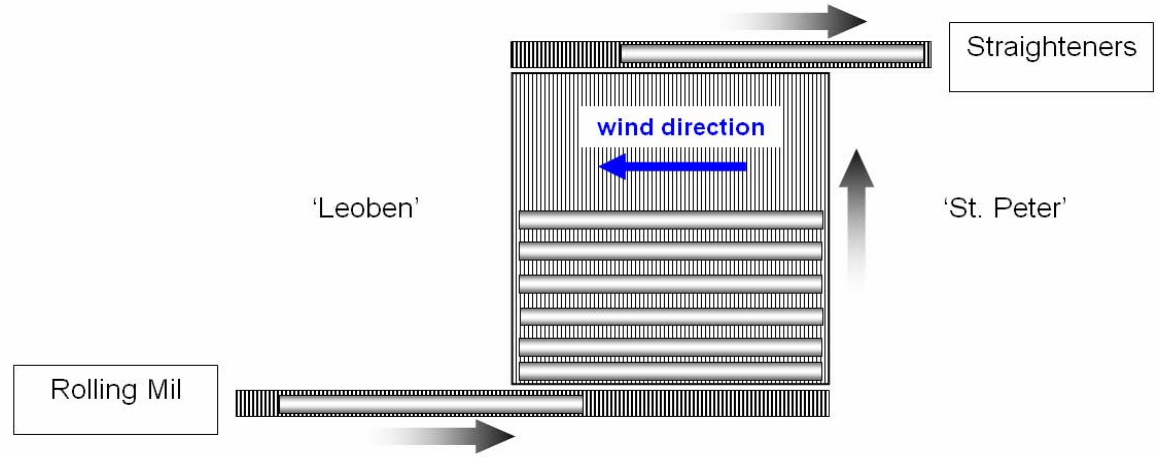


*Figure 56. General cooling bed configuration. Also in the figure, the principal wind direction: 'St.Peter-Leoben'.*

The air flow conditions were measured with rails on the cooling bed, and the average magnitude obtained was 1.5 m/s.

The rails input temperature was about 850 ºC and the correspondent output temperature was from about 20 to 50 ºC. In general, the rails were cooled for approximately three hours.

Two main positions of the rails on the cooling bed were considered: standing position and lie-down position. The rails are cooled down one after the other in their way to the straightening process.

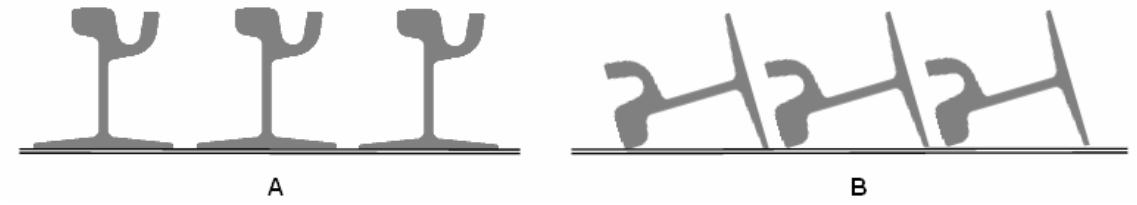


*Figure 57. Rails' configurations simulated. A. Standing position, B. Lie-down position.*

The lie-down configuration (B) is the one used normally at the enterprise. Nevertheless, the study of the residual stresses development in both configurations was considered interesting.

### 3.1.3.2 EXPERIMENTAL VALUES: RAIL'S SURFACE TEMPERATURE DURING COOLING ON THE COOLING BED; RESIDUAL STRESSES AFTER COOLING PROCESS

Experimental values to compare with the simulation of the models were measured by the enterprise (VA) in the development of the European project. VA kindly authorized the use of these experimental data also in this dissertation.

#### *EXPERIMENTAL TEMPERATURE VALUES DURING COOLING PROCESS*

The temperature histories during cooling process at some interesting surface points were measured using NiCrNi-thermocouples of diameter 1.5 mm. The thermocouples were located at 1.5 m from the rail's edge. Both configurations were measured.

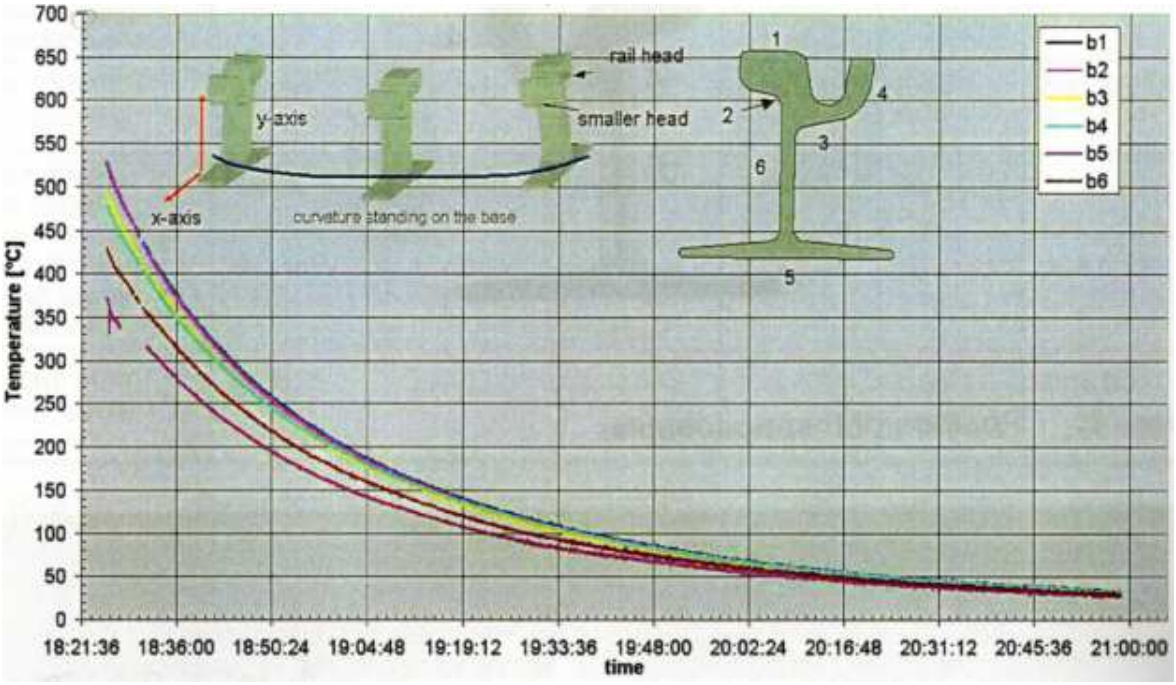


*Figure 58. Cooling history for rail Ri60, steel grade EN200 cooled in standing position.*
*Figure courtesy of VA.*

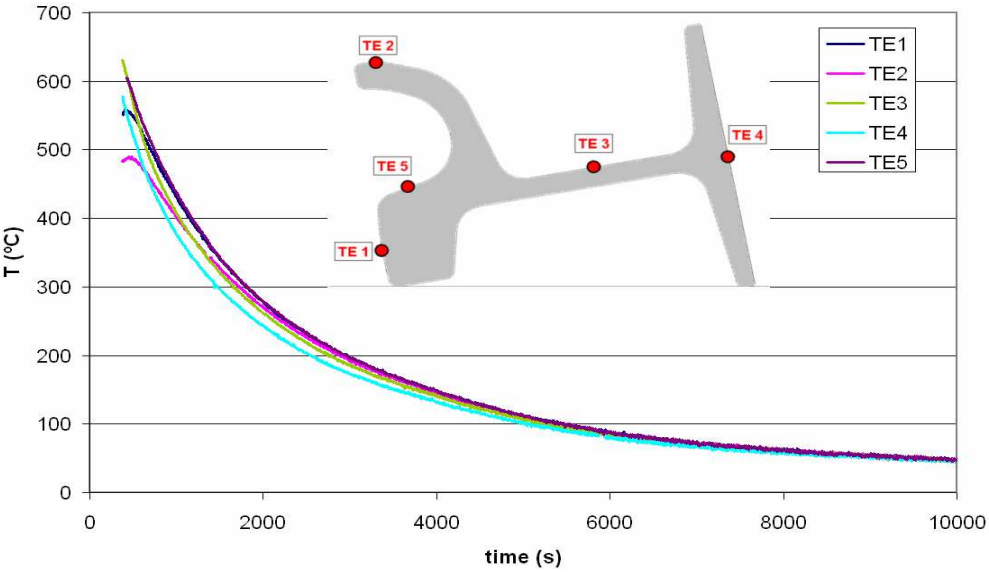


*Figure 59. Cooling history for rail Ri60, steel grade EN200 cooled in lie-down position. Figure courtesy of VA.*

## EXPERIMENTAL RESIDUAL STRESSES VALUES AFTER COOLING PROCESS

The residual stresses after cooling process for the rail cooled in standing position were measured using the sectioning method (following the procedural specified for rails in EN 13674-1). Pieces of 20mm thick were cut from 1m central rail section. The results are displayed in Figure 60.

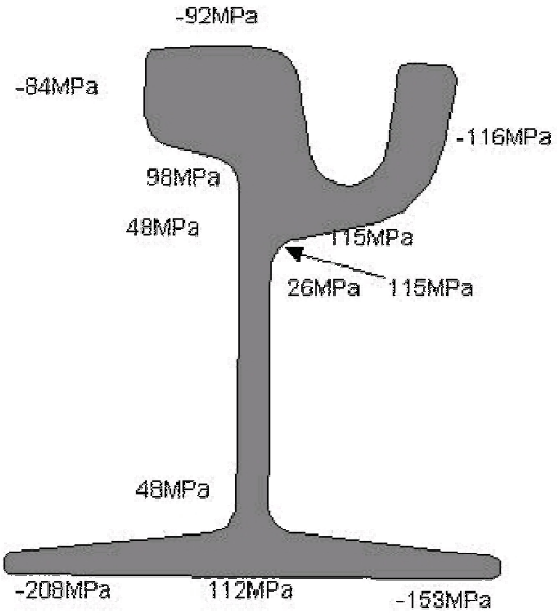


*Figure 60. Experimental residual stresses after cooling for rail Ri60, steel grade EN200, for standing position. Figure courtesy of VA.*

### 3.1.3.3 FE-THERMAL MODEL FOR THE GROVED RAIL'S COOLING PROCESS IN STANDING POSITION

As for the 'H' profile, the thermal model for the grooved rail's cooling process was designed using the powerful software FLUENT®. The model included the following characteristics:

a) The rail's cooling was simulated by means of the heat transfer, achieved by conduction inside the beam and convection and radiation to the air. The influence of heat transfer by conduction between the rails and the cooling bed's supports was considered not relevant in this study.

b) The model incorporates the influence of the surrounding rails on the cooling of the studied rail: heat from the rails located at both sides (Figure 61). To represent this fact the model included lateral symmetry planes.

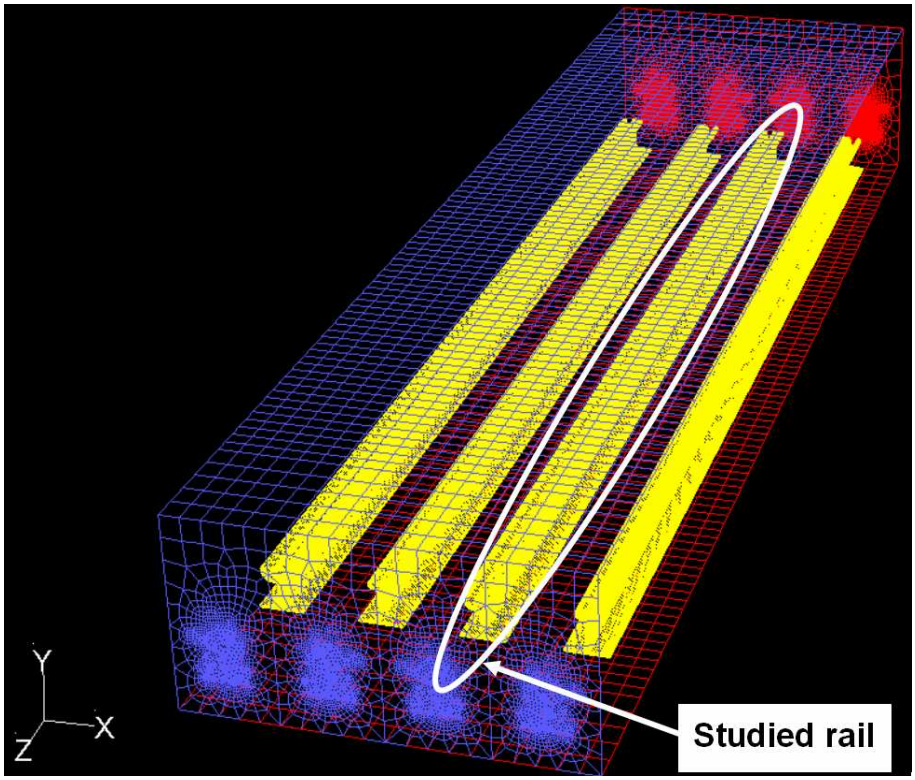


*Figure 61. Thermal model view activating the symmetry planes.*

c) The model included the boundary conditions related to the wind speed magnitude and direction: 1.5 m/s in 'St.Peter-Leoben' direction (Figure 62).

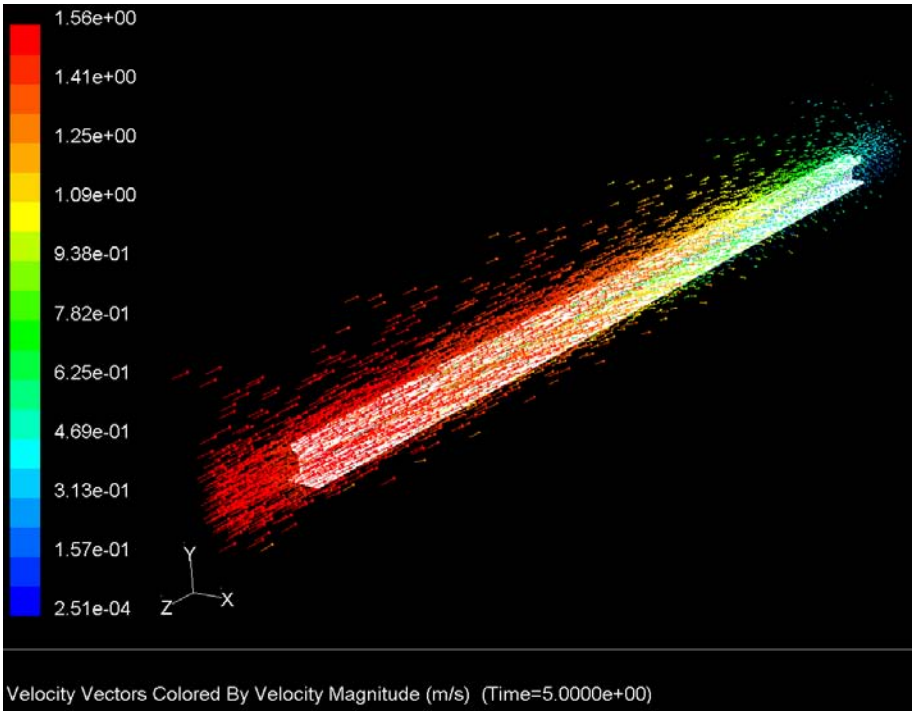


*Figure 62. Velocity Vectors (from west to east) in m/s, at time 2015 s.*

d) The Ri60 rail simulated was 5 m length (long enough to avoid the border effects and to make us able to perceive the rail's bending during the process). The meshing was based on 3D hexahedral elements. A plane view of the mesh is presented in Figure 63. The element length in the *Z* direction was 62.5 mm.

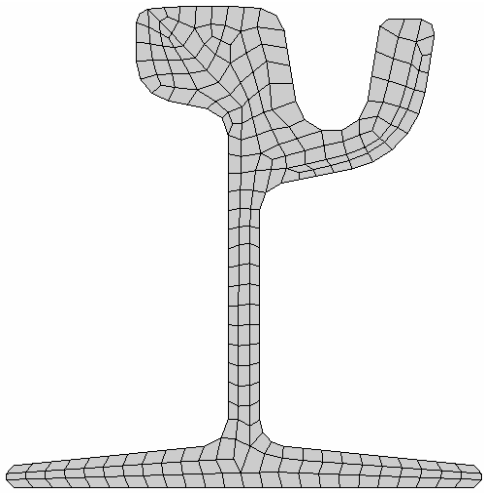

*Figure 63. Mesh of the Ri60 rail.*

e) The material thermal properties for the studied steel, the EN200, are presented in Table 4.

*Table 8. Thermal properties for steel S235.*

| ºC | *k* (W/mºC) | *c* (J/kg ºC) |
|---|---|---|
| 20 | 48.5 | 485 |
| 200 | 45.2 | 540 |
| 400 | 38.5 | 625 |
| 600 | 32.7 | 712 |
| 800 | 24.5 | 800 |
| 1000 | 16 | 950 |

This information was found in reference (Basu, et al., 2004) for a similar steel grade.

## RESULTS OF THE THERMAL MODEL SIMULATIONS

### COMPARISON OF EXPERIMENTAL AND SIMULATED VALUES DURING THE COOLING PROCESS

The temperature evolution of the rail's head surface can be seen in next figure.

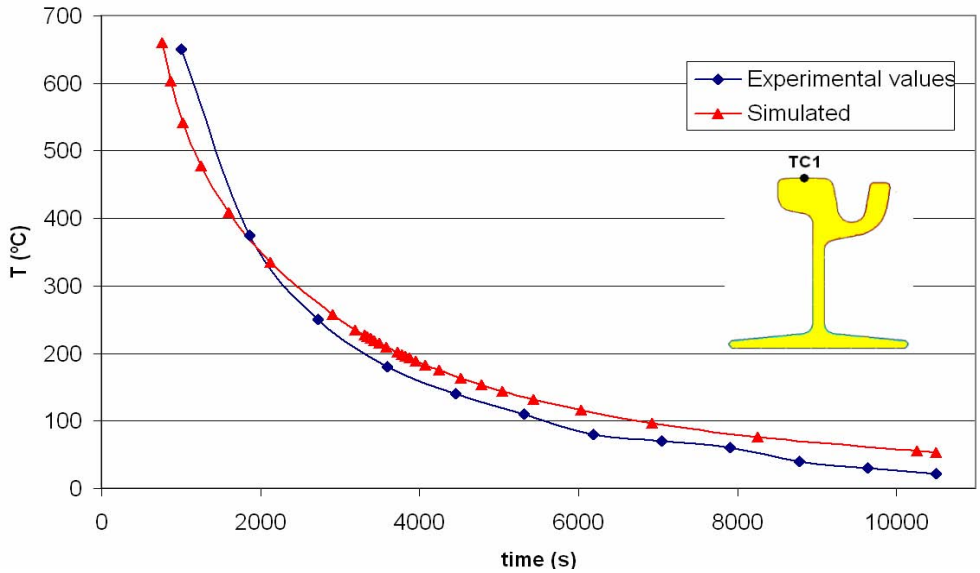


*Figure 64. Comparison of the temperature history for the head-surface: experimental and simulated values (standing position).*

The temperature evolution obtained by the FE model is very similar to the experimental one.

A general view of the surface temperatures at the end of the cooling is presented in next figure. The final time of the cooling process was around 3 hours. Axis X, Y and Z correspond to 1, 2 and 3 respectively in the rest of figures.

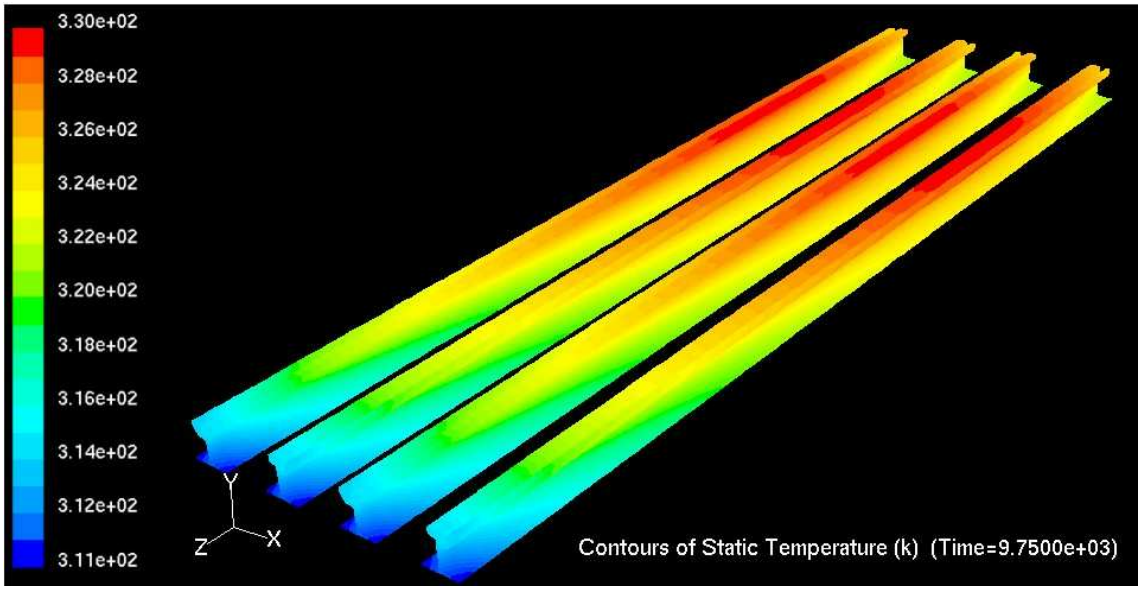


*Figure 65. Temperature contour plot of rails at ending time (9750s). The scale is Kelvin. It corresponds to a range from 38 to 57ºC in Celsius degree.*

We can see that the rails' cooling is not uniform, because of the wind in the principal direction. The front part ('St. Peter') cools down faster than the back part ('Leoben'). As a result, the effect of this unsymmetrical cooling on the residual stresses could be studied.

### 3.1.3.4 FE-STRESS/DISPLACEMENT MODEL OF THE RAIL'S COOLING PROCESS IN STANDING POSITION

Similar to the 'H' profile, the FE model for the stress/displacement analysis was developed using ABAQUS®. The model presented the characteristics listed bellow:

a) The model included the gravity forces: 9.81 m/s$^2$.

b) The rail laid on a plane table with friction. The friction value was set on 0.07, as an approximation for the support bars friction presented in the cooling bed.

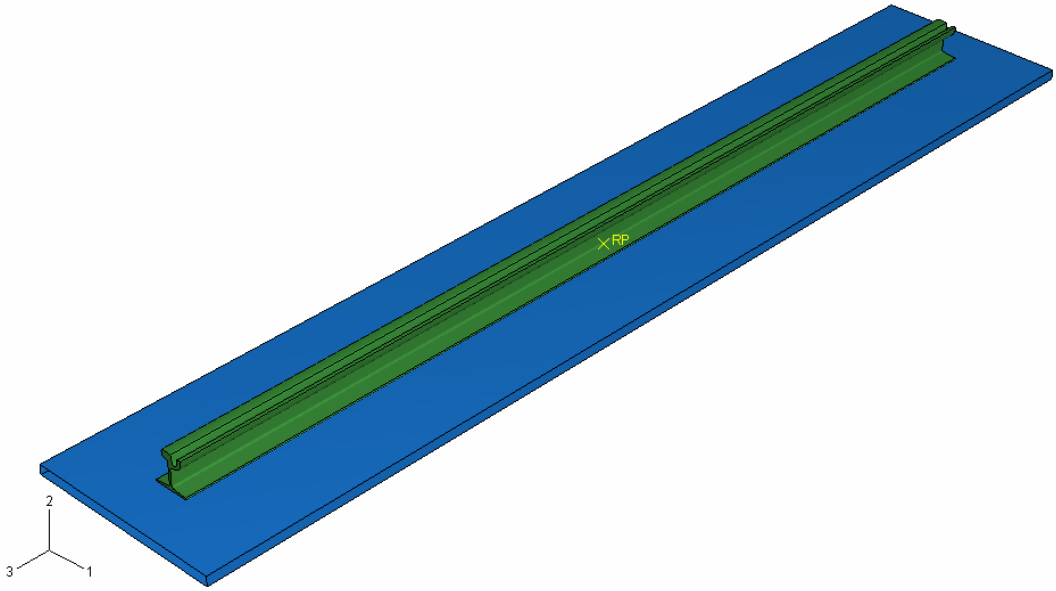


*Figure 66. FE-stress/displacement model created in ABAQUS® for the rail's cooling process.*

c) The mechanical properties for the rail's steel, the EN200, were also taken from (Basu et al., 2004). In this reference the elastic and plastic behaviour for similar steel was found.

*Table 9. Elastic behaviour and thermal expansion coefficient for steel EN200.*

| ºC | *E*(GPa) | *v* | *α*(e-5/ºC) |
|---|---|---|---|
| 20 | 212 | 0.28 | 1.08 |
| 200 | 180 | 0.28 | 1.15 |
| 400 | 155 | 0.28 | 1.31 |
| 600 | 140 | 0.28 | 1.40 |
| 800 | 130 | 0.28 | 1.49 |
| 1000 | 100 | 0.28 | 1.50 |

*Table 10. Yield stress vr. Plastic Strain for EN200 steel grade*

| | **Yield stress (GPa)** | | | | | |
|---|---|---|---|---|---|---|
| **Plastic Strain** | **20ºC** | **200ºC** | **400ºC** | **600ºC** | **800ºC** | **1000ºC** |
| 0 | 540 | 334 | 180 | 90.8 | 30 | 10 |
| 0.1 | 765 | 480 | 330 | 190 | 74 | 67 |

.

d) As before, the mesh of the profile for this FE model was exactly the same as for the FE-thermal model in order to facilitate the job of the conversion code (Section 3.2).

## RESULTS OF THE STRESS/DISPLACEMENT MODEL SIMULATION

### COMPARISON OF EXPERIMENTAL AND SIMULATED RESIDUAL STRESSES VALUES

The stress distribution of the residual stresses at the surface and inside the rail's cross section (at the rail's center) is displayed in the following figure.

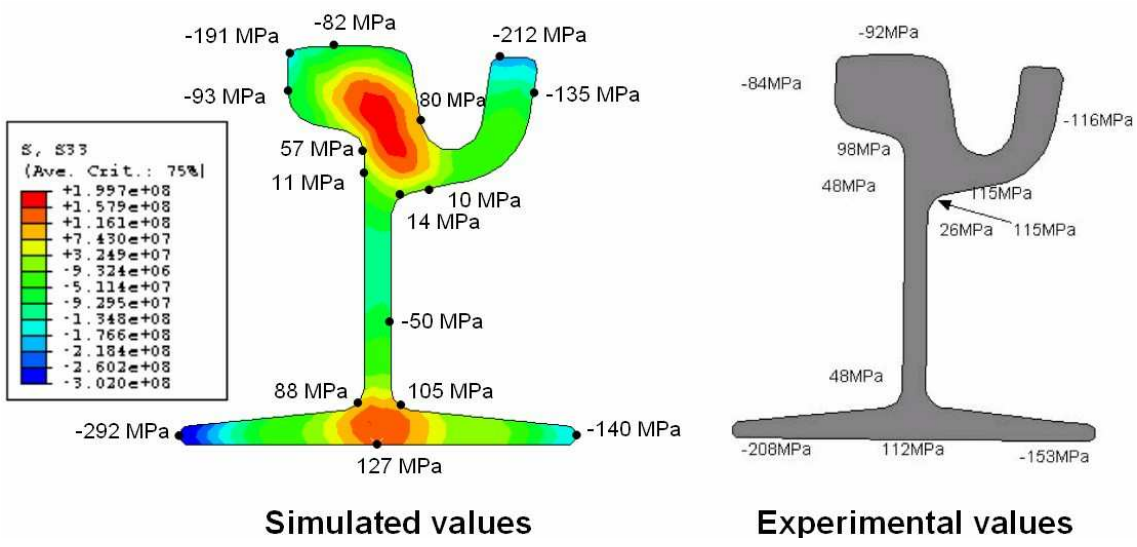


*Figure 67. S33 contour plot of rail's center from simulated and experimental tests.*

There was an agreement between the simulated and the experimental values in nature (compression-tension) and also in magnitude. Next figure presents the same result in another format for the ten points of the experimental tests.

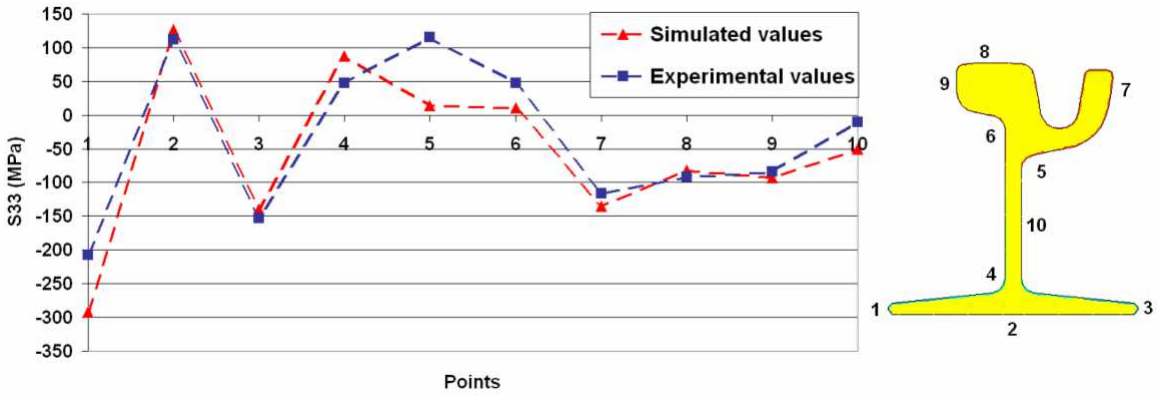


*Figure 68. Comparison of simulated and experimental S33 values for several interesting surface points.*

Point 5 presented the higher deviation. Nevertheless, this point, as well as point 4 and 6, is located in areas quite complicate to reach for the experimental measurement. Also, it is important to point out that the experimental-measurement-method's tolerance is about ±25MPa. Therefore, the differences between experimental and simulated values were acceptable.

It can be seen in Figure 67 that the biggest tensile residual-stresses were located in the rail's big-head center and in the rail's base-center. The biggest compression residual-stresses were located in the base-tip corresponding to the big-head side and also at the top of the small-head.

The evolution of S33 (in Pa), temperature (in ºC) and deformation during cooling is displayed in next figures. For a better understanding, the temperature contour plot was also included. The displacement in the YZ-plane (or 2-3 plane) can be seen at the top of the figures, and the displacement in the XZ-plane (or 1-3 plane) at the right side of the figures (the contour plot is referred to the longitudinal stresses: S33). On the left side, the temperature of the center cross-section is displayed. Beside it, at the right side, the longitudinal stress (S33) of the same cross-section is showed.

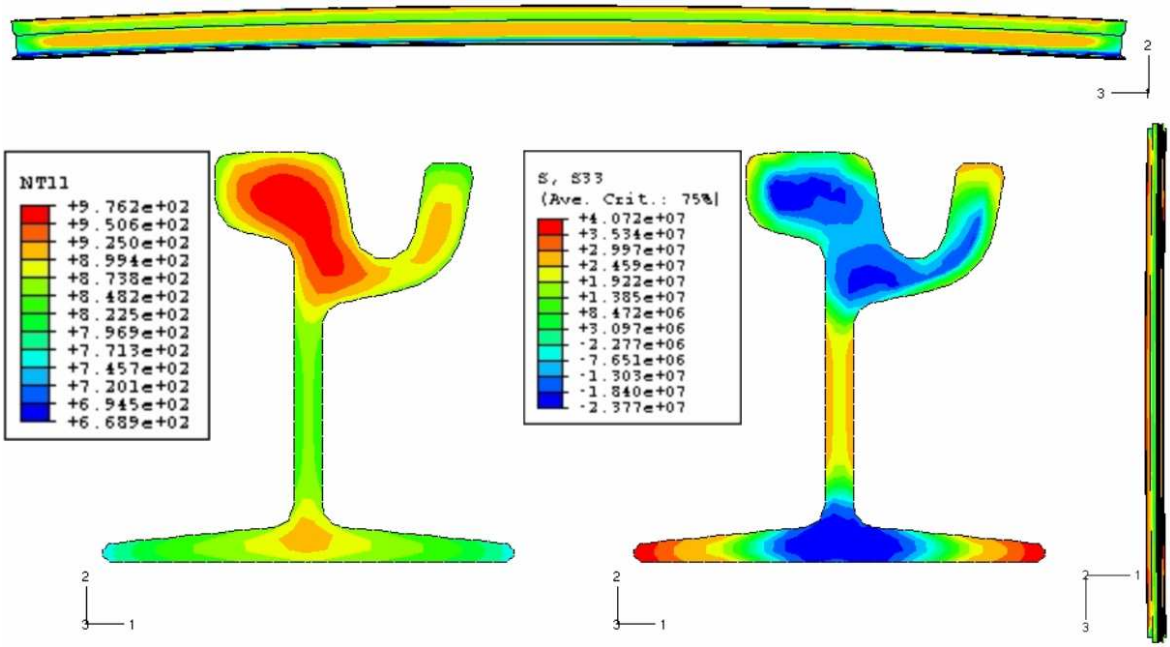


*Figure 69. Stress (S33 in Pa), displacement behavior (two plane views) and temperature (NT11 in ºC) at the beginning of the cooling process (time 32 s).*

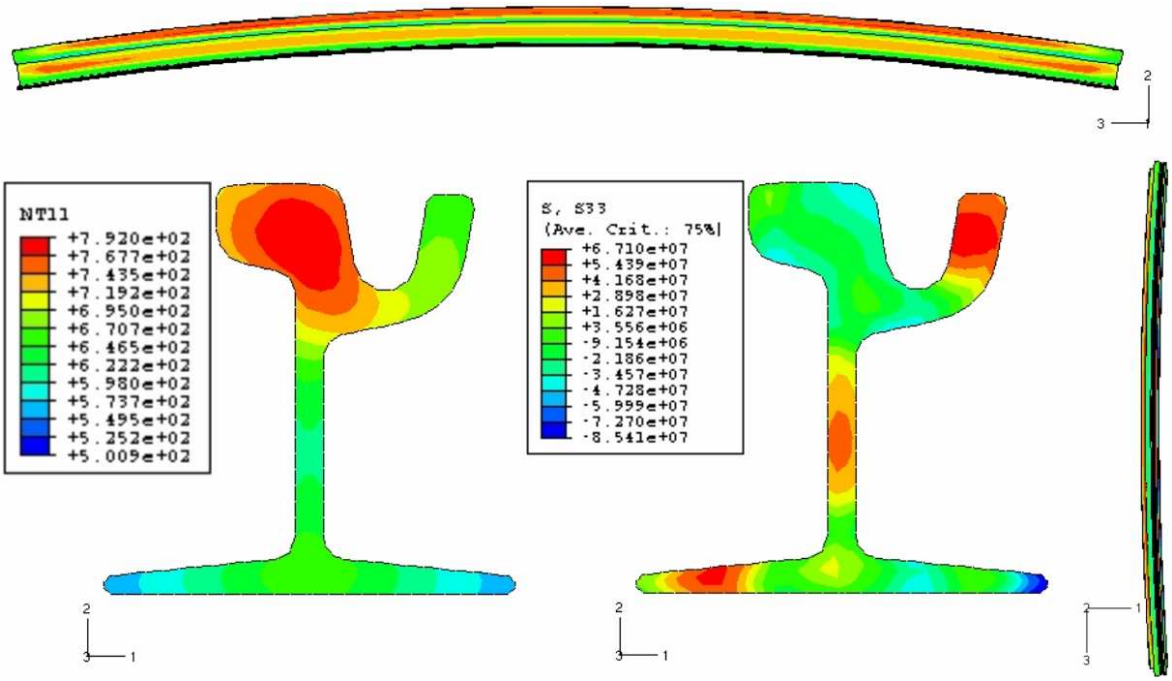


*Figure 70. Stress (S33 in Pa), displacement behavior (two plane views) and temperature (NT11 in ºC) at time 152 s.*

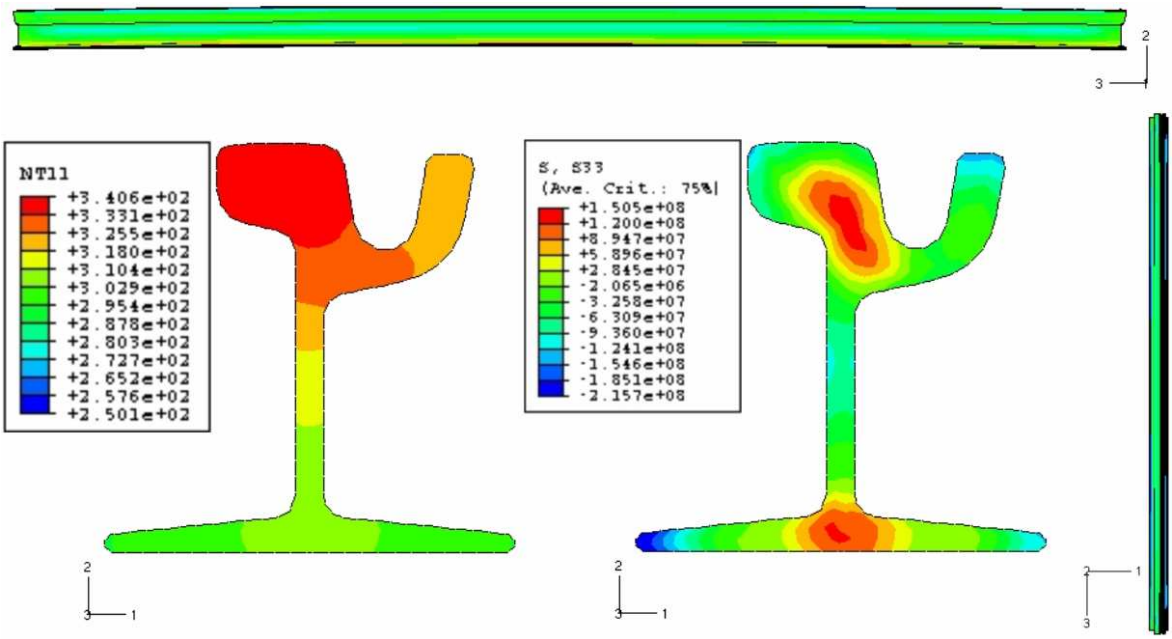


*Figure 71. Stress (S33 in Pa), displacement behavior (two plane views) and temperature (NT11 in ºC) at time 1623 s.*

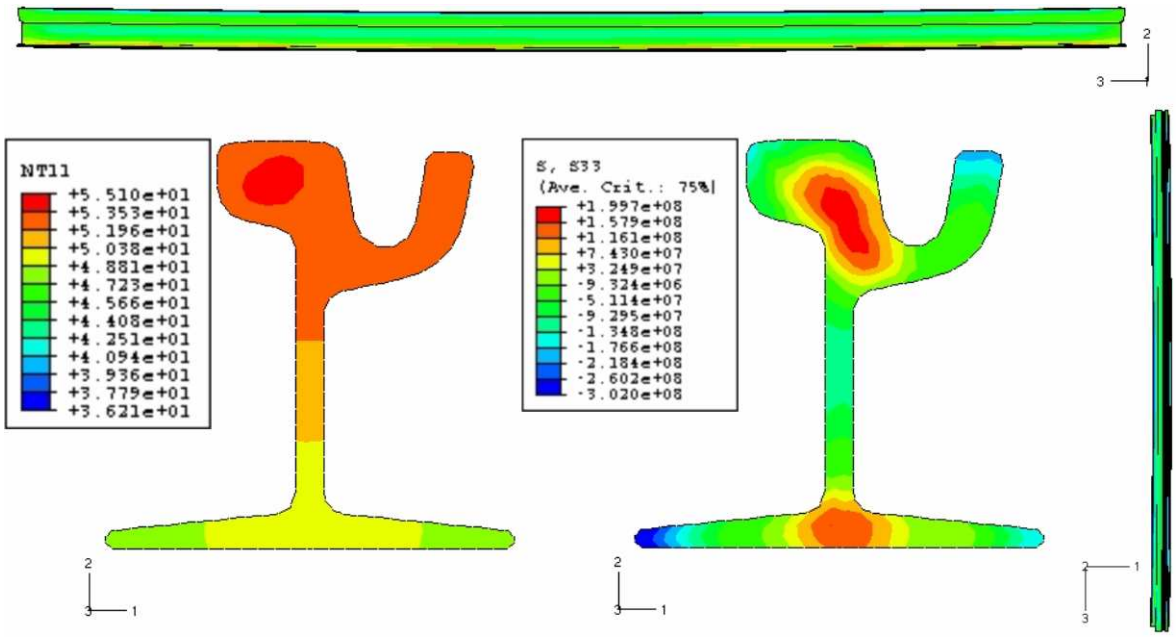


*Figure 72. Stress (S33 in Pa), displacement behavior ((two plane views)) and temperature (NT11 in ºC) at final time (10000 s).*

These figures show how the different parts of the rail changes the sign of their longitudinal stresses (compression/tension), along the cooling process. The reasoning is similar as the exposed for the 'H' profile:

a) At the beginning of the cooling process the rail's base-tips, web and small-head-tip (which were the parts that had larger external surface) cool down and shrink faster that the parts that had more material inside as the big-head. Therefore, these parts tended to pull the rail's base-center and big-head, and, as a reaction, they contracted (Figure 69). Once again, points where the stresses reached the yielding stress (which is low for high temperatures), suffered plastic deformation.

b) At the final phase of the cooling process (Figure 71 y Figure 72), the base and web reached a more uniform temperature and was the big-head and base-center that started to cool down with a higher rate. This caused the opposite reaction than before: pressure stresses in the web, base-tips and small-head-tip, and tensile stresses in the big-head and base-center.

c) About the bending, it can be said that as the base and the small-head were the parts of the rail that cooled down faster at the beginning of the cooling, the rail bended around these parts (around the base and around the small-head), as displayed in Figure 70. Later on, these parts reached a more uniform temperature and was the big-head that starts to cools down in a faster way causing the bending around it. This was the final bending observed in VA's cooling bed (Figure 72).

d) In this case, because of the asymmetry of the profile, the residual stresses had a non symmetric distribution in the base.

The rail's bending along the time in the two main bending planes, XZ-plane and YZ-plane, are displayed in Figure 73 and Figure 74 respectively.

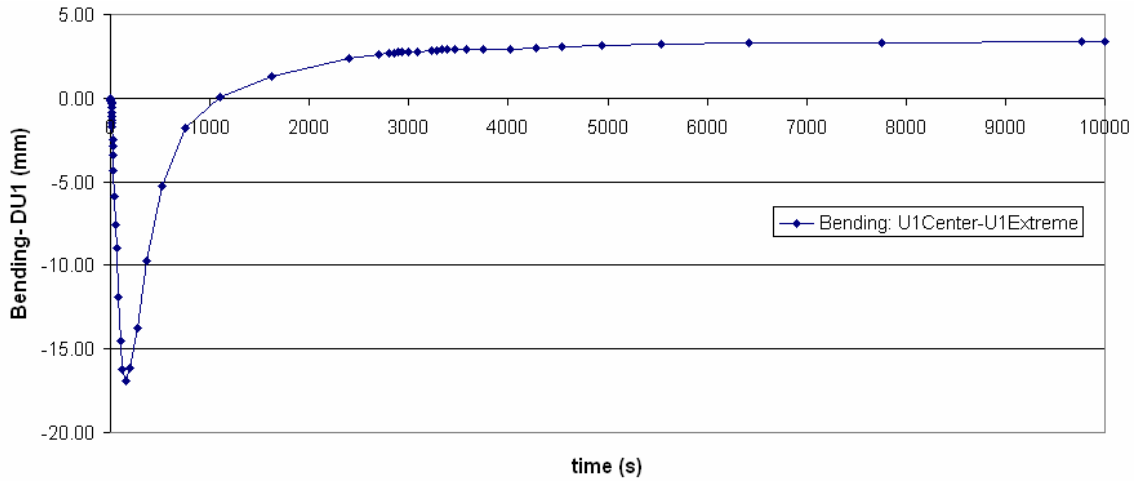


*Figure 73. Rail's bending history for standing position, referred to the XZ-plane.*

Once again, it can be seen how, at the beginning of the process, the bending developed around the small-head, but as the rail cooled down, the bending changed sing and remained around the big-head.

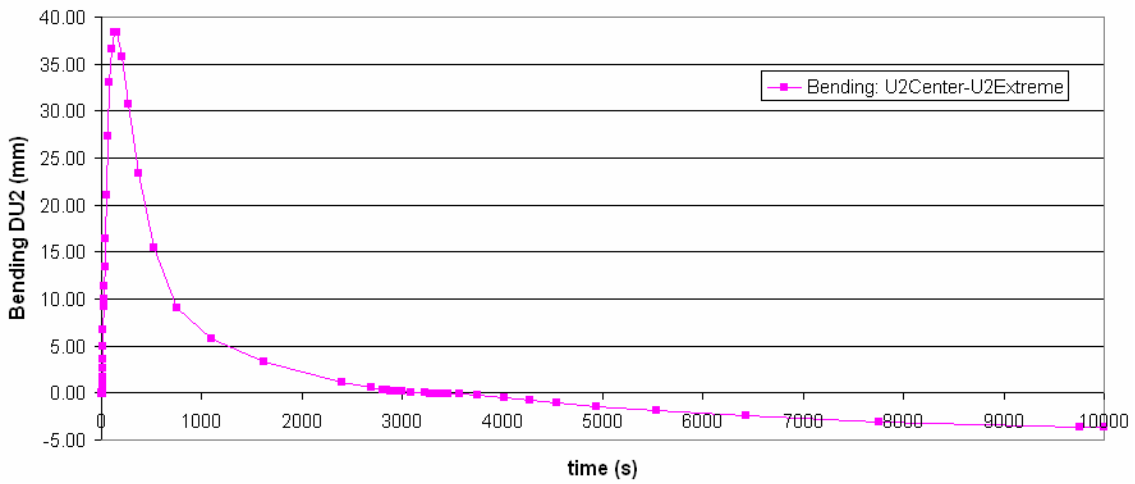


*Figure 74. Rail's bending history for standing position, referred to the YZ-plane.*

In this figure (Figure 74) one can observe that, at the beginning of the cooling process, the rail bended around the base and then it changed sing and remained around the rail's heads, as observed in the reality.

To conclude, we can say that the cooling rate, residual stresses (S33) and bending trend closely follow experimental observations and values.

### 3.1.3.5 FE-THERMAL AND STRESS/DISPLACEMENT MODEL OF THE RAIL'S COOLING PROCESS IN LIE-DOWN POSITION

The rail-by-rail in lie-down position is the configuration usually applied in VA's cooling bed. Therefore it was consider interesting the simulation of this configuration and the comparison with the results from the models for the standing position.

Basically, the models were conceptually the same. The only difference was the position of the rails, as in this case the lie-down configuration was adopted.

#### *RESULTS OF THE THERMAL MODEL SIMULATION*

The rail head-surface history obtained from the FE thermal model and the obtained experimentally are presented in next figure.

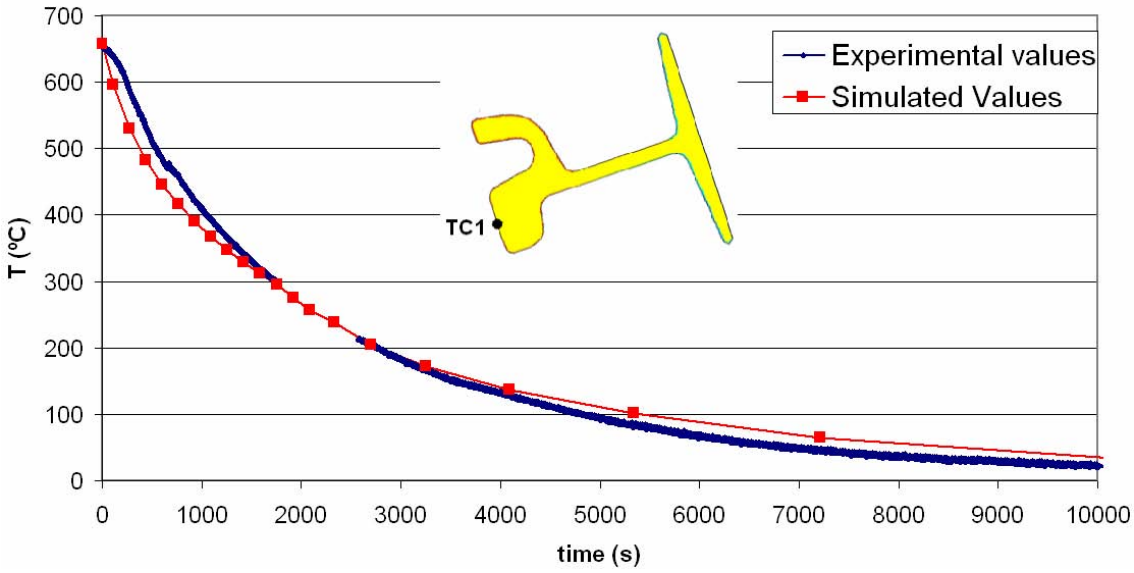


*Figure 75. Comparison of temperature history for the head-surface: experimental and simulated values (lie down position).*

Both temperature evolutions were very similar. Therefore, the thermal model simulated the cooling with a proper cooling rate.

## RESULTS OF THE STRESS/DISPLACEMENT MODEL SIMULATION

The distribution of the residual stresses at the surface and inside the rail's cross section (at the rail's center) is displayed in the following figure.

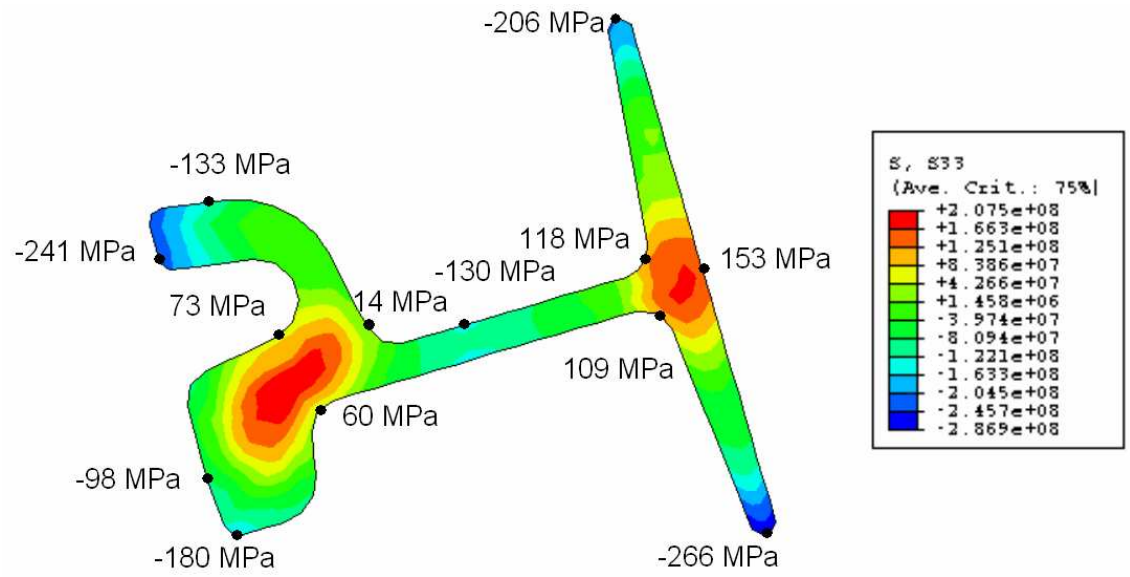


*Figure 76. Longitudinal residual stresses (S33) for lie down position.*

The contour plot is very similar to the one obtained with the rail cooled in standing position.

In a further section we compare the residual stresses obtained in both configurations: standing and lie-down in a more extensive way.

The evolution of S33 (in Pa), temperature (in ºC) and deformation behavior in YZ-plane and XZ-plane, during cooling is displayed in following figures.

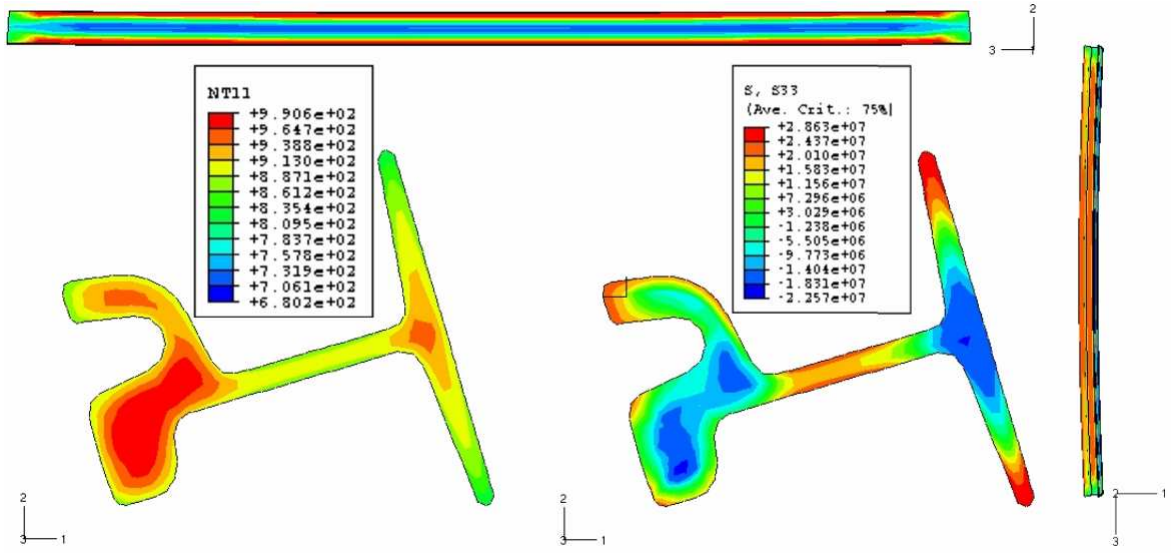


*Figure 77. Stress (S33 in Pa), displacement behavior and temperature (NT11 in ºC) at the beginning of the cooling process (time = 20 s).*

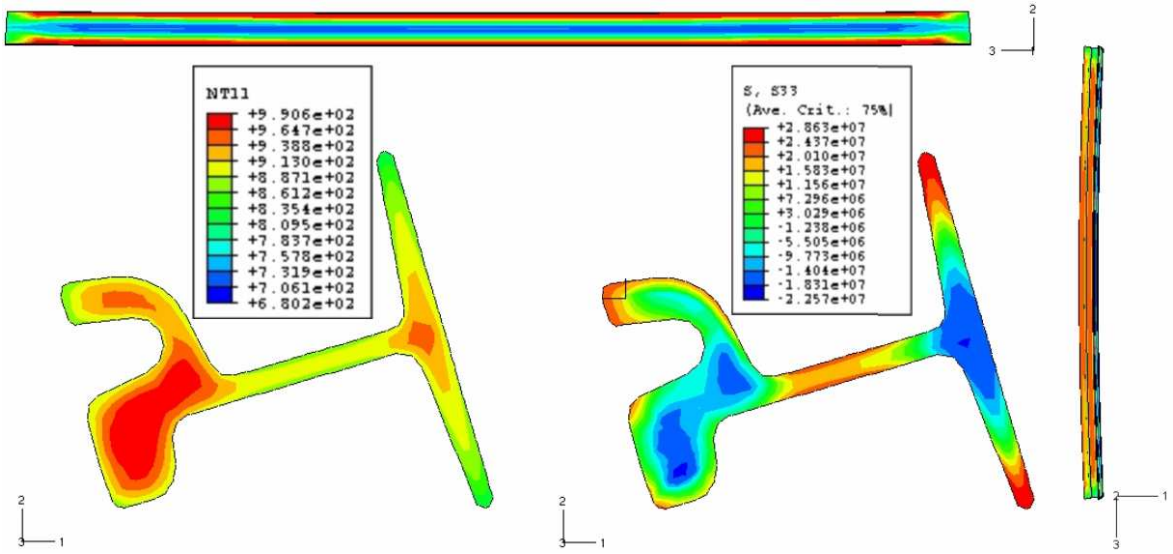


*Figure 78. Stress (S33 in Pa), displacement behavior and temperature (NT11 in ºC) at time 182 s.*

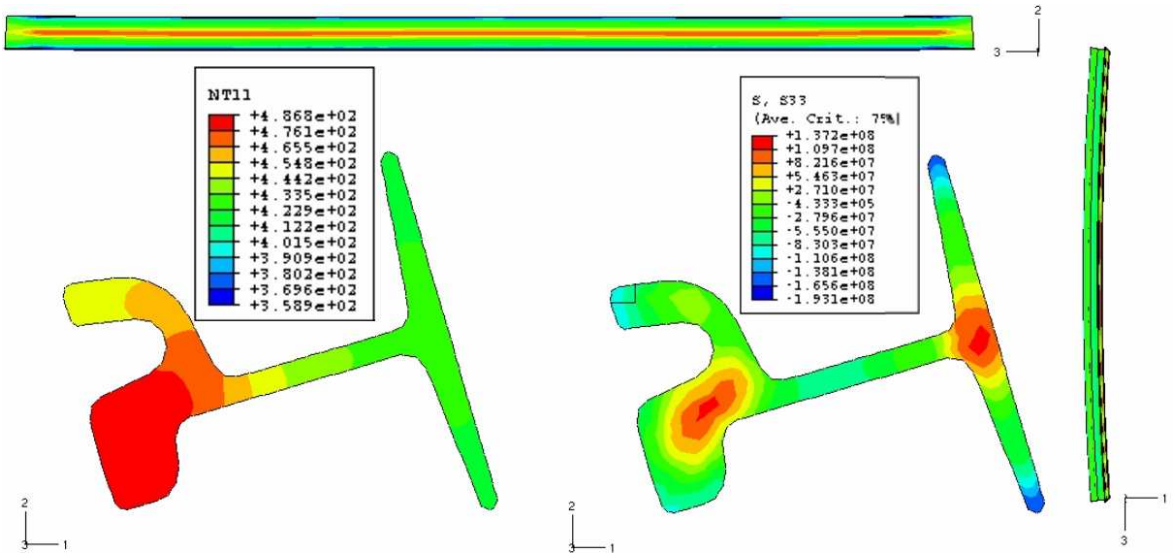


*Figure 79. Stress (S33 in Pa), displacement behavior and temperature (NT11 in ºC) at time 694 s.*

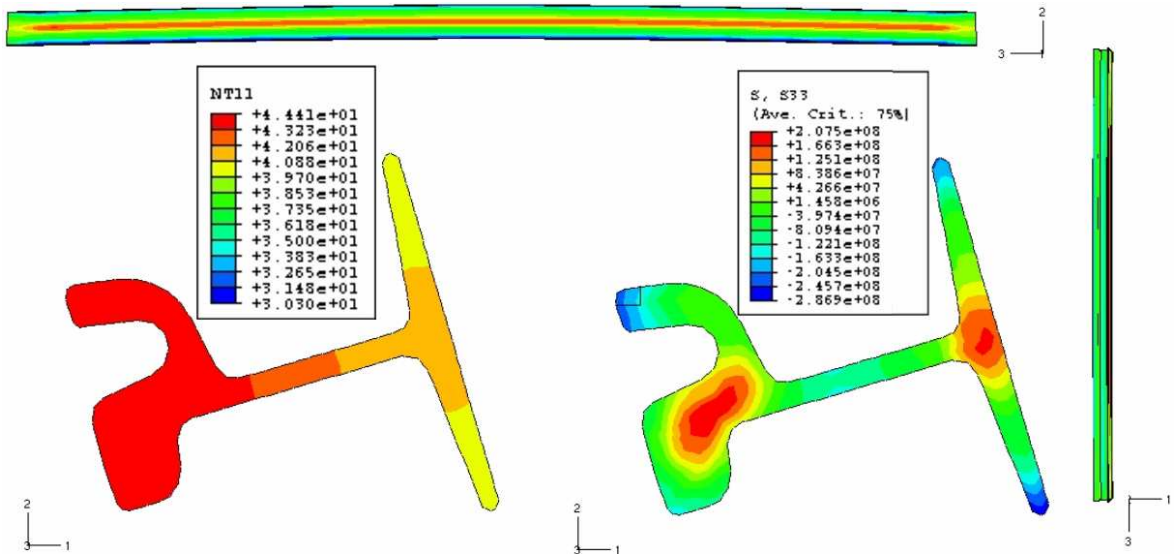


*Figure 80. Stress (S33 in Pa), displacement behavior and temperature (NT11 in ºC) at final time (12000 s).*

The causes of these stresses evolution and displacement behaviors were the same as the one exposed in the previous section.

The rail's bending along the time in the two main bending planes (XZ-plane and YZ-plane) are displayed in next figures.

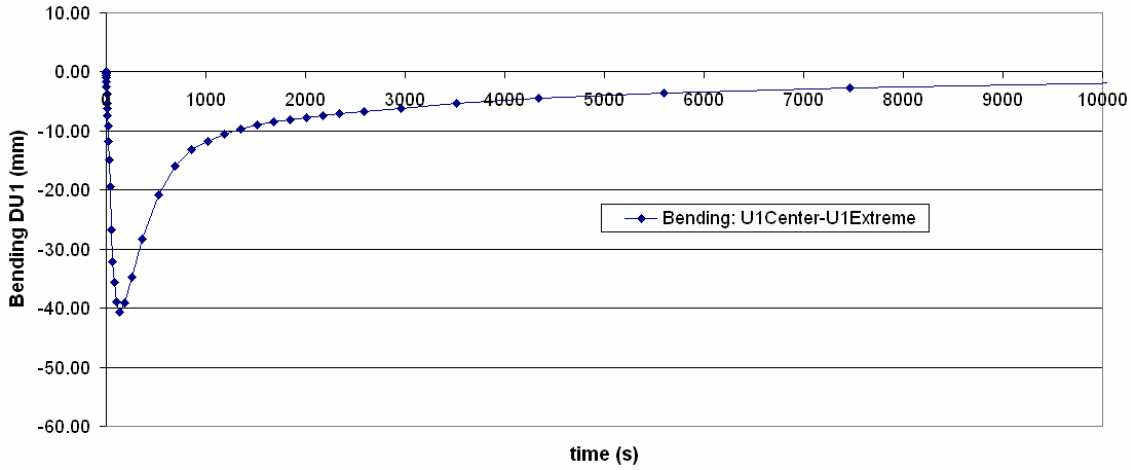


*Figure 81. Rail's bending history for lie-down position, referred to the XZ-plane.*

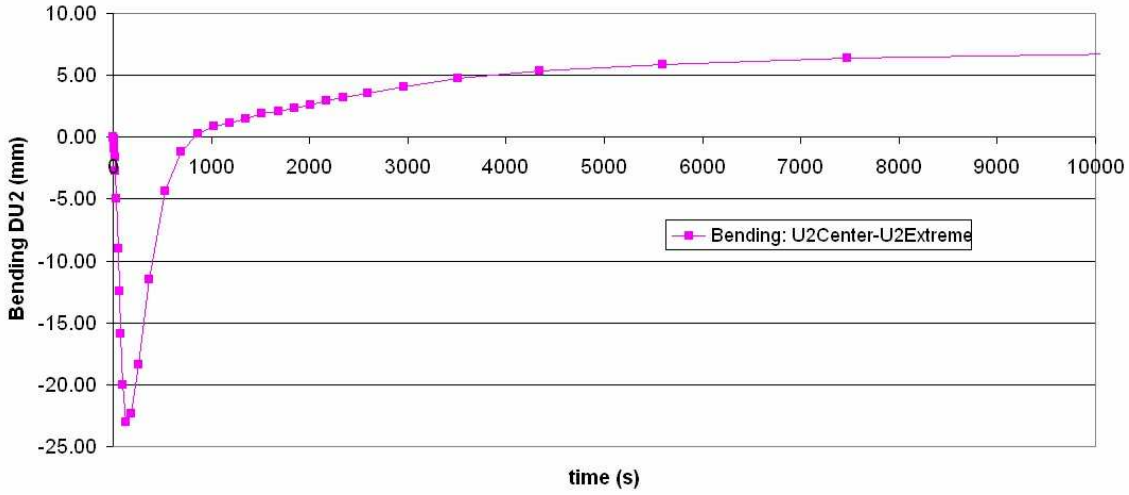


*Figure 82. Rail's bending history for lie-down position, referred to the YZ-plane.*

Once again, the bending sings and magnitudes were very similar to the one observed in the real process.

### 3.1.3.6 COMPARISON OF RESIDUAL STRESSES VALUES FOR THE RAIL'S COOLING IN STANDING POSITION AND IN LIE DOWN POSITION

We present in this section a comparative of the longitudinal residual stresses generated during cooling when the rails were situated in standing and lie-down position.

Figure 83 represents the longitudinal residual stresses of the center cross section of rails in standing and lie-down positions. We have also added the experimental results for standing position, just to have an experimental reference.

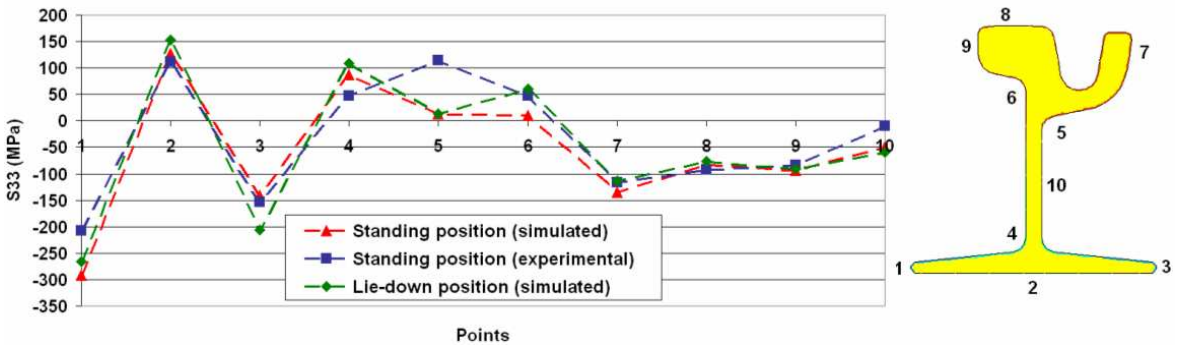


*Figure 83. Comparison of simulated and experimental S33 values for several interesting surface points for both positions. (A) Standing and (B) Lie down position.*

In general terms, at these surface points, there were not big differences between cooling the rail in any of the two positions.

Nevertheless, along the rail length there were appreciable differences. Next figure shows this fact.

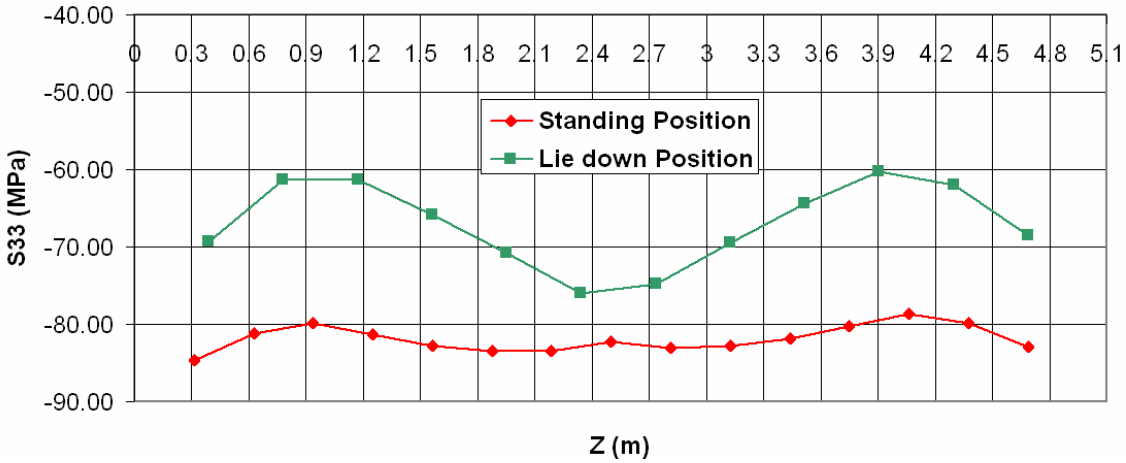


*Figure 84. Residual stresses (S33) at the rail's big-head-surface (point 8), along the rail length.*

There are two main differences in this figure between both curves: the shapes and the magnitudes. The residual stresses in the big-head-surface along the rail was more constant when the rail cools down in standing position. The reason could be that the bending affecting this point (bending around the big-head) is more significant in lie-down position than in the standing position, mainly because in this last position the gravity forces act against the bending. The magnitudes in standing position were higher than in the lie down position (with a maximum difference between both positions of 18.5MPa). This could be caused by the slower cooling (smaller cooling rate along the cooling process) in lie-down

position than in standing position. In lie-down position the rail beside the studied rail radiate its heat directly on this point (point 8), different situation than in standing position where this point is free to radiate its heat to the ambient.

However, using FE model simulations one can also observe the differences between the inner parts of the rails in both positions. In next figures we present the residual stresses of the rail's big-head-center and base-center, which were the points with maximum S33.

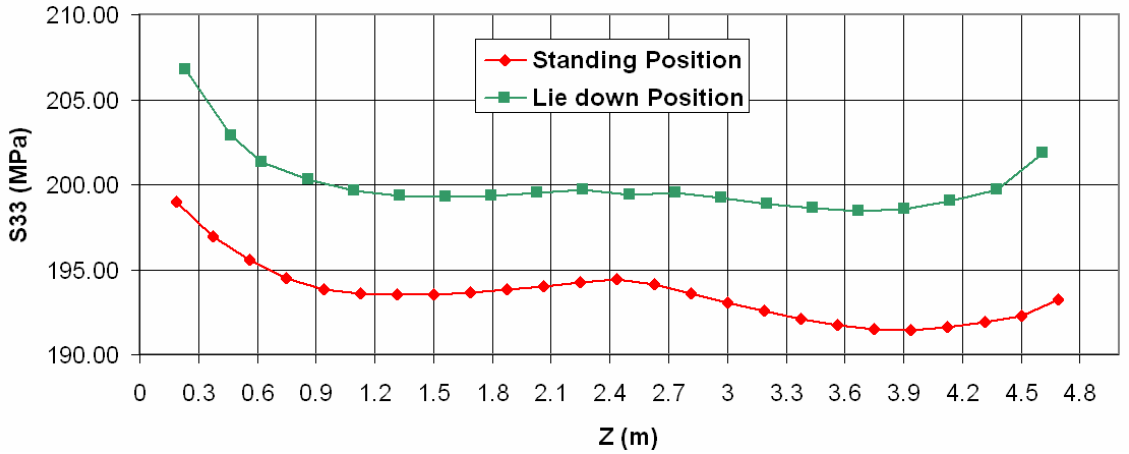


*Figure 85. Residual stresses (S33) at the rail's big-head-center, along the rail length.*

At this point, the maximum difference was 8.6 MPa, which is not quite significant. More important, in this figure we can appreciate the effect of the unsymmetrical cooling caused by the wind. In the figure the wind is coming from the 0m extreme to 5m extreme. We can see that the front part of the rail (0 m extreme) cooled down faster than the back part and as a consequence it developed higher residual stresses. In this case, with this 5m rail, the difference between the front and back extremes was not so significant (5.72 MPa), but it evidences the effect of the wind (or its consequence: the unsymmetrical cooling).

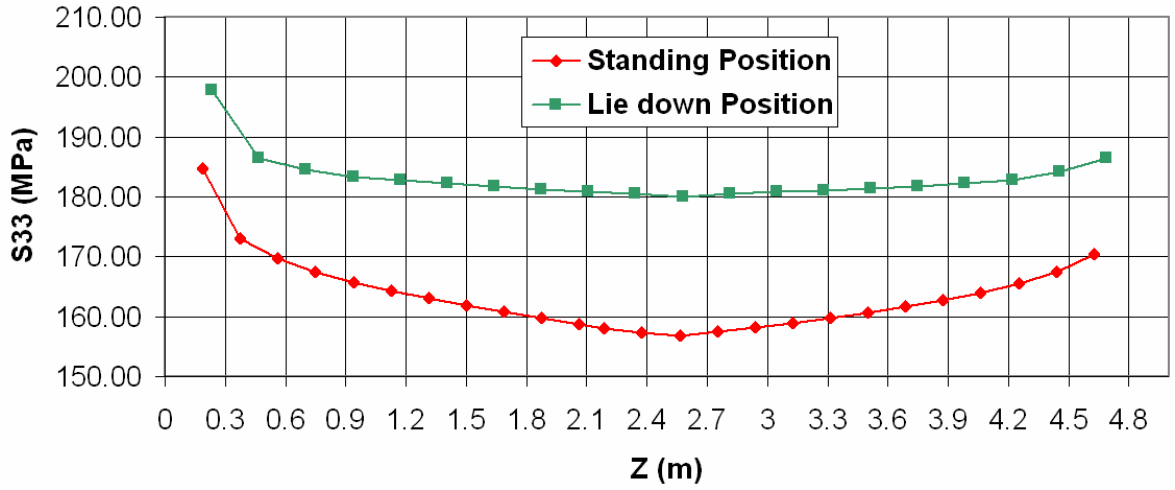


*Figure 86. Residual stresses (S33) at the rail's base-center, along the rail length.*

Once more we can appreciate the higher value of the residual stresses on the front part of the rail that cooled down faster than the back part. In this case there were higher differences in the residual stresses between of both positions. The maximum difference at the base-center happens in the rail's center and was of 24MPa. This is again caused by the cooling rate differences of the base-center during the cooling in both positions: the base-center cools down slower in standing position than in lie-down positions, where the base of the rail is freer to radiate its heat to the ambient.

As a result, some differences were evident in the longitudinal residual stresses by cooling the rail in standing position or in lie-down position. It seems that the tendency is that the cooling in lie-down position develops higher residual stresses, but to arrive to a solid conclusion, a more exhaustive study is necessary.

## 3.2 CONVERSION CODE TO COMMUNICATE FLUENT® RESULTS TO ABAQUS®

As said previously, in the sequentially coupled thermal-stress analysis adopted, there was a need to create a conversion code to communicate the temperature results from the FE-thermal model, formulated in FLUENT® (v6.0), to the FE-stress/displacement model, created in ABAQUS® (v6.4 or v6.5), in order to analyze the stresses and deformations produced by the temperature changes.

### *GENERAL DESCRIPTION*

The program, named *conv_flu_abq.sh*, was developed using freeware:

- Linux shell programming (by means of awk scripts),
- R® (GNU software),
- C programming (by means of gcc, also GNU software).

Using these tools, the conversion code presented time and memory efficient execution.

A general description of the sequentially coupled thermal-stress analysis, including the conversion code, is presented in the Figure 87.

To simplify the communication, the profile's mesh analyzed in FLUENT® and in ABAQUS® was the same (i.e. the nodes location were identical for both analysis). This was possible by creating a unique mesh using I-deas® (v9.2m), and exporting it to FLUENT® format as well as to ABAQUS® format.

ABAQUS® is able to carry out a sequentially coupled thermal-stress analysis but by using its own thermal results files ('.inp', '.prt', and '.fil' files) (ABAQUS, 2005). Therefore, to develop the conversion code, the general idea was to modify the thermal results file ('.fil') provided by a "fake" thermal simulation in ABAQUS®.

The modifications were not too obvious because of the special arrangement of the '.fil' file, which is the file that contains the node temperatures and times. (We worked with the ASCII version of the '.fil' file, the '.fin' file. The original '.fil' file was written in binary format).

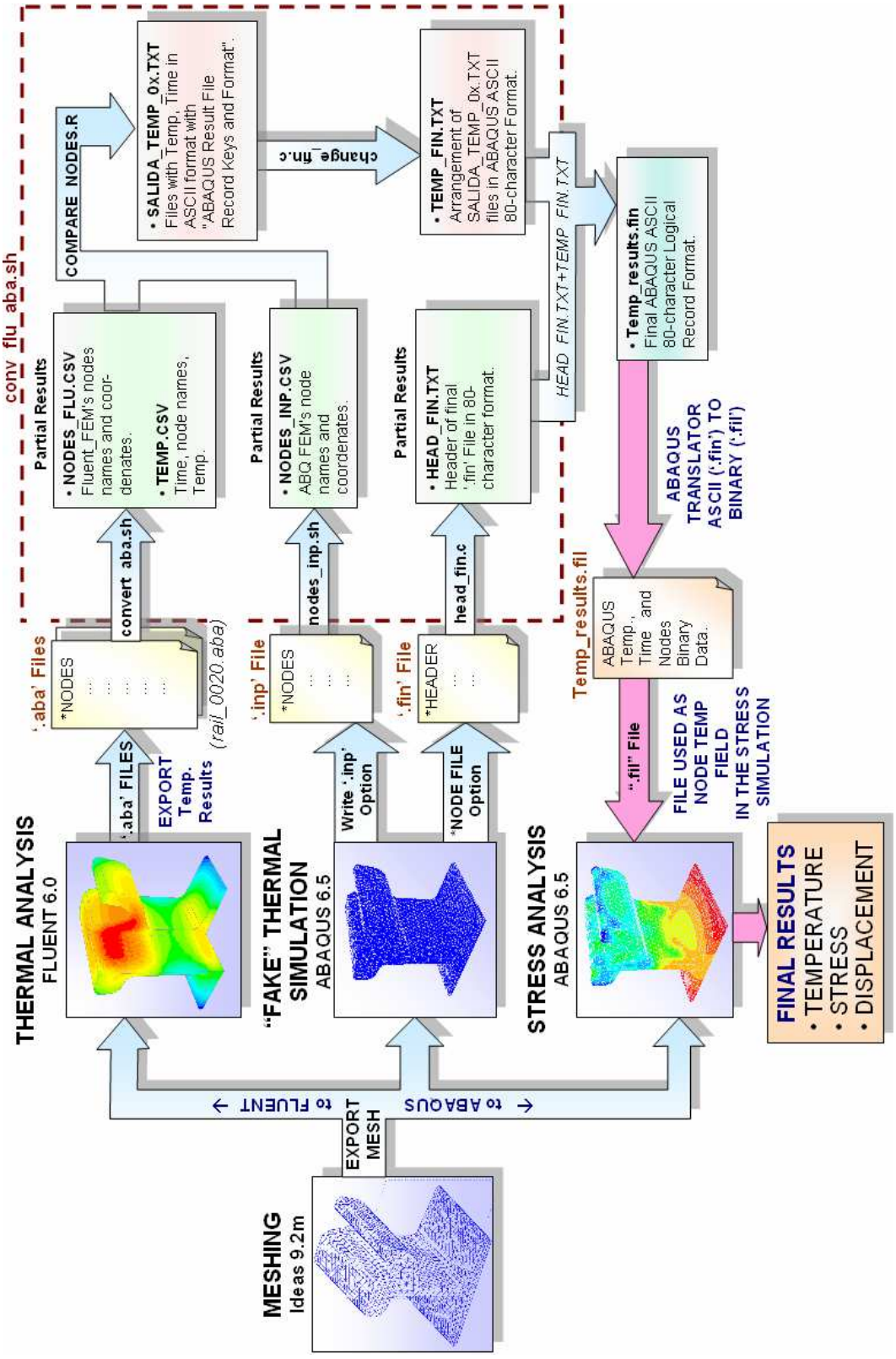


*Figure 87. General description of the sequentially coupled thermal-stress analysis using the conversion code: conv_flu_abq.sh.*

For memory storage efficiency, ABAQUS® write its results in a 80-character logical records, in the order described in the record definitions presented in the ABAQUS User's Manual (see reference ABAQUS, 2005). For example, the line bellow represents a record for the temperature of the node number 2:

```
*I 14I 3201I 12D 8.019542800000005D+01
```

The beginning of each "record" is indicated by an asterisk (*). The first part "*I 14", indicates that this is a record of "4" words. The second part "I 3201" indicates the record key "201" which represents: node temperature. The third part "I 12" indicates the node number: "2". And the last part "D 8.019542800000005D+01" indicates the temperature of that node as a floating point number (represented by the "D"). Each 80-character logical record is completely filled before the next one is started, so that any data item can be split. Hence, a general view of the '.fin' would be:

```
11D 8.105193500000001D+01*I 14I 3201I 12D 8.019542800000005D+01*I 14I 3201I 13D
8.817138100000000D+01*I 14I 3201I 14D 8.028179300 000005D+01*I 14I 3201I 15D 8.81
6335400000003D+01*I 14I 3201I 16D 8.040282600000000D+01*I 14I 3201I 17D 8.814409
```

After modify the '.fin' file with the valid profile's temperatures obtained by FLUENT®, it was possible to perform the stress/displacement analysis in ABAQUS®, using this final '.fin' file as a prescribed temperature field.

## CONVERSION CODE

The conversion code, *conv_flu_abq.sh*, was composed by several subprograms. The list of the subprograms and a general description of their functions are presented bellow.

1. convert_abq.sh: takes the '.abq' files, exported from FLUENT's FE-thermal model, obtains its node's names and coordinates and store these values in "NODES_FLU.CSV". It also obtains the temperature history (temperature and its times) for each node and stores it in "TEMP.CSV". From this program the rest of the subprograms were required.

2. nodes_inp.sh: takes the ABAQUS's problem-definition-file, '.inp' file, produced by the "fake" ABAQUS thermal analysis, obtains the node's names and coordinates and store these values in "NODES_INP.CSV".

3. head_fin.c: takes the ABAQUS's thermal-result-file, '.fin' file, produced by the "fake" ABAQUS's thermal analysis, obtains the header of this file and stores it in "HEAD_FIN.TXT".

4. COMPARE_NODES.R: takes "NODES_FLU.CSV" and "NODES_INP.CSV" and generates "SALIDA_TEMP_0x.TXT" files with the data of times (represented in the file's name by "0x"), nodes and temperatures, in the ABAQUS's 80-character logical records format.

5. change_fin.c: arrange the contents of each "SALIDA_TEMP_0x.TXT" files, in a unique file "TEMP_FIN.TXT".

6. And finally, the same COMPARE_NODES.R code, adds "HEAD_FIN.TXT" and "TEMP_FIN.TXT", to obtain the final and valid '.fin' file: "Temp_results.fin".

With this conversion code was possible to introduce the temperature history of each node obtained through the FLUENT® FE-thermal model to the FE-stress/displacement model developed in ABAQUS® in a simple and computational efficient way.

## 3.3 CONCLUSIONS

The FE models for the cooling process of the 'H' profile and the grooved rail 'Ri60' were developed successfully. Both processes were in essence the same but there were some remarkable differences as the location: the cooling bed for the 'H' profile was outdoors and the one for the grooved rail was indoors. The models included as the boundary conditions the weather characteristics presented in the real plants.

FLUENT® demonstrated to be suited for the simulation of both cooling bed thermal conditions. Using this powerful CDF (Computational Fluid Dynamics) software it was possible to model the cooling of the rail through conduction, convection and radiation specifying only geometries, steel thermal properties and boundary conditions. Using FLUENT® was possible to incorporate the wind magnitude and direction resembling the field measurements carried out in the real plant. From these parameters FLUENT® was able to calculate the temperatures, the heat transfer, the film heat transfer coefficient and other interesting thermodynamic variables in the system necessary to obtain a more realistic thermal model than previous found in the literature. The stress/displacement behaviour was modeled using ABAQUS® and through these FE models was possible to observe the longitudinal stress evolution during the cooling processes and explain the final curvatures observed in the plants. Also residual stresses pattern provided in the literature and by experimental tests was verified.

Two cooling configurations were simulated and compared for the cooling of the grooved rail (Ri60): cooling in standing position and in lie-down position. There were some differences in the residual stresses obtained and the tendency seems to indicate that in

general, the configuration given less residual stresses values was the 'standing position' one.

Also, an informatics tool was developed to make possible the communication of the thermal results, obtained by FLUENT®, to the FE-structural/displacement model created in ABAQUS®. The conversion tool was created using freeware and demonstrate to be computational efficient.

The final stress profile, temperatures and bending obtained in the cooling were the initial conditions for the downstream process: the straightening process. Chapter 5 presents the coupling procedure to integrate the cooling process and the straightening process.

# RESUMEN DEL CAPÍTULO 4

## EL PROCESO DE ENDEREZAMIENTO

En este capítulo se presentan los pasos seguidos en la creación y calibración del modelo del proceso de enderezamiento de perfiles de acero. Este modelo presentó un reto importante en lo relativo al modelado del comportamiento plástico durante las cargas cíclicas a las que estaba sometido el perfil. En particular se muestran las acciones que fueron necesarias para poder simular correctamente con ABAQUS® el proceso de enderezamiento de perfiles IPE100.

El proceso de enderezamiento se realiza mediante una máquina compuesta por 8 o 9 rodillos que cíclicamente doblan el perfil hacia arriba y abajo con el objetivo de superar el límite plástico en varias ocasiones durante el proceso. De esta forma, se puede reducir y homogeneizar las tensiones residuales, además de disminuir la curvatura final del perfil.

Modelar este proceso con elementos finitos es altamente complicado pues, para poder explicar convenientemente el comportamiento elástico-plástico del acero estudiado, es necesario contar con valores experimentales que expliquen el comportamiento cíclico del material, además de definir una gran cantidad de parámetros en ABAQUS®. Para el caso en cuestión, al no contar con los parámetros del modelo plástico de los aceros estudiados (a pesar de una búsqueda exhaustiva en la literatura y bases de datos de materiales en Internet) estos debieron obtenerse empíricamente, comparando numerosas simulaciones con los datos experimentales disponibles. Posteriormente estos valores fueron ajustados mediante técnicas de optimización. Además, al resultar un proceso muy costoso en términos computacionales, fue necesario optimizar al máximo los tiempos de simulación empleando la herramienta de 'escalamiento de masa'.

En este capítulo se muestra, el proceso de creación del modelo y cómo se realizó el ajuste de los parámetros de simulación en el ABAQUS®. En particular, se explican los ajustes necesarios correspondientes a los parámetros de control de las simulaciones (el control de la deformación de los elementos: *hourglassing*; el escalamiento de masa; entre los más importantes), los diferentes modelos plásticos probados, los efectos a considerar y sus posibles soluciones.

Después de numerosas simulaciones para ajustar todos los parámetros de simulación, se concluyó que la mejor configuración correspondía con: un modelo de simulación no lineal de grandes desplazamientos; control de la deformación *hourglassing* del tipo *stiffness* (que incluye una matriz de estabilización en la matriz de rigidez); y un modelo de plástico del tipo isotrópico/cinemática no lineal (*nonlinear isotropic/kinematic*). Este modelo plástico

resultó el más conveniente para simular el comportamiento cíclico al considerar el efecto *Bauschinger*, entre otros efectos importantes.

Finalmente, se muestran los resultados obtenidos del modelo calibrado y la buena correspondencia respecto los datos experimentales obtenidos en planta la planta piloto de BFI (la *HSM* o *Hot Straightening Machine*).

CHAPTER 4

# THE STRAIGHTENING PROCESS

## 4.1 STRAIGHTENING PROCESS MODELING

### 4.1.1 INTRODUCTION

In general terms, the straightening processes for both profiles are very similar: the straightener machine receives the profile from the cooling process at a suited temperature and curvature. The straightener machine, composed by 8 or 9 rollers, cyclically bends the profile upwards and downwards in order to achieve the plastic behaviour and homogenize the residuals stresses. Moreover, the aim of the straightening process is to reduce the profile's curvature.

The main difference between both straightening processes consists in the straightened axis involved. The 'H' profile suffers the straightening process only in the secondary axis (axis along the height of the section). On the other hand, the rail suffers the straightening in both, the primary axis and, successively, about the secondary axis.

The main experimental data available to study and tune the straightening model was obtained from the BFI's Hot Straightening Machine (*HSM*) pilot plant. This pilot plant resembles the conditions of the industrial 'H' profile straightening process. The profile processed in this case is the IPE100, made in the same steel grade as the 'H' profile. The roller deflections established for the experimental tests were very demanding and therefore the modelling of this process required a deeper study of the control parameters of the software and to establish the adequate meshing size to obtain a compromise between the accuracy and computing time.

Therefore, the 'I' straightening process model was the base for the modelling of the straightening process for the 'H' and grooved rail long products.

In this chapter the development of the straightening process for the 'I' profile is presented. And because the experimental data available was obtained from the straightening of a profile at ambient temperature the process was modelled as an isolated process (i.e. no coupling with the previous cooling process was consider) in order to simplify the tuning of the model. Once the models were adjusted and verified, the coupling with the cooling

process was achieved for the 'H' and rail profiles, establishing the output of the cooling process as the initial conditions of the straightening process. This coupling is presented in the next chapter (chapter 5).

Consequently, the FE model for the *HSM* was developed using ABAQUS® stress/displacement analysis, in the modality of the 'Explicit' integration approach. This is the approach recommended for contact problems. Additionally, the ABAQUS/Explicit count on a tool to improve the computational efficiency: the *mass scaling*. The mass scaling increases the material density allowing a larger time step, and decreasing in this way the total computing time. This tool was possible to be adopted because the profile's speed throughout the straightener was relatively slow and therefore the inertial forces were not significant.

Special efforts were also invested in obtaining a suited material model for the plastic behaviour. There was no mention in the literature or data bases available about the plastic model parameter for the steel grades used. The final parameter were calibrated by trial and error, changing the parameters and observing the profile behaviour throughout the straightener machine (profile's velocity, stresses, final bending and residual stresses), comparing the results with the experimental data available. Then a Newton –Rapson based methodology helped to adjust these parameters in a finer way.


*Figure 88. BFI's Hot Straightening Machine (HSM). Picture courtesy of BFI.*

## 4.1.2 STRAIGHTENING PROCESS MODELING FOR THE 'I' PROFILE

### 4.1.2.1 DESCRIPTION OF THE PROBLEM

As said before, the straightening process modelled was the Hot Straightening Machine (*HSM*) pilot plant constructed by BFI to simulate the real PTG's 'H' profile straightening process.

The machine is composed by 9 rollers arranged with its axes in horizontal position, in such a way that they bended the beam by its web, in two areas near the roots (see Figure 89). This made possible the straightening about the secondary straightening axis only. This type of process is also called "second moment of area straightening process" (Schleinzer, 2000). The rollers involved were composed by the so called *conventional* discs (the *HSM* count also with *Flange Supported* discs, patented by BFI, with very interesting performance. Nevertheless, in this research work we focused only on the *conventional* discs).

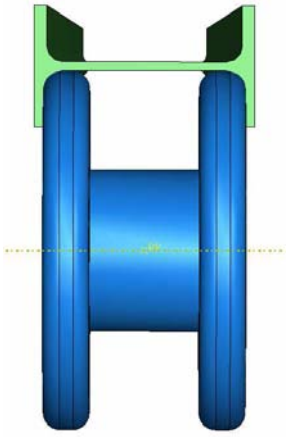

*Figure 89. Roller with 'conventional disc' acting in the IPE100 profile.*

The straightener configuration is presented in the next figure and table.

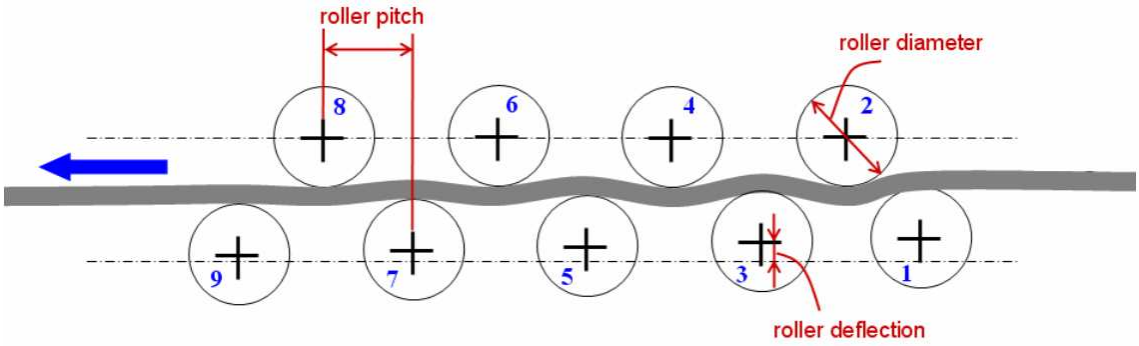


*Figure 90. Straightener configuration.*

*Table 11. Straightener values used in the experimental test.*

| Roller Nº | 1 | 2 | 3 | 4 | 5 | 6 | 7 | 8 | 9 |
|---|---|---|---|---|---|---|---|---|---|
| Diameter (mm) | | | | | 155 | | | | |
| Pitch (mm) | | | | | 250 | | | | |
| Deflection (mm) | 10.15 | 0 | 9.65 | 0 | 9.00 | 0 | 8.50 | 0 | 6.88 |

This is the so called 9-rolls-configuration-straightener, with deflection in rollers 1, 3, 5, 7 and 9. The deflection values represented an important challenge as the bending produced at the beginning of the process was quite large.

#### 4.1.2.2 EXPERIMENTAL STRESSES VALUES

BFI kindly provided experimental values regarding the beam's stresses produced by each roller during the straightening process and the residual stresses after it.

The experimental test was achieved in a beam at 20ºC, with an initial bending produced artificially (i.e. the bending was not caused by the cooling process). Unfortunately, the beam's curvatures before and after the experimental test was not available.

The stresses values were obtained by the sectioning method and are displayed in Figure 91.

In sections 0 and 1, the stresses produced by the artificial bending are showed. The non symmetries in the experimental results were caused by the rollers' axes tilting produced when the beam pass through the straightener.

#### 4.1.2.3 FE-STRESS/DISPLACEMENT MODEL

The problem was analyzed in a mechanical aspect only as the experimental data regarding the beam's stresses produced by each roller and the residual stresses was measured in a cold beam (20ºC).

The FE model simulated an IPE100 beam of 4 m length, straightened with conventional disc. The rollers velocity used for the process was: 0.086 rpm. This resulted in a linear beam velocity of 0,4 m/min.

The main assumptions in the developing of the model were:

- The rollers were rigid without bending axes. Therefore the asymmetries displayed in Figure 91 were not presented in the simulations.
- The initial beam's temperature was uniform (20ºC).
- The camber of beams caused by cooling was ignored.
- There were no residual stresses before straightening.

In next chapter all of these factors, except the tilting, were considered on the model, as the output from the cooling process model (non uniform temperature, bending and residual stresses) were the input of the straightening process model.

The element used to mesh the beam was the C3D8R (continuum solid eight node element), i.e. hexahedral element. The rollers were generated with Analytical Rigid Surfaces. Between the rollers and the beam the basic Coulomb friction was used with a friction coefficient of 0.25. The element length in the beam direction was of 20 mm (see Figure 92).

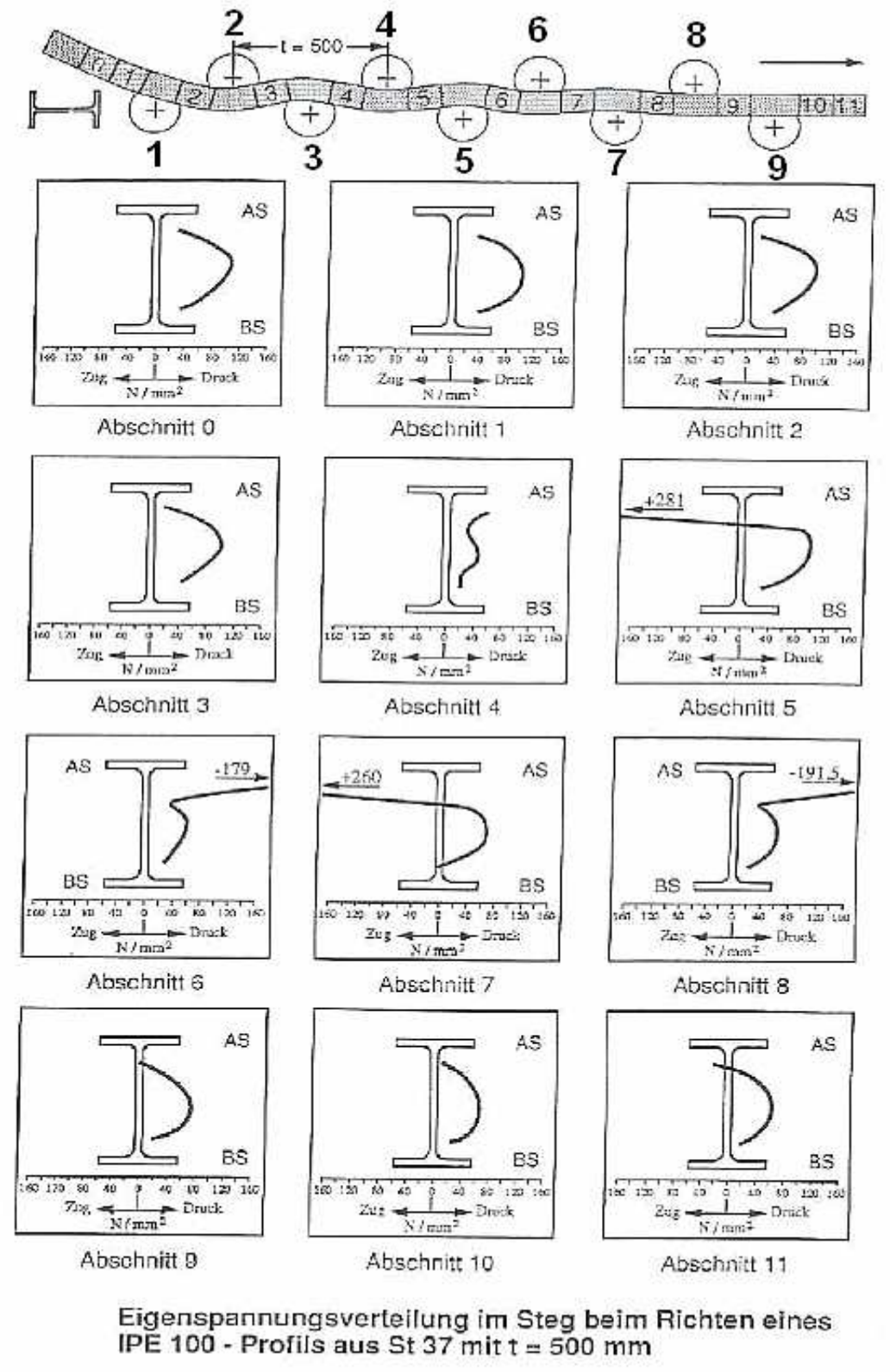


*Figure 91. Experimental results provided by BFI.*

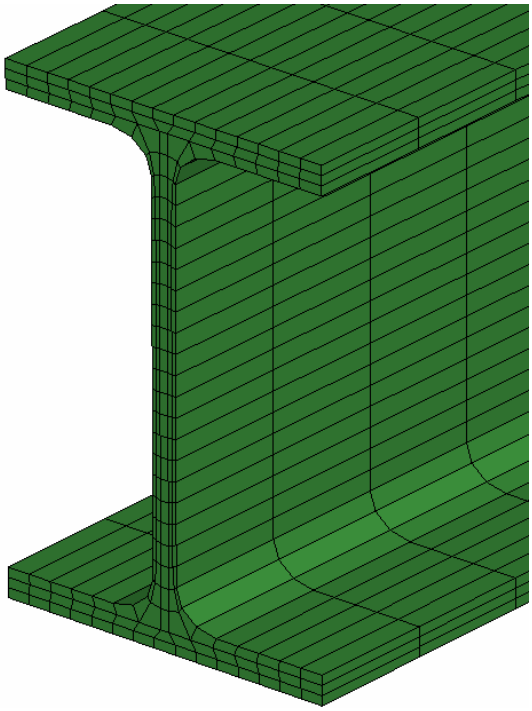

*Figure 92. Detail of the beam's mesh.*

A general view of the FE model assembly is presented in the next figure.

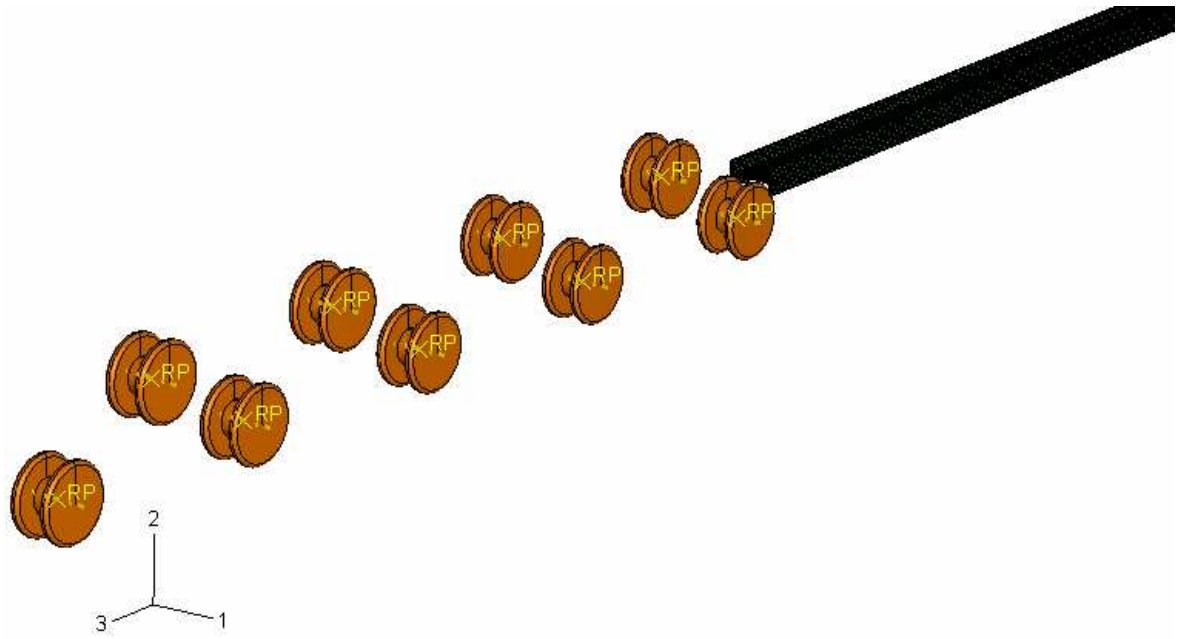


*Figure 93. BFI's Hot Straightening Machine (HSM) FE model.*

## *ABAQUS® PARAMETERS CONFIGURATION*

The straightening process model was a demanding model because of the contact involved and the type of load applied to the profile (cyclic loads). This is why it was necessary a deep study of the control parameters available in ABAQUS®.

Therefore, the next items were studied:

- Non linear stress analysis options.
- Element's deformation controls (hourglass controls).
- Mass scaling tool.
- Plastic models.

### NON LINEAR STRESS ANALYSIS OPTIONS

A non linear stress analysis problem can contain up to three sources of nonlinearity: material nonlinearity, geometrical nonlinearity and boundary nonlinearity (ABAQUS, 2005).

***Material nonlinearity***: The material is history dependent. In this case, as it will be seen in next section, the material (steel S235) presented nonlinearities on the plastic model chosen.

***Geometric nonlinearity***: it is possible to define a problem as a 'small-displacement' analysis, which means that geometrical nonlinearity is ignored in the element calculation (the kinematic relationships are linearized), or as a 'large-displacement' analysis, where elements can distort in a nonlinear manner. In this case, the use of the 'large-displacement' option was fundamental.

***Boundary nonlinearity***: This commonly appears in contact problems, as in this case.

Therefore, a nonlinear material model (see the plastic model used in next sections) has been defined, and the NLGEOM (large-displacement) option has been applied on the simulation.

### ELEMENT DISTORTION CONTROLS

There are several ways to overcome the problems derived from the *reduced integration* technique (used to improve the stability and convergence of an incompressible stress analysis). One of the biggest consequences of using reduced integration is the hourglass

distortion in elements. To solve this problem, ABAQUS® count with several hourglass-controls. The main controls are:

***Enhanced***: Provides improved coarse mesh accuracy with slightly higher computational cost and performs better for nonlinear material response at high strain levels when compared with the default total stiffness formulation. Based on the enhanced assumed strain method; no scale factor is required. Although generally beneficial, this may give overly stiff response in problems displaying plastic yielding under bending.

***Stiffness***: This is the most common approach to suppress hourglassing, as it involves the addition of a stabilization matrix to the reduced the integrated stiffness matrix. This stabilization matrix should preserve the conditions of "invariance" and "consistency".

Therefore, we have adopted the *stiffness* element control. Nevertheless, the rest of the controls were tested as well to observe the simulation performance. As predicted, the best result was obtained with the *stiffness* control.

### MASS SCALING OPTION

As said before, mass scaling is often used in ABAQUS/Explicit for computational efficiency in quasi-static analyses. Because the explicit central difference method is used to integrate the equations in time, the discrete mass matrix used in the equilibrium equations plays a crucial role in both computational efficiency and accuracy. When used appropriately, mass scaling can often improve the computational efficiency while retaining the necessary degree of accuracy required for a particular problem.

In several tests carried out it was observed that this parameter had a crucial effect on the simulations, even though the problem could be considered as a quasi-static analysis (because of the low velocities involve: beam's line-speed equal to 0.4 m/min). The smaller the mass scaling factor was, the stable and accurate the stress results were. Nevertheless, as the straightening process model represents a high computational cost simulation, it was necessary to find the equilibrium between efficiency and accuracy though this parameter.

### PLASTIC MODEL

ABAQUS® offers several plastic models (ABAQUS, 2005). The classical plasticity model (isotropic hardening model), and the models for metals subjected to cyclic loading (linear kinematic and nonlinear isotropic/kinematic hardening models).

***Isotropic hardening**:* The yield surface changes size uniformly in all directions such that the yield stress increases (or decreases) in all stress directions as plastic straining occurs.

***Linear kinematic hardening model:*** The evolution law of this model consists of a linear kinematic hardening component that describes the translation of the yield surface in stress space through the backstress, $\alpha$. When temperature dependence is omitted, this evolution law is the linear Ziegler hardening law:

$$\dot{\alpha} = C \frac{1}{\sigma^0} (\sigma - \alpha) \dot{\bar{\varepsilon}}^{pl} \tag{1}$$

where

$\dot{\bar{\varepsilon}}^{pl}$ : equivalent plastic strain rate.
$C$ : kinematic hardening modulus.
$\sigma^0$ : equivalent stress that defines the size of the yield surface.
$\sigma|_0$ : reference equivalent stress (at zero plastic strain).
$\gamma$ : rate at which $C$ decreases with increasing plastic deformation.

In this model the equivalent stress defining the size of the yield surface, $\sigma^0$, remains constant, $\sigma^0 = \sigma|_0$, where $\sigma|_0$ is the equivalent stress defining the size of the yield surface at zero plastic strain.

***Nonlinear isotropic/kinematic hardening model:*** The evolution law of this model consists of two components: a nonlinear kinematic hardening component, which describes the translation of the yield surface in stress space through the backstress, $\alpha$; and an isotropic hardening component, which describes the change of the equivalent stress defining the size of the yield surface, $\sigma^0$, as a function of plastic deformation.

The kinematic hardening component is defined to be an additive combination of a purely kinematic term (linear Ziegler hardening law) and a relaxation term (the *recall* term), which introduces the nonlinearity. When temperature and field variable dependencies are omitted, the hardening law is

$$\dot{\alpha} = C \frac{1}{\sigma^0} (\sigma - \alpha) \dot{\bar{\varepsilon}}^{pl} - \gamma \alpha \dot{\bar{\varepsilon}}^{pl} \tag{2}$$

where $C$ and $\gamma$ are material parameters that must be calibrated from cyclic test data. $C$ is the initial kinematic hardening modulus, and $\gamma$ determines the rate at which the kinematic hardening modulus decreases with increasing plastic deformation (see Figure 94). The kinematic hardening law can be separated into a deviatoric part and a hydrostatic part; only

the deviatoric part has an effect on the material behavior. When $C$ and $\gamma$ are zero, the model reduces to an isotropic hardening model. When $\gamma$ is zero, the linear Ziegler hardening law is recovered.

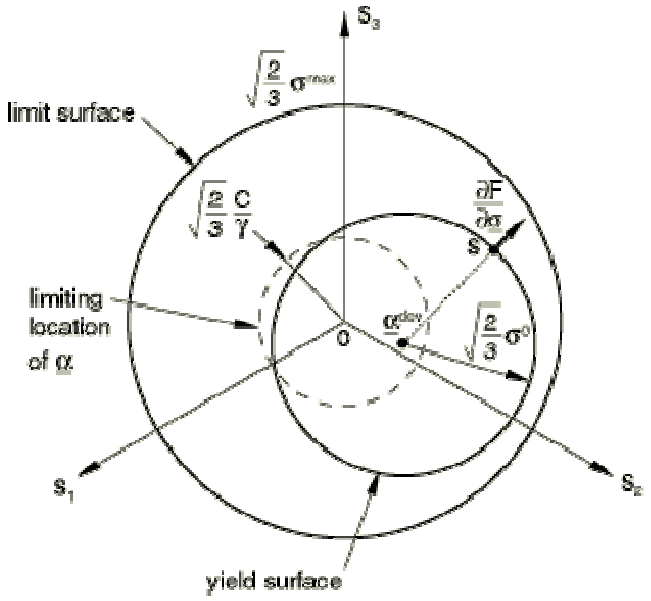


*Figure 94: Three-dimensional representation of the hardening in nonlinear isotropic/kinematic model (taken from ABAQUS, 2005).*

As the beam was alternately bended in opposite directions (upward and downward) it can be said that the metal is subject to cyclic loading, that generates nonlinearities. Several tests on the straightening process model have proved that the better steel behavior was obtained through the last of these three models: the *nonlinear isotropic/kinematic hardening model*. Furthermore, this model takes into account several important material behaviours as (ABAQUS, 2005):

**Bauschinger effect**: This effect is characterized by a reduced yield stress upon load reversal after plastic deformation has occurred during the initial loading. This phenomenon decreases with continued cycling.

**Cyclic hardening with plastic shakedown**: This phenomenon is characteristic of symmetric stress- or strain-controlled experiments. Soft or annealed metals tend to harden toward a stable limit, and initially hardened metals tend to soften. The kinematic hardening component of the models used alone predicts plastic shakedown after one stress cycle. The combination of the isotropic component together with the nonlinear kinematic component predicts shakedown after several cycles.

**Ratchetting**: Unsymmetrical cycles of stress between prescribed limits will cause progressive "creep" or "ratchetting" in the direction of the mean stress. Typically, transient ratchetting is followed by stabilization (zero ratchet strain) for low mean stresses, while a constant increase in the accumulated ratchet strain is observed at high mean stresses. The nonlinear kinematic hardening component, used without the isotropic hardening component, predicts constant ratchet strain. The prediction of ratchetting is improved by adding isotropic hardening, in which case the ratchet strain may decrease until it becomes constant.

## *CALIBRATION THE STRAIGHTENING PROCESS FE MODEL*

The problem was simulated using several combinations of the previous section options in order to arrive to an optimal solution. The calibration parameters where:

a) The beam's linear velocity (that can be affected by the mass scaling and other parameters as the hourglass control).
b) The longitudinal residual stresses (comparing them with the experimental values).
c) The final beam's curvature.
d) The behavior and magnitudes of the stresses while the beam was passing through the rollers.

Taking into account all these factors, and after about 60 trials simulations, the best combination of all parameters was the follow:

- We consider the 'large-displacement' analysis by chosen: *NLGEOM=YES*
- Hourglass control: *Stiffness*
- Mass scaling: semiautomatic, to target an increment time of *5e-4s*.
- Plastic model: *nonlinear isotropic/kinematic hardening model*.

The parameters of the plastic model for the studied steel (S235) were not possible to find in the literature. So we calibrate the values of $C$ and $\gamma$ using Newton-Rapson optimization method through 20 simulations varying the model parameters till reach the real beam's velocity. The final values chosen were: $C$ = 410 GPa and $\gamma$ = 37,7.

With all these final parameters we could reach the right linear beam velocity; an acceptable beam's final curvature; the longitudinal residual stresses had acceptable shape and magnitudes; and the computational time per simulation was not so high (45 h).

## *RESULTS*

In this section we compare the results obtained with the FE straightening process model and the experimental values produced by BFI.

Two general view of the longitudinal stresses contour plot at the middle stage (time=515s) of the FE model simulation is displayed in the follow picture. The aim of the figures is to display how the beam goes through all rollers and leave the straightened with an acceptable bending.

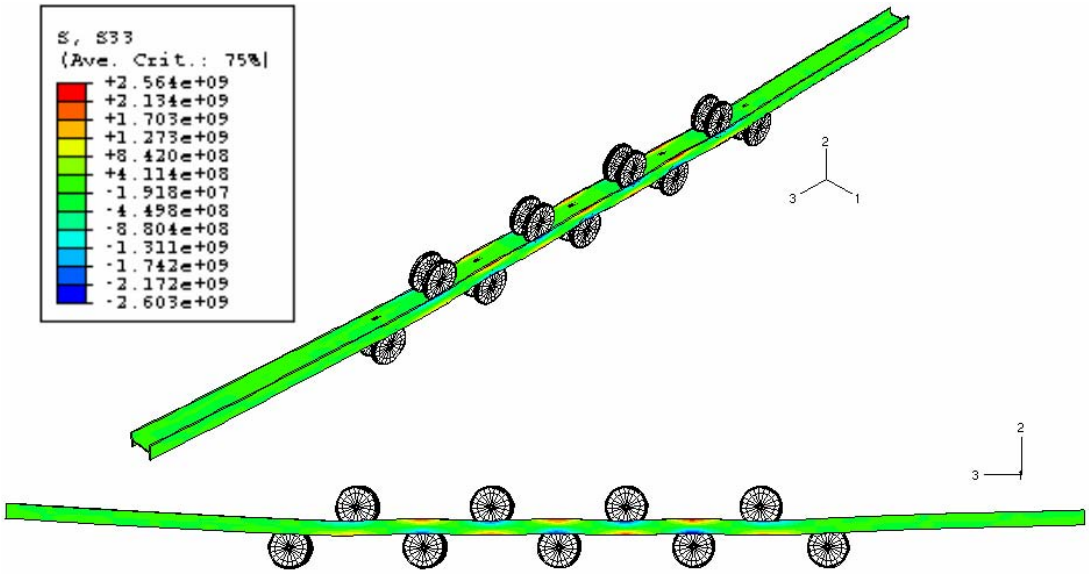


*Figure 95. Two general view of the straightener FE model at time 515s. S33 contour plots.*

The longitudinal stresses (S33) results were obtained by taking the average of the web's elements located in the same perpendicular position, as showed in Figure 96. In doing so, the sectioning method was imitated in order to compare the simulated and the experimental values.

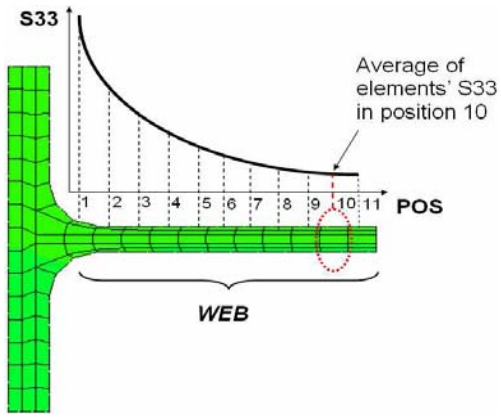


*Figure 96. Procedure to obtain S33 at the web from the simulation results.*

The results of the simulation are presented in Figure 98 and Figure 99. As the problem is symmetric about the web, the right side of the figures is the mirror of the left side. There are three curves displayed at each figure that corresponds to:

- *Black curve*: S33 of the web's elements of a segment 2.5 m from the front of the beam. (Each segment is 20 mm long).
- *Red curve*: S33 of the web's elements of a segment located right beside the previous one.
- *Blue curve*: Is the average of the black curve and the red curve.

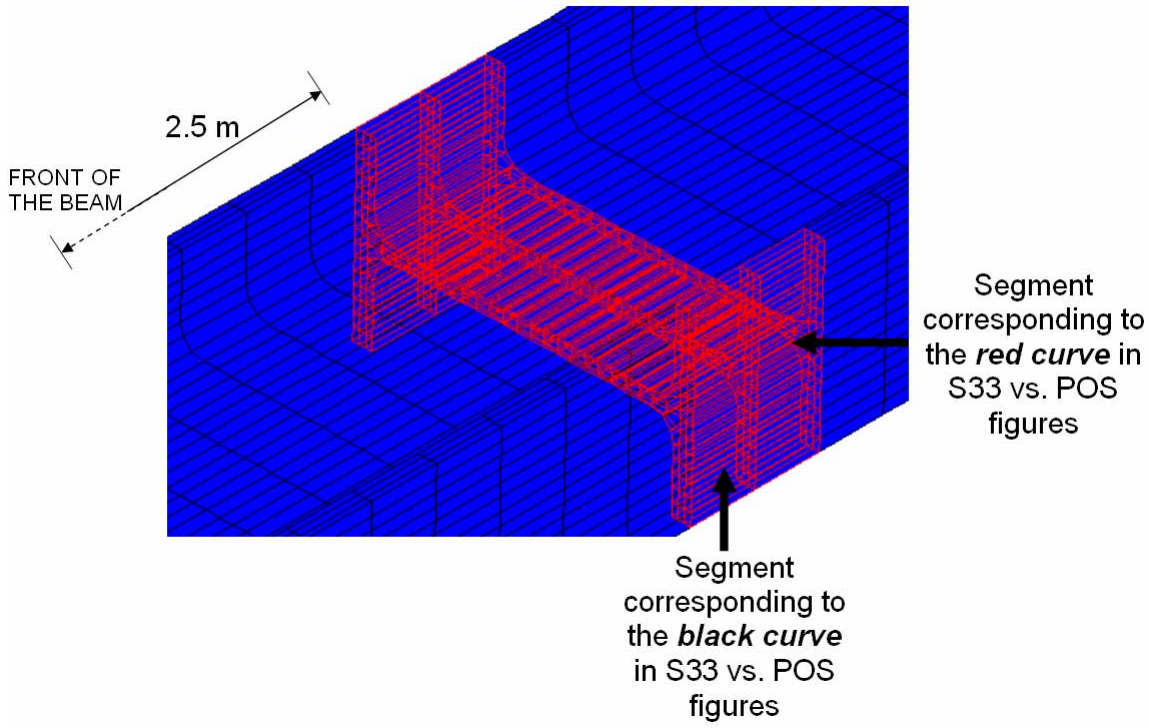


*Figure 97. Segments chosen to get the S33 vs. Position curves.*

The representation of these three curves was chosen in this way because the areas compared (sections between two rollers) were transitional areas where the stresses changed from tension to compression and vice versa (see Figure 100). As a result, in this way, what was happening in the nearby segments could be observed (and also the average produced by these two segments).

As in the simulations of the straightening FE model an initial straight beam was used, only sections from 2 to 11 were compared.

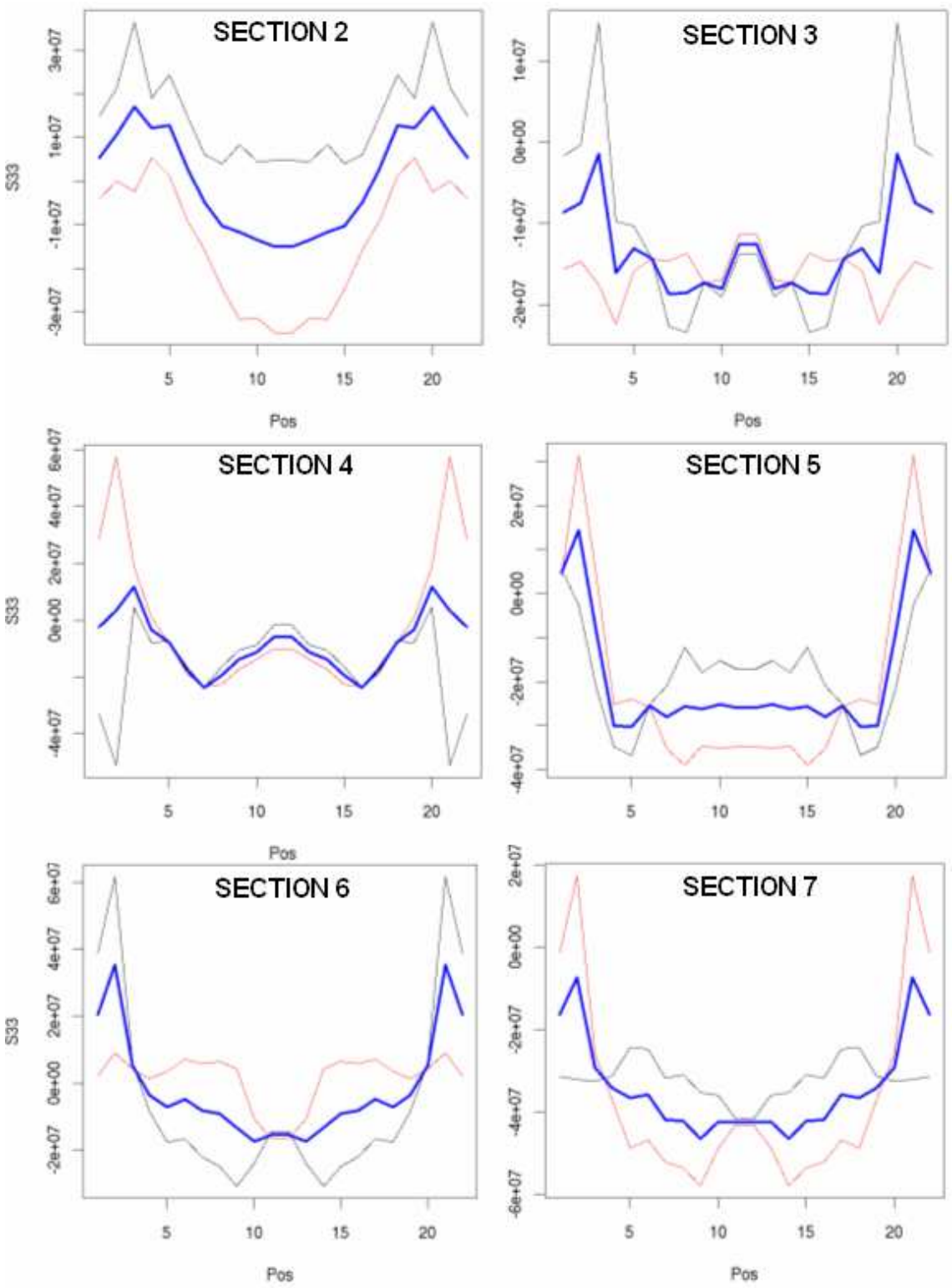


*Figure 98. Longitudinal stresses (S33 in Pa) at the web in sections from 2 to 7.*

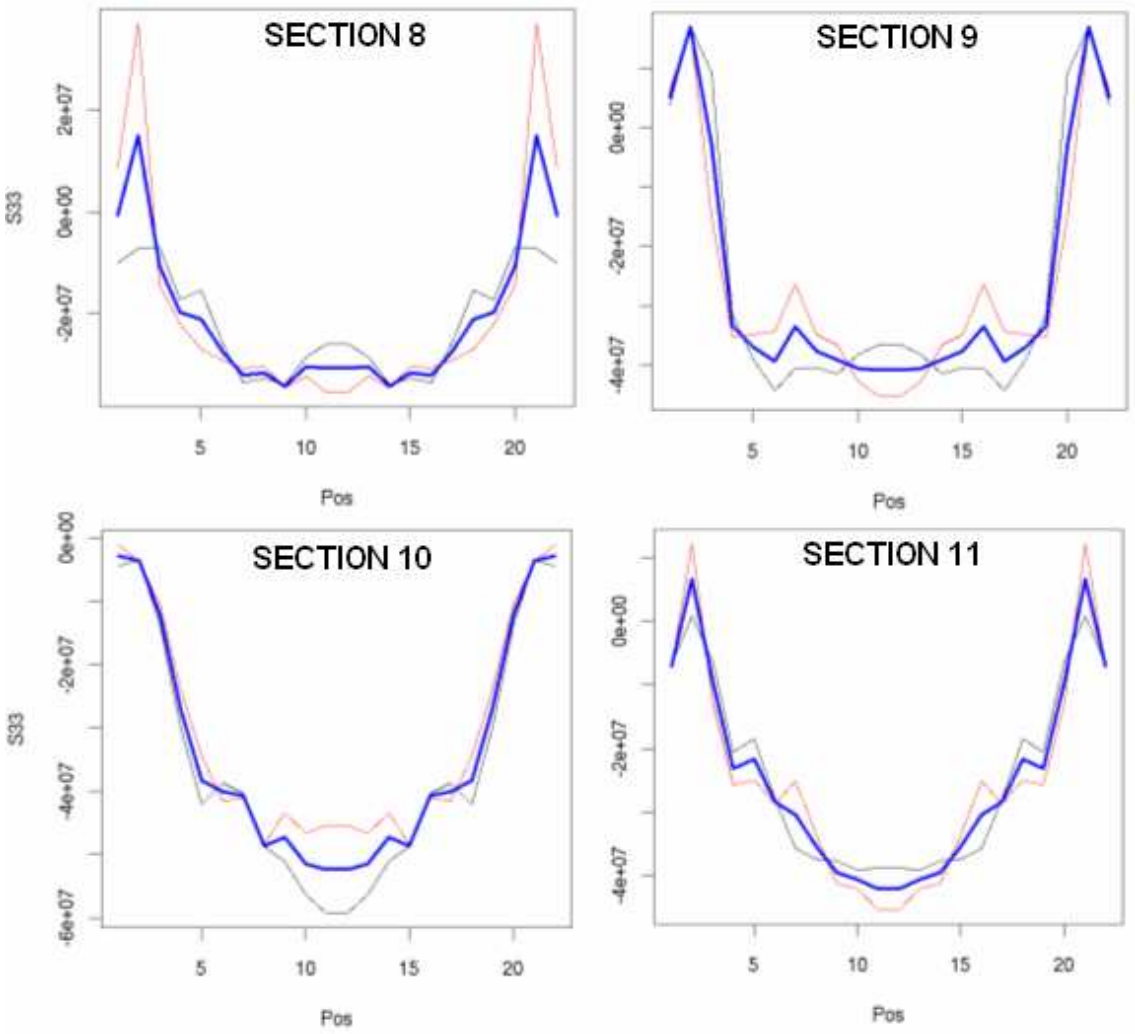


*Figure 99. Longitudinal stresses (S33 in Pa) at the web in sections from 8 to 11.*

The shape of most of the figures agrees with the experimental results. About the magnitudes, in sections 2 and 3 lower values were observed comparing them with the experimental results. This could be produced by the initial residual stresses inherent to the previously bended beam used in the experimental test.

Other reason for the differences between experimental and simulation results in sections form 2 to 7 could be that the sections compared, as we have said before, were in transitional areas, between two rollers, and as can be seen in next figure, it is a position where the stress sign changes from tension to compression and vice versa.

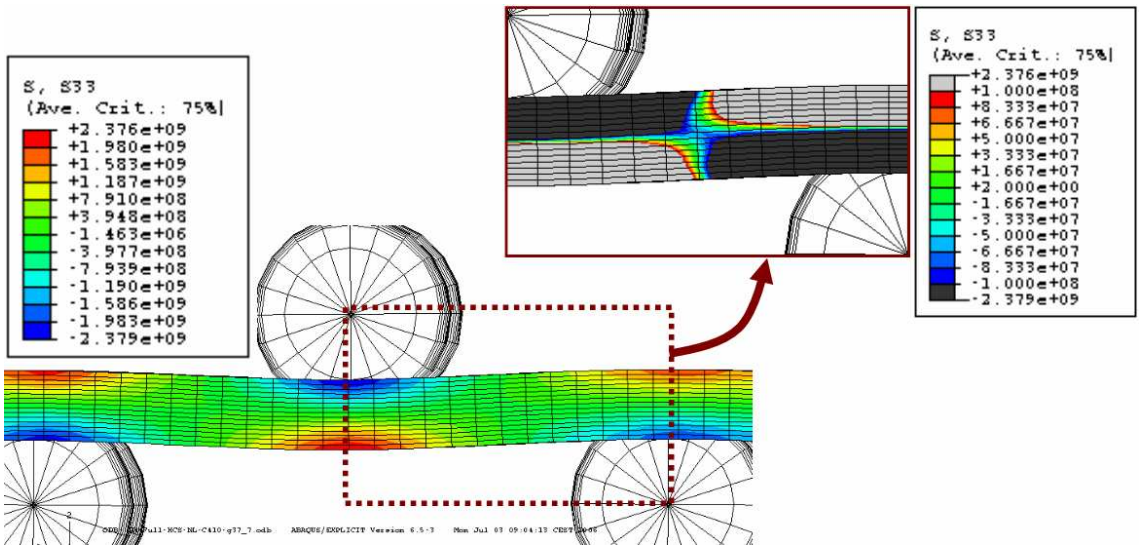


*Figure 100. Stresses transitional area between rolls 3, 4 and 5.*
*Detail of transitional zone between rolls 3 and 4.*

The final curvature reached with the definitive FE model was 55.01 mm. Nevertheless, it was observed that the curvature could be reduced by reducing the mass scaling factor: the curvature with MS-target 1e-3s was 12.7% higher than the one obtained with MS-target 5e-4 s. In next figure both curvatures are compared.

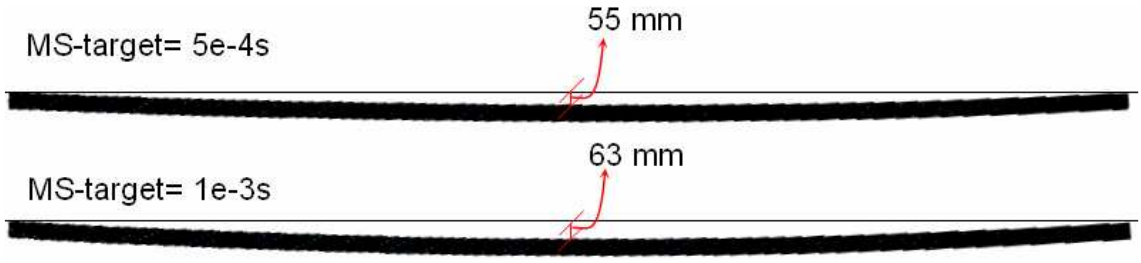


*Figure 101. Final beam's curvature for MS-target= 5e-4 s and MS-target= 1e-3 s.*

## 4.2 CONCLUSIONS

The stress/displacement model for the IPE100 straightener process have been developed using ABAQUS® software. The machine modeled was the BFI's HSM.

For this process the plastic model required was a quite complex model: a non linear cyclic model that takes into account the *Bauschinger* effect and other important characteristics. The model parameters for the studied steel were not possible to find in the literature so it

was necessary to calibrate them comparing the simulations with the experimental data and observations. At the end, Newton-Rapson optimization method was used for a finer tune. In addition, the effect of the mass-scaling factors was patent. The lower the mass-scaling factor, the more realistic the results. However, in decreasing this factor the computational effort can be increased in hug way. Therefore, it was necessary to reach a compromise between the accuracy of the results and the simulation time. This solution provided acceptable results but a deeper study to find the precise model parameters is advisable. Much more if the plastic behaviour during the straightening for different beam's temperatures have to be simulated.

# RESUMEN DEL CAPÍTULO 5

## ACOPLAMIENTO DE LOS PROCESOS DE ENFRIAMIENTO Y ENDEREZAMIENTO

En este capítulo se muestran el trabajo desarrollados para acoplar los modelos de los procesos de enfriamiento y enderezamiento de los perfiles de acero estudiados. El acoplamiento de ambos procesos es de gran importancia debido a que ofrece la oportunidad de estudiar de forma integrada la evolución de las tensiones residuales a lo largo de todo el proceso de fabricación de estos perfiles.

Hay que destacar, que uno de los objetivos primordiales del proceso de enderezamiento consiste en reducir y homogeneizar las tensiones residuales provenientes del proceso anterior de fabricación, el enfriamiento. Debido a esto, para poder simular y optimizar convenientemente este proceso, es necesario que el perfil entrante presente unos mapas de temperaturas y tensiones residuales realistas.

El proceso de acoplamiento parte del modelo creado en FLUENT® del enfriamiento de los perfiles según la condiciones ambientales existentes en la realidad. El objetivo inicial fue obtener la evolución del mapa de temperaturas del perfil a lo largo del tiempo para exportarlo al modelo mecánico creado en ABAQUS®. Una vez importados estos resultados térmicos al ABAQUS®, se procedió a simula el mismo proceso de enfriamiento pero esta vez con la intención de obtener la evolución de las tensiones y deformaciones del perfil a lo largo del tiempo. Cabe destacar que, para poder exportar los mapas de temperatura a lo largo del tiempo del FLUENT® al ABAQUS®, fue necesario desarrollar una herramienta software específica, que se denominó *conv_flu_abq.sh*.

Una vez obtenidas las tensiones residuales y deformaciones finales del proceso de enfriamiento, se introducen éstas (acompañadas del mapa de temperatura final) como condiciones de partida para la simulación del proceso de enderezamiento (cuyo modelo fue creado en ABAQUS®). De esta forma, el inicio del proceso de enderezamiento se simula con las temperaturas, tensiones residuales y deformaciones que presenta el perfil después de haber sido enfriado.

Como demostración de la metodología planteada, se muestran los resultados obtenidos en el acoplamiento de la simulación de los procesos de enfriamiento y enderezamiento para las vigas ‘H’ y raíles Ri60.

En los casos estudiados, los resultados de simulación fueron comparados con los resultados experimentales, mostrando una alta similitud. Existen algunas discordancias en la

curvatura final de los productos que puede ser debida a la falta de unos parámetros más realistas del modelo plástico y adicionalmente dependientes de la temperatura. Estos valores están siendo buscados actualmente por el grupo de investigación EDMANS por considerarlos de vital importancia para un estudio más profundo de la influencia de la temperatura en el procesos de enderezamiento. Los modelos por EF fueron desarrollados tomando en cuenta este hecho y están preparados para la inclusión de estos valores sin realizar ninguna modificación adicional.

Una ventaja sustancial del uso de la metodología de acoplamiento propuesta, es que permite estudiar la evolución de las temperaturas, tensiones, deformaciones y cualquier otro parámetro que nos proporcionen las simulaciones en cualquier localización interna del perfil y en cualquier momento durante el desarrollo de los procesos.

CHAPTER 5

# COUPLING THE COOLING AND THE STRAIGHTENING PROCESSES

It was explained in the introduction chapter that the cooling and the straightening of the long products were sequential processes. Therefore, it is important to consider the output of the cooling as the input of the straightening, as happens in the reality. This chapter focused on the coupling of the cooling process with the straightening process for the 'H' beam and grooved rail Ri60. The straightening processes were modeled as thermal-stress/displacement coupled analysis, to be able to consider the temperature map coming from the cooling process. First a general explanation of the coupling methodology carried out is reported. Afterward, the coupling of both processes and the results for the 'H' is exposed followed by the coupling and results for the Ri60 profile.

## 5.1 COUPLING THE COOLING AND THE STRAIGHTENING PROCESSES

Summarizing the proceeding to simulate the two sequentially manufacturing processes for the profiles studied, first the cooling process was modeled in two parts: the thermal behaviour was developed in FLUENT® and the mechanical behaviour in ABAQUS/Standard. A conversion program (*conv_flu_abq.sh*) was necessary to communicate the results from one model to the other. Second, the straightening process was modeled using ABAQUS/Explicit in a coupled thermal-stress/displacement approach. Figure 102 displays the general steps.

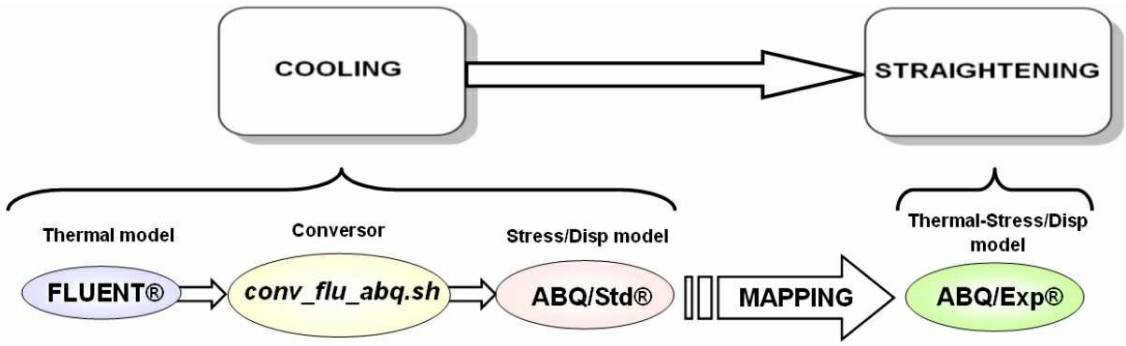


*Figure 102. Coupling of the cooling process and the straightening process*

Even though the initial values for the straightening process model created in ABAQUS®, were provided by a mechanical model created also in ABAQUS®, the mapping process from a *standard*-stress/displacement model to an *explicit*-thermal-stress/displacement model is not automatic. It was necessary to create an intermediate analysis to translate or 'map' the final results (stresses, temperatures and displacements) from the cooling process to the straightening process.

The main problem was the type of elements involved in the analysis and the temperature variable imported from the previous thermal model. To be able to import the results from an ABAQUS/Standard to an ABAQUS/Explicit analysis it is necessary that both models contain the same element type.

As explained in the preceding chapter, in the previous *standard*-stress/displacement model the element type used was the pure stress/displacement element C3D8R: continuum solid 8-node element, (where the 'R' means: reduced integration with hourglass control), including in the analysis the temperature as an independent field variable.

To be able to import the final temperature form the *standard*-mechanical model, the straightening process was modeled as a coupled thermal-mechanical problem. In this way, the material properties, which were temperature-dependent, could be applied in a proper manner. Therefore, the element used for this analysis was the C3D8RT: coupled temperature-displacement elements, 8-node displacement and temperature (also with reduced integration with hourglass control).

To make possible the mapping, the ABAQUS function *MAP SOLUTION was used. This function is normally used when severe distortion occurs in an analysis and it is necessary to remesh the part, i.e. to create a new mesh better designed to continue the analysis, and therefore it is required to map the old-model solution onto this new mesh (ABAQUS, 2005). In this case the mesh in both models was the same, and the mapping function just provided a way to change the element type.

The other tool used to complement the mapping was the *IMPORT function. With this function was possible to import the material state of the elements at the specified step and time of the previous ABAQUS/Standard analysis (the cooling process).

## 5.2 STRAIGHTENING PROCESS MODELING FOR THE 'H' PROFILE, INCLUDING COUPLING WITH PREVIOUS COOLING PROCESS.

### 5.2.1 DESCRIPTION OF THE PROBLEM

As established in previous chapter the straightening process for the 'H' profile is very similar to the one for the 'I' profile studied (the BFI's *HSM*) as this pilot plant resemble its behaviour. Therefore, the straightening configuration modelled was the same as in Figure 90.

The values for the roller's deflections and pitches tested in the simulation are presented in next table.

*Table 12. Deflection and pitch for the HEM500's straightener with conventional (konv) and flange supported (FS) discs.*

| **Roller Nº** | **1** | **2** | **3** | **4** | **5** | **6** | **7** | **8** | **9** |
|---|---|---|---|---|---|---|---|---|---|
| Pitch (mm) | | 1100 | 1100 | 1050 | 1050 | 1000 | 1000 | 1000 | 1000 |
| Deflection (mm) | 0.5 | - | 11.2 | - | 8.2 | - | 7.3 | - | 4.2 |

Whit these deflections, nine HEM500 beams of 18.1 m long were straightened after cooling at the PTG's cooling bed. These beams were the same that provided the experimental results of chapter 3, section 3.1.2.3.

The curvatures for these beams after cooling were in a range from 12 to 43 mm. And after the straightening the values were from 5 to 25 mm. It is important to point out that several initial temperatures at the straightening process were tested for the project, and that was why there was such a wide range of bending before and after the straightening process. The maximum curvature a beam can have, according to quality specification, is 1 mm per meter. Therefore, some of these beams (the one with more than 18.1 mm) had to be passed again for the straightener machine in order to be able to sell them.

Also, it have been used for a basic verification of the simulation results the same experimental values obtained from the IPE100 straightening process presented in chapter 4, Figure 91.

### 5.2.2 FE-THERMAL-STRESS/DISPLACEMENT MODEL

For the straightening process a beam of 9 m length was used. This beam was previously cooled using the thermal-model developed in chapter 3. The type of discs used was the 'conventional' discs. The linear velocity of the beam was set on 0.5 m/s, which resulted in

an angular velocity for the rollers of 0.72 rpm. This value corresponds to the real velocity in the PTG plant.

The only assumption that remained from the previous IPE100 straightening model was the nature of the rollers (rigid without axes tilting). The rest of the assumptions were not valid anymore as in this case the coupling with the previous process, the cooling process, was achieved. In this way, the initial conditions of the beams, in the sense of temperature, camber and residuals stresses, were the final results obtained in the cooling process.

As explained in section 5.1, the element used to mesh the beam was the C3D8RT (coupled temperature-displacement continuum solid eight node element), i.e. hexahedral element. Again, the rollers were generated with Analytical Rigid Surfaces and a Coulomb friction between rollers and beam with a value of 0.25 was used. The element length in the beam direction was of 100 mm (see Figure 103).

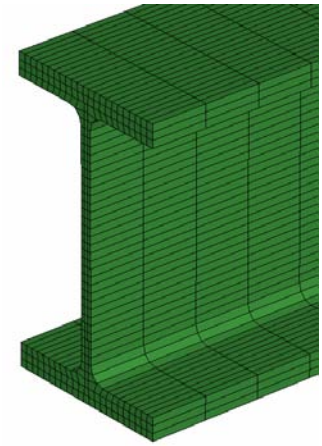

*Figure 103. Detail of the beam's mesh.*

A general view of the FE model assembly is presented in the next figure.

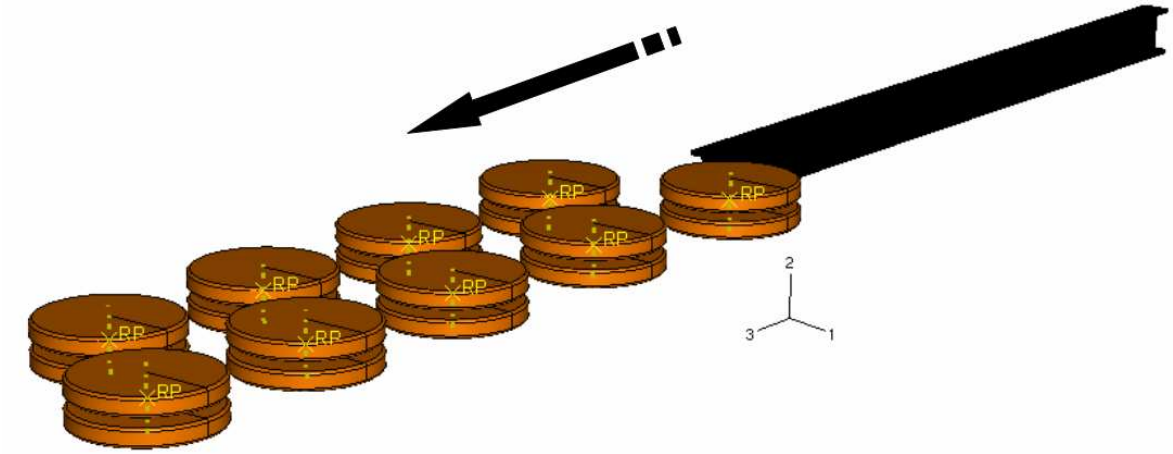


*Figure 104. HEM500 straightening machine FE model.*

The ABAQUS® control parameters were set following the study made in Chapter 4: 'large-displacement' analysis; hourglass control: *Stiffness*; mass scaling factor: 200 in semiautomatic mode; plastic model: *nonlinear isotropic/kinematic hardening model,* with $C$ = 410 GPa and $\gamma$ = 37,7.

The straightening conditions for this model, in the sense of rollers' deflections, were less demanding that for the IPE100 and therefore a small mass scaling factor could be set. This caused more stable stress results as will be see in next section. Nevertheless, as this is a temperature dependent problem, the plastic-model parameters should be also temperature dependent. As was explained in chapter 4, these values were not found in the references and represent important information to be able carry out a deeper study of the process.

### 5.2.3 RESULTS

Figure 105 display the initial conditions for the HEM straightening process, considering as initial temperature and stresses values the result from the cooling process. The bending for this beam (9 m long) after cooling was of 5 mm.

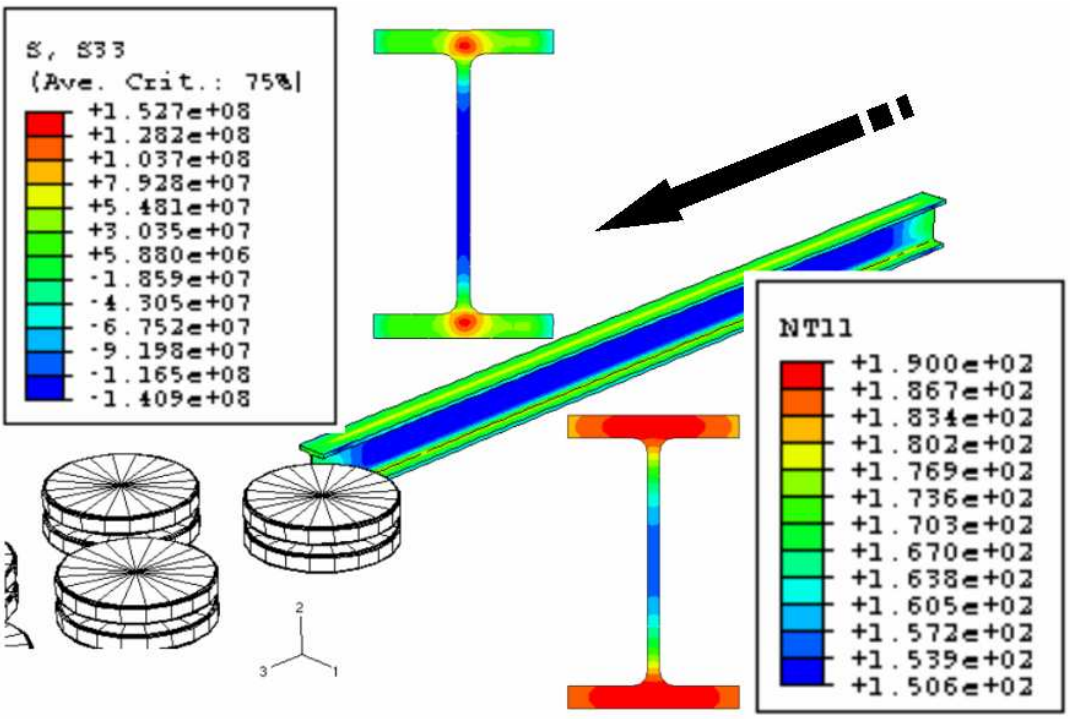


*Figure 105. Temperature (NT11 in ºC) and longitudinal stresses (S33 in Pa) at the straightening process input. Initial values taken from the cooling process.*

After the straightening process the beam present the residual stresses and bending displayed in Figure 106.

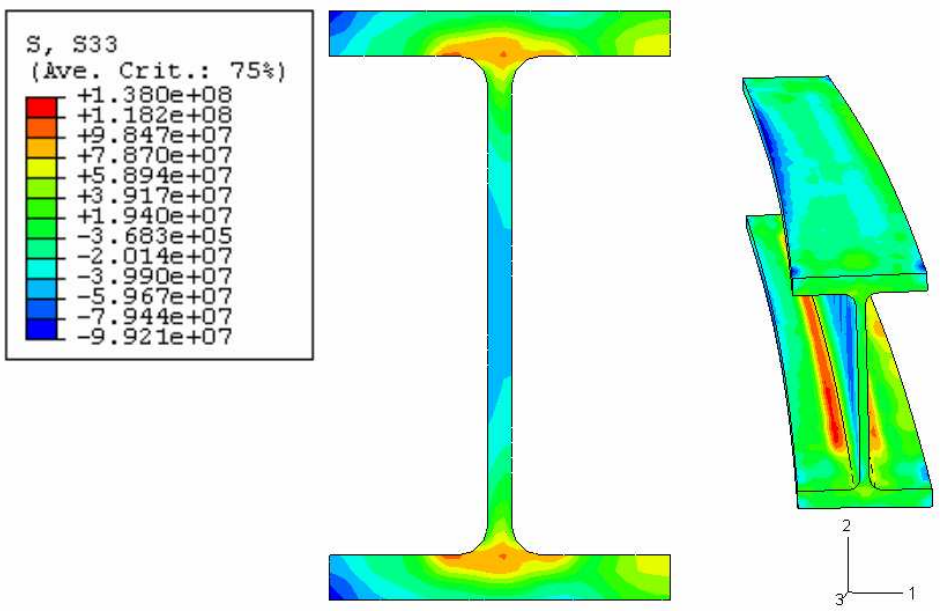


*Figure 106. Residual stresses (S33 in Pa) contour plot of the HEM500 beam after the straightening process. The cross section corresponds to the center of the beam. At the right side, the final bending is also displayed.*

Comparing Figure 105 and Figure 106, regarding the residual stresses before and after the straightener machine, it is evident the reduction of the magnitudes after the straightening process. We can also observe how the maximum tensile residual stresses remained near the beam's root and the web center area conserved compressive stress. The final stress profile at the flange tips was according the final bending of the beam.

Next figure shows the history of the longitudinal stress in an interior point of the beam. The point chosen was located in the flange center, near the root of the beam, which is the place where the maximum tensile residual stresses were located before and after the straightening process (see Figure 105 and Figure 106).

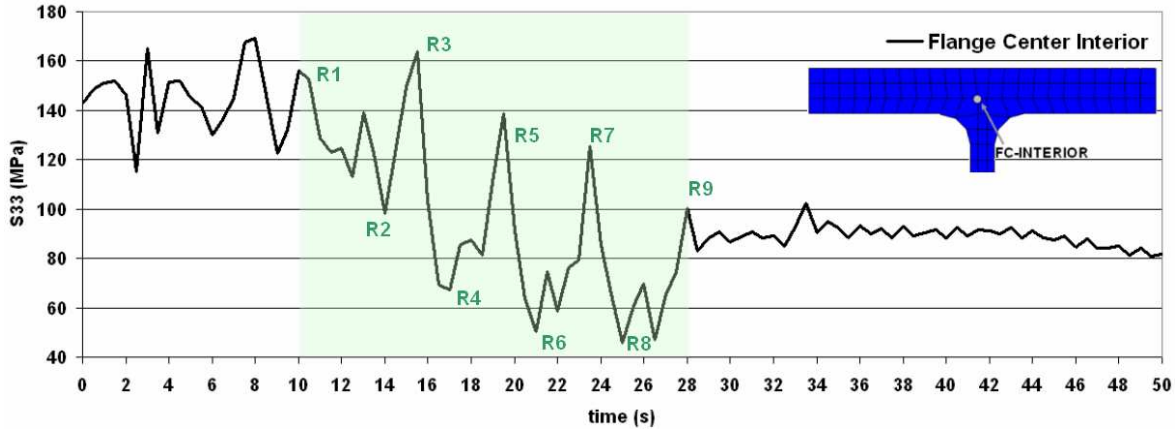


*Figure 107. S33 history of a point located near the root of the beam during the straightening process.*

It is possible to observe in Figure 107 the effect of each straightening rollers and the reduction of the initial residual stresses after the process. In this case the reduction was of 43%. Another characteristic observed at the end of the straightening process is the trend of the residual stresses to decay. The reason could the 'springback' resilience, i.e. the recovery from the elastic deformation after the straightening. Nevertheless, a deeper study is necessary to justify this behaviour.

Nevertheless, regarding the beam's curvature, the reduction was not achieved. In this case, the beam's bending after the straightening was of 11 mm, a value much higher than the initial curvature (5 mm, after cooling). This could mean that maybe the roller deflection were not suited for the initial curvature provided by the cooling process for this case. However, before to arrive to a conclusion, the simulations have to be repeated using more realistic plastic-model parameters (temperature dependent).

Next figures present the longitudinal stresses at the web of a cross section located at the center of the beam while passing through the straightener rollers. The complete set of 'sections' (from 0 to 11) of the experimental test (Figure 91) could be compared as in this case there were values in 'sections' 0, and 1 coming from the cooling process. As before (for the IPE100), the longitudinal stresses (S33) results were obtained by taking the average of the web's elements located in the same perpendicular position, as showed in Figure 96.

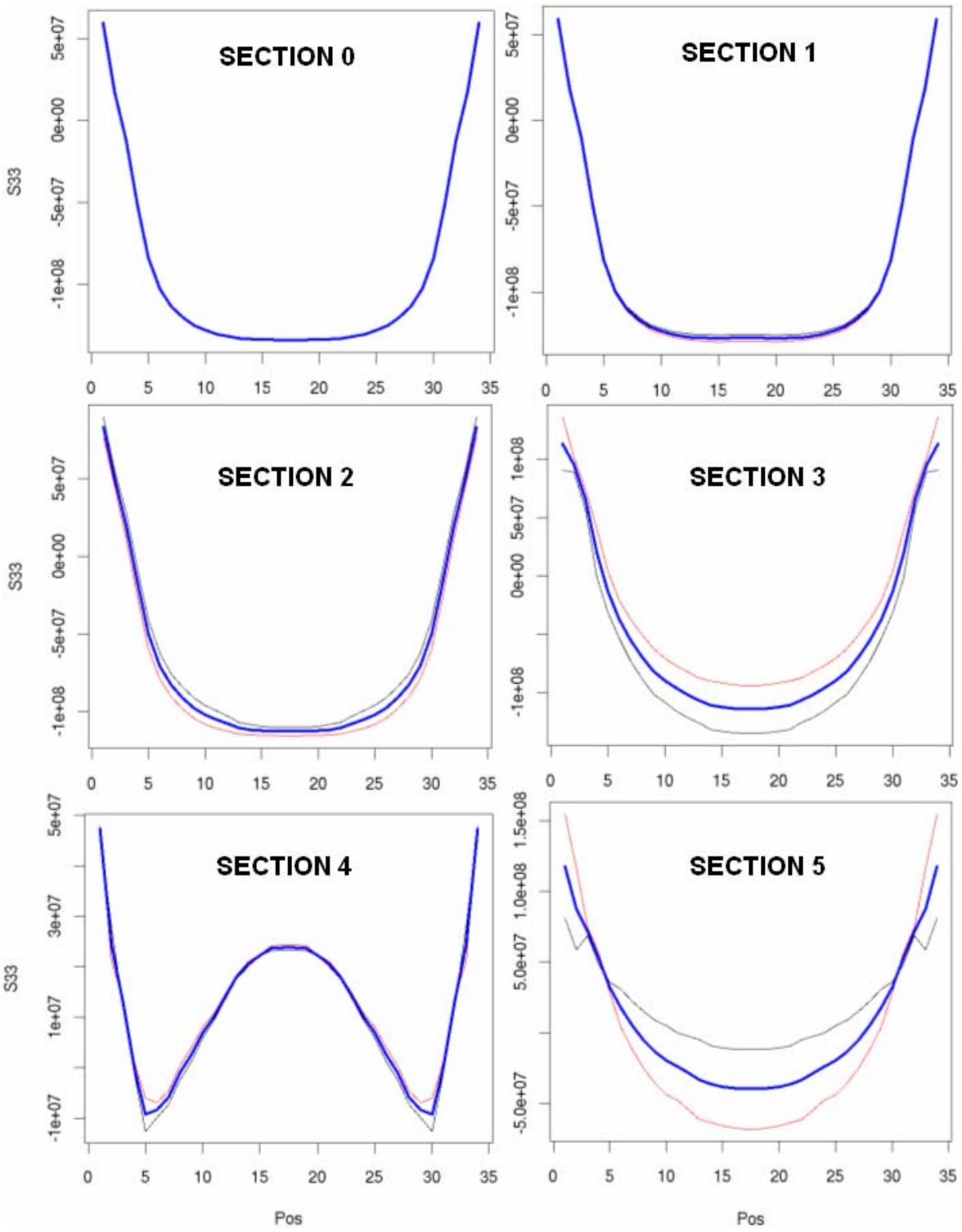


*Figure 108. Longitudinal stresses (in Pa) at the web in 'sections' from 0 to 5 regarding Figure 91.*

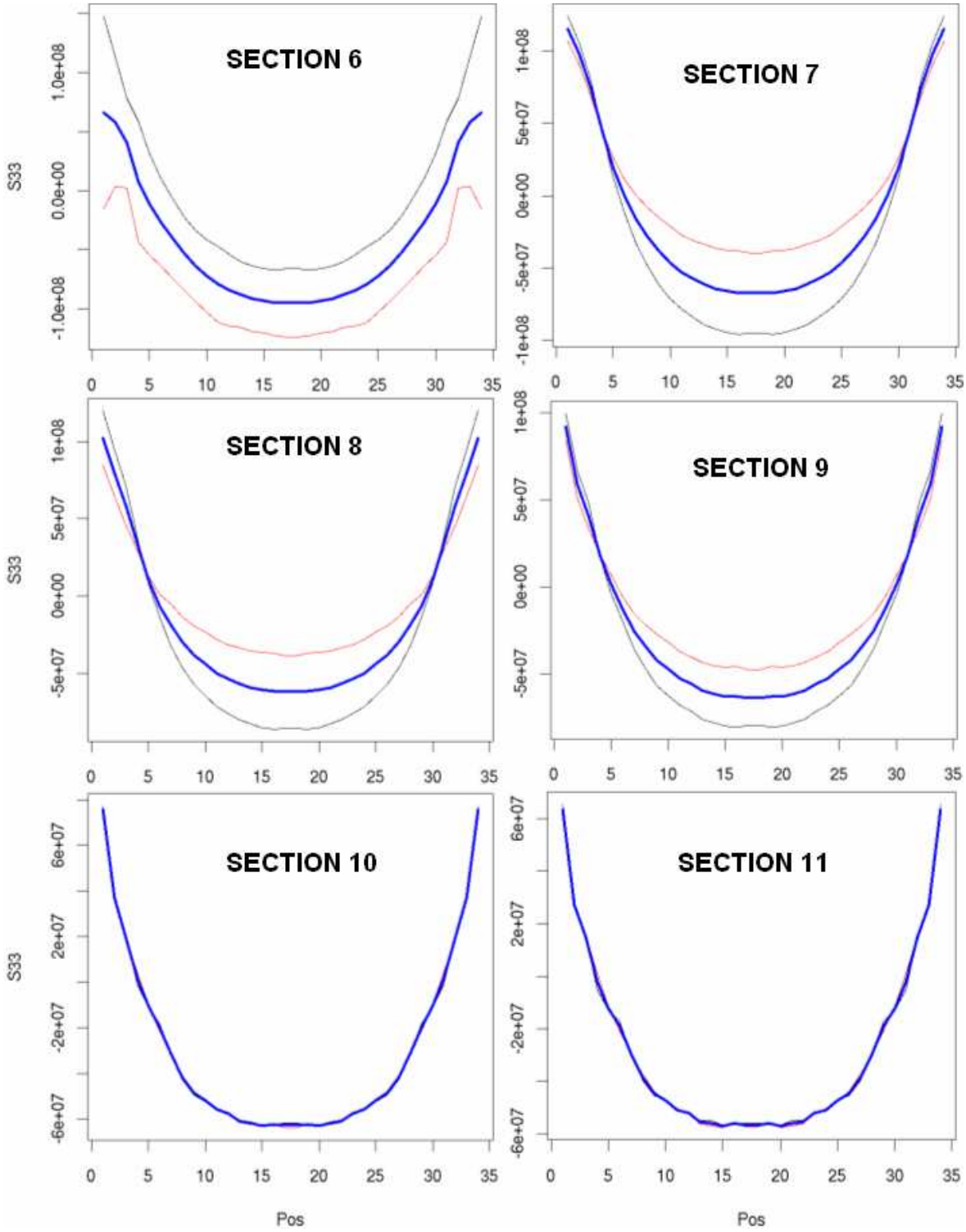


*Figure 109. Longitudinal stresses (in Pa) at the web in 'sections' from 6 to11 regarding Figure 91.*

In all sections, the black and red curves were very close to each other. Also the shapes of the curves were smoother. This means more stability in the model, provided by a smaller "mass scaling" factor. As said before, this could be possible because the roller deflection were less demanding than in the case of the IPE100 *HSM* (chapter 4).

In Figure 108, 'sections' 0 and 1 represents the residual stresses values from the cooling process. The rest of the sections follow very close the shapes of the curves obtained experimentally (Figure 91). In Figure 109, 'sections' 10 and 11 represents the residual stresses after the process. Also, through this graphics is evident how the straightening process reduces the initial residual stresses values. In the web, the reduction was of 57%.

The following graphics in Figure 110 display the longitudinal stresses values of the same cross section but regarding the upper flange of the beam before and after the straightening process.

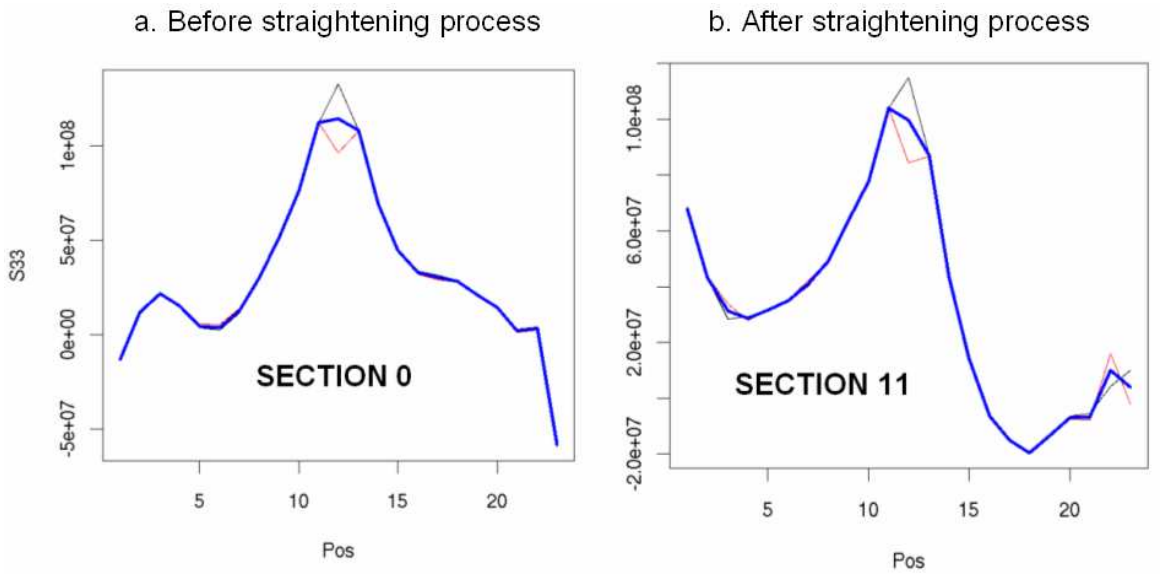


*Figure 110. Longitudinal stresses (in Pa) at the flange of the beam before (graphic on the left side) and after (graphic on the left side) the straightening process.*

The reduction of the residual stresses in this case, regarding the flange, was of 68%.

### 5.2.4 CONCLUSIONS

The coupling of the cooling process and the straightening process for the HEM500 beam has been achieved successfully. The simulation results present good agreement with the experimental data available for a similar process (the *HSM* for the IPE100). The results demonstrate how the initial residual stresses (formed in the cooling process) were reduced significantly by the straightening process. Nevertheless, the curvature was not improved after the process. The main reason could be the lack of plastic-model parameters temperature-dependent. However, the straightening process model was developed considering the inclusion of these parameters, i.e. the model is ready to receive these values without any modification.

## 5.3 STRAIGHTENING PROCESS MODELING FOR THE GROOVED RAIL INCLUDING COUPLING WITH PREVIOUS COOLING PROCESS

### 5.3.1 DESCRIPTION OF THE PROBLEM

The straightening process for the grooved rail studied (Ri60) is in essence the same as for the 'H' and 'I' beams. Nevertheless, this process counts on two straightener machines, one for each of the axis involved in this process. First the rail is straightened about the primary axis through the 'horizontal straightening machine' and successively about the secondary axis through the 'vertical straightening machine. The complete configuration can be seen in Figure 112.

The roller's deflection values were omitted in this case as they represent relevant information for the enterprise. Experimental data regarding the residual stresses after straightening process for the same 10 points evaluated in Chapter 3 were kindly provided by VA.

### 5.3.2 FE-THERMAL-STRESS/DISPLACEMENT MODEL

A rail of 5 m length cooled in rail-by-rail configuration and in standing position was straightened by the horizontal and vertical straightening machines. The rail's linear velocity through the straightener machines was set on 0,5 m/s. The discs were created as Analytical Rigid Surfaced and following the dimensions obtained from VA.

As for the previous case, the initial conditions of the beams, in the sense of temperature, curvature and residuals stresses, were the final results obtained in the cooling process.

Once more, the element used to mesh the beam was the C3D8RT (coupled temperature-displacement continuum solid eight node element), i.e. hexahedral element. The friction coefficient between rollers and beam was set on 0.25. The meshing of the rail can be seen in Figure 111.

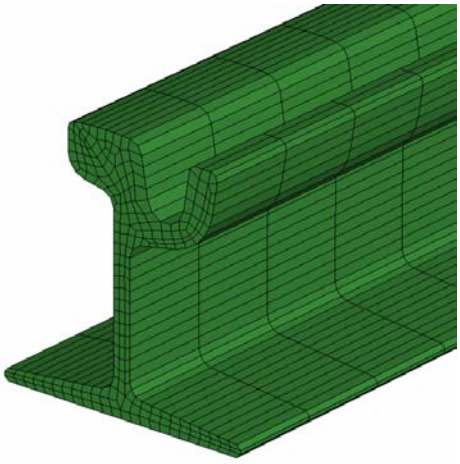

*Figure 111. Detail of the beam's mesh.*

The ABAQUS® control parameters were set in the same way as for the previous straightening model. Nevertheless the mass scaling factor was set in 500 to obtain an acceptable computing time. The plastic model parameters for the steel grade were calculated following the methodology presented in chapter 4, as they were not found in the literature. The values obtained were $C$ = 650 GPa and $\gamma$ = 40. As is previous section, more realistic parameters and also temperature-dependent for the steel EN200 are necessary for a deeper study of the process.

A general view of the FE model assembly can be seen in Figure 112.

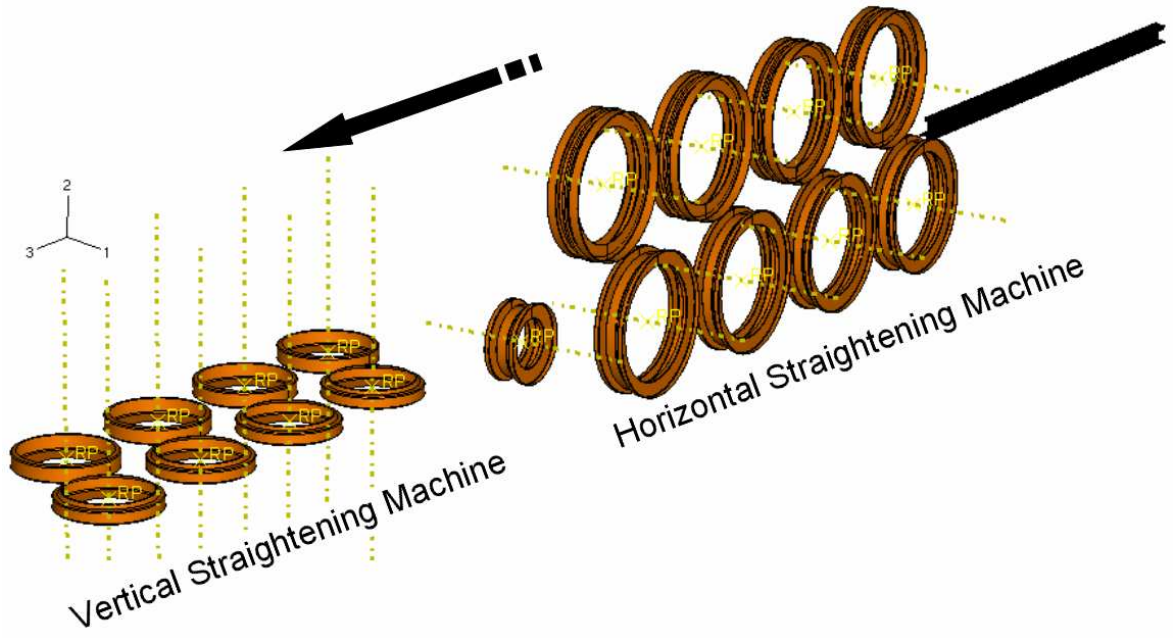


*Figure 112. Assembly of the straightening process FE model for the Ri60 rail.*

### 5.3.3 RESULTS

In the next figure a general view of the initial conditions of straightening process, considering the temperature and stresses values resulting from the cooling process, is displayed. The initial curvatures in the main planes were: 3.6 mm in XZ-plane and 4.1 mm in YZ-plane.

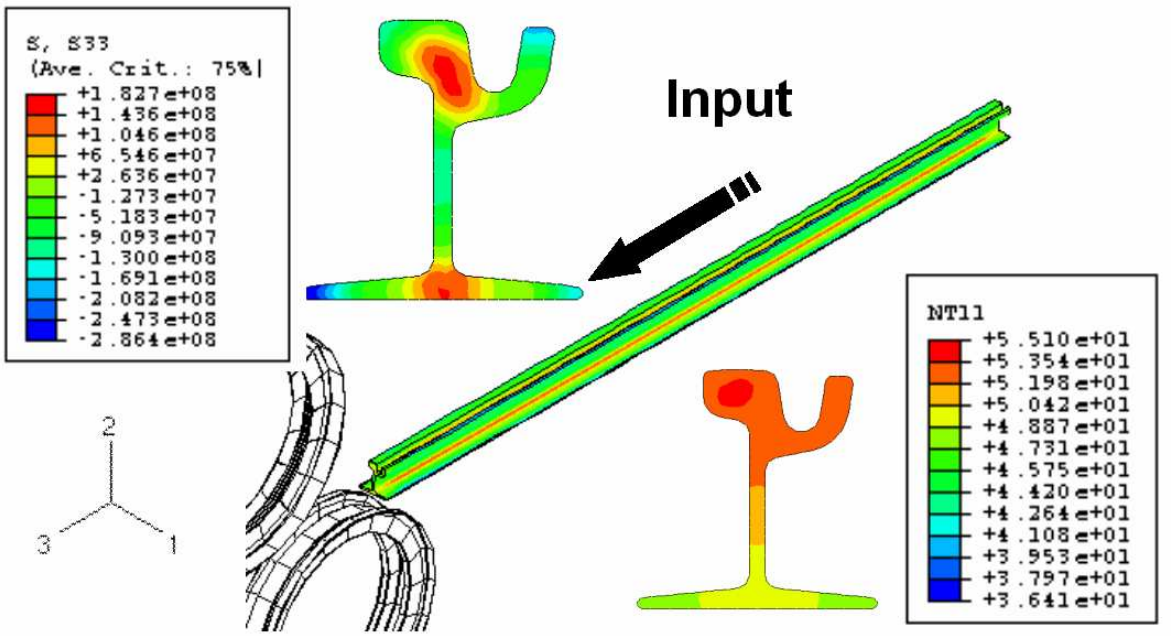


*Figure 113. Temperature (NT11) and longitudinal stresses (S33) at the straightening process input. Initial values taken from the cooling process.*

After the straightening process, i.e. after the rail has passed through both straightening machines (horizontal and vertical), the residual stress contour plot obtained was the one displayed in Figure 114.

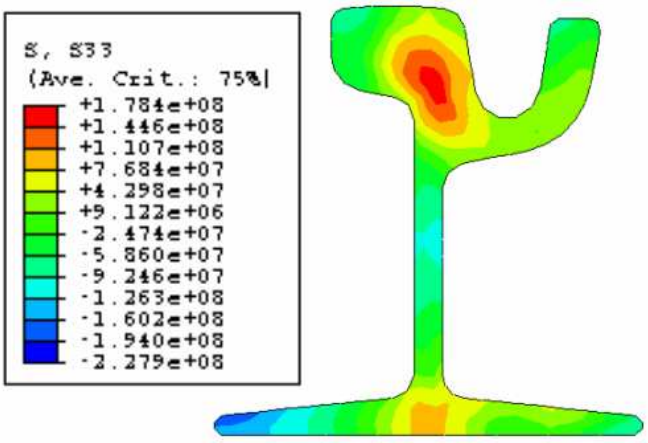


*Figure 114. Residual stresses contour plot of the rail after passing through both horizontal and vertical straightening machines.*

In Figure 114 it can be observed how the maximum tensile and compressive longitudinal residual stress remained in the same areas than before the straightening process (after the cooling process), but with lower magnitudes. Therefore, as well as in the reality the straightening process have reduced the residual stresses produced by the cooling process. Nevertheless, once more, the final curvature was not improved. The final values in the main planes were: 12 mm in XZ-plane and 25 mm in YZ-plane. The reasons could be the same as before, the lack of more realistic plastic-model parameters, temperature-dependent. Again, the model have been developed thinking on this fact and the inclusion of these values will not represent any problem.

Specifically, in order to compare the simulated results with the experimental values available, the residual stresses in some interesting points are presented in Figure 115.

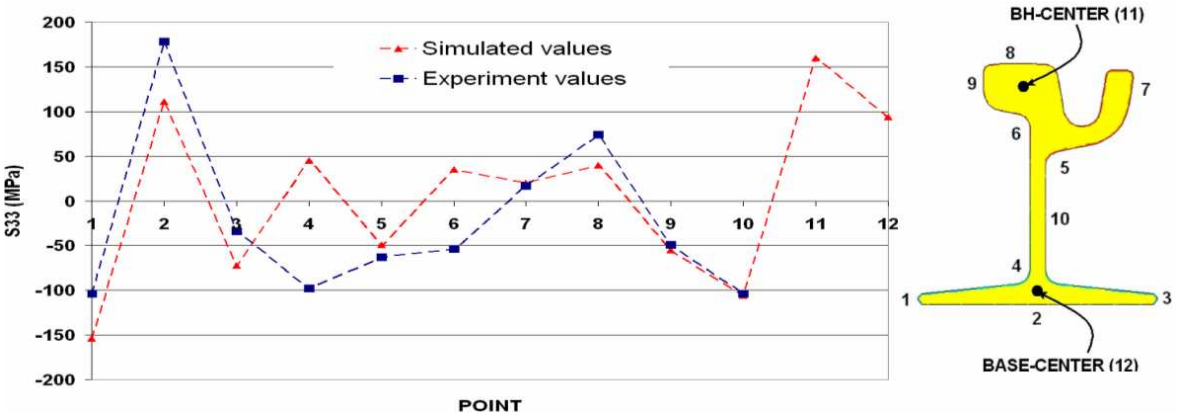


*Figure 115. Comparison of simulated and experimental S33 values for 12 interesting points..*

Most of the points were in agreement with the experimental results provided by VA. Nevertheless, points 4 and 6 seems to be located in areas difficult to measure and therefore the experimental results provided regarding there point were quite unstable.

The time evolution of the longitudinal stresses of point 11 (situated in the center of the big head), at the central cross-section, along the straightening machines is presented in Figure 116. As can be seen in Figure 113 and Figure 114 this point represent the area where the maximum tensile stresses were located, before and after the straightening process.

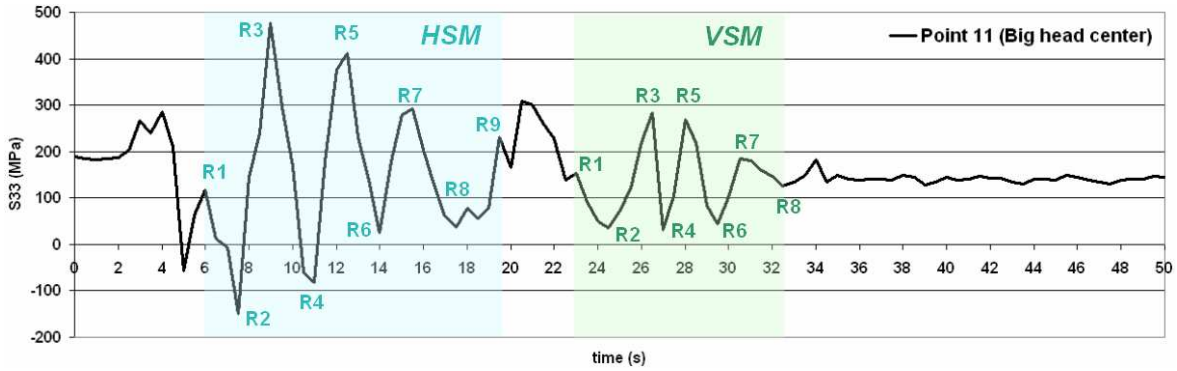


*Figure 116. S33 history of point 11 during the straightening process.*

In Figure 116 it is clear how the initial residual stresses were reduced after the straightening process. Specifically, for this point (point 11) the decrease on the residual stresses was of 28%. Once more, there were some oscillations after the straightening process that need a deeper study.

## 5.4 CONCLUSIONS

The proceeding for coupling the cooling and the straightening processes developed in this chapter demonstrate simplicity and good performance. The simulation time for both long products was also acceptable: 12 days for the HEM500 and 15 days for the Ri60. In this way was possible to integrate both processes as happens in the reality, and made possible the study of the residual stresses formation along these manufacturing processes.

Specifically, for the HEM500, the residual stresses were reduced after the straightening in 57% in the web and 68% in the flange. The shape of the curves and magnitudes showed good agreement with the existing experimental data.

Regarding the Ri60, the 10 surface points studied after the straightening process showed good agreement with the experimental values provided. The simulations also demonstrate the decrease of the residual stresses after the process. A point in the rail's big-head center reduced its residual stress value in 28%.

In both cases simulated (the one for the 'H' beam and the one for the grooved rail), the curvature of the long products were not improved after the straightening process. The answer for this result could be the lack of more realistic parameters for the plastic-model, which have to be also temperature dependent, as the problem demands it. The UR research group, EDMANS, is currently searching a laboratory where to perform the experimental test to find these values. We are aware of the importance of these parameters for a deeper study of the temperature influence in the process. The models were developed considered the addition of these values without further modifications. In addition, and maybe related

to this topic, a deeper study of the residual stresses behaviour after the straightening (oscillation and decreasing of the magnitude) is necessary.

# RESUMEN DEL CAPÍTULO 6

## METODOLOGÍA PARA LA OPTIMIZACIÓN DEL PROCESO DE ENDEREZAMIENTO BASADA EN ALGORITMOS GENÉTICOS

En este capítulo se propone una metodología, basada en el uso de Algoritmos Genéticos, para la optimización del proceso de enderezamiento de perfiles de acero a partir de los modelos con elementos finitos creados en los capítulos previos. La propuesta, basada en técnicas de programación evolutiva, se enfoca en la búsqueda de la mejor posición de los rodillos que proporcione un perfil con tensiones residuales mínimas y una curvatura que esté dentro de una tolerancia de fabricación preestablecida. En este capítulo se ha aplicado la metodología al proceso de enderezamiento del perfil IPE100, pero ésta puede extenderse fácilmente a cualquiera de los perfiles estudiados.

La metodología comienza con la creación de la generación inicial (generación 0) de $N$ individuos (o soluciones). Cada uno de los individuos corresponde a una posición aleatoria de los rodillos 3, 5, 7 y 9 que intervienen en el proceso de enderezamiento. De esta forma, el cromosoma de cada individuo está formado por las posiciones de los cuatro rodillos anteriormente citados.

Una vez creada la generación 0, se simula cada uno de sus individuos mediante el modelo creado en ABAQUS®. Para ello, se modifican las posiciones de los rodillos del modelo según el cromosoma de cada individuos, se procesa con ABAQUS® y se obtienen las tensiones residuales y la curvatura final del perfil simulado.

Después de la simulación de cada individuo, se calcula la función objetivo de cada solución, que involucra las tensiones residuales tanto del ala como del alma del perfil. Se seleccionan las $M$ individuos que menores valores presentan. De ellas, se penalizan aquellas en las que la deformación del perfil no ha pasado por el régimen plástico y/o la curvatura final del mismo ha superado la tolerancia de fabricación propuesta. En conclusión, la mejores soluciones de la generación serán aquella en las que el perfil haya presentado una deformación plástica importante, la curvatura final del mismo no haya superado la tolerancia preestablecida y las tensiones residuales sean las menores posibles.

El proceso de optimización continúa mediante la creación, a partir de las $M$ mejores soluciones de la generación anterior, de otros $N$ individuos correspondientes a la nueva generación. Es decir, ésta se crea mediante operaciones de selección ($M$ mejores de la anterior generación), cruce ($K$ individuos creados por combinación o cruce de los $M$ mejores) y mutación de cromosomas ($L$ individuos obtenidos por mutación). De esta forma, el problema converge a una solución óptima a medida que se simulan sucesivas

generaciones. La ventaja adicional de esta metodología es que se puede contar con varias soluciones que ofrezcan buenos resultados (los mejores individuos de la última generación).

Los valores iniciales de la posición de los rodillos, a partir de los cuales se creó la primera generación, fueron proporcionados amablemente por BFI de acuerdo con pruebas experimentales en su planta piloto *HSM*.

Para implementar esta metodología se desarrolló una aplicación informática mediante programación con diversos lenguajes GNU o software libres (*Bash* en Linux, *R*® y *C*-gcc). Se contó además con varios servidores para agilizar la obtención de las soluciones de cada generación. Y por último, para poder monitorizar la evolución de las generaciones a distancia se creó una herramienta on-line que desplegaba los datos más importantes de cada solución (servidor donde se estaba ejecutando, si había terminado o no de ejecutarse, fecha y hora de finalización y función objetivo). Además contaba con la opción de poder visualizar las tensiones residuales y descargar los archivos solución (.odb). Todo esto ayudó a realizar un seguimiento de la metodología y comprobar de esta forma su buen funcionamiento.

CHAPTER 6

# METHODOLOGY FOR STRAIGHTENING PROCESS OPTIMIZATION BASED ON GENETIC ALGORITHMS

In this chapter a methodology based on genetic algorithm is proposed to improve the straightening process. The methodology expects to be an automatic tool used to find the right rollers' deflections in order to obtain a product with minimum residual stresses and with a bending value into an acceptable tolerance.

Initially the proposal was applied to the IPE100 profile and its straightener machine (the *HSM*). Nevertheless, it was built up in such a way that can be extended to any of the other profiles studied.

In order to test the methodology with several generations a rather coarse mesh and a considerable mass scaling factor was introduced in the simulations.

## 6.1 A BRIEF INTRODUCTION TO GENETIC ALGORITHMS

Genetic algorithms (Mitchell, 1996 and Goldberg, 1989) are systematic methods used to solve optimisation problems. The method applies to such problems the principles of biological evolution, namely: selection of the "fittest", sexual reproduction (cross-over) and mutation.

To explain the optimisation process followed by this technique, suppose we have a mathematical model or function $f(x_1,...,x_n)$ and we want to find a solution $(x_1,...,x_n)$ that maximizes or minimizes that function. First, a basic genetic algorithm creates an initial generation of $N$ individuals of random solutions $G_0(k) = (x_{k11},...,x_{kn})$. Each solution is encoded in chromosomes and evaluated using the model $f(x_1,...,x_n)$ in such a way that the best individuals will be those whose result approaches the desired maximum or minimum. Based on the best individuals (the ones that provide best solutions) a new generation is created and evaluated. A repetitive process is achieved until the result, provided by the best individual of each generation, converges to a value near the desired local optimum.

Generally, each generation of individuals $G_n(k)$ is created using the previous generation $G_{n-1}(k)$ as follow: a small percentage is formed by the best individuals (the "fittest", similar to natural selection theory); other percentage (usually high) is created from the cross-over of chromosomes of individuals from the previous generation (sexual reproduction); and the rest (small percentage) is created randomly altering selected genes of chromosomes from previous generation (mutation).

## 6.2 APPROACH FOR AN AUTOMATIC STRAIGHTENING PROCESS IMPROVEMENT USING GENETIC ALGORITHM.

The proposal, based on evolutive techniques (genetic algorithms), focused on the search for the best positions of rollers number 3, 5, 7 and 9 of the straightening process (see chapter 4 in order to identify these rollers). The beam's bending of the best solution was restricted according to a predefined tolerance value. Another important restriction was to achieve the plastic behavior in several moments during the process. The details of the methodology to achieve all this are explained in the next section.

The methodology was developed using the following freeware:

- Linux shell programming (by means of awk scripts),
- R® (GNU software),
- C programming (by means of gcc, also GNU software).

Combining these tools was possible to attain time and memory efficient execution.

### 6.2.1 METHODOLOGY

1. The optimization process began with the initial generation, named *generation 0*. It was composed by 20 individuals corresponding to different positions for rolls 3, 5, 7 and 9. The position values were random variations (maximum ±5 mm) of the original values provided by BFI: 6, 4.7, 2.8 and 1.3 (all in mm) for the IPE100 straightening process. These random values were assigned in such a way that the position of a roller was always greater than the position of the following roller (descendant order).

   The chromosome of each individual was composed by the position of the four rollers. For example, the first individual, with the original position values {6, 4.7, 2.8, 1.3}, was codified (using 2 integers and 2 decimals) like this: {0600,0470,0280,0130}. The same code but without colon was set as its chromosome: {0600047002800130}.

2. Once the positions for the 20 individuals were set, the program generated 20 ABAQUS's input files (.inp) with each case. Then, these files were given out to the

servers for simulation. The UR research group EDMANS count with 4 dual servers (2 CPUs), so it was possible to simulate 8 cases at the time. The servers uses Linux as operating system

3. The mass scaling and the beam's mesh were such that a computing time of 40 hours was possible for each case. The length of the beam was also reduced to 2 m. In this way we assured small simulation times, risking accuracy. Nevertheless, it was enough as the main goal at this stage was to test the methodology proposed.

4. After the simulation of the 20 individuals of the first generation, the goal function of each case was calculated. The goal function ($J_i$) was directly related to the residual stresses, and was set as the mean value of the residual stresses' absolute value for web and flange of a predefined 1m beam's section, located in the beam's center part. The following formula defines the goal function for individual number *i*:

$$J_i = \frac{1}{n}\left(\sum_{k=1}^{n}\left(\frac{1}{m}\cdot\sum_{h=1}^{m}\left|Sweb_{kh}\right|\right)+\sum_{k=1}^{n}\left(\frac{1}{p}\cdot\sum_{u=1}^{p}\left|Sflange_{ku}\right|\right)\right) \qquad (3)$$

where

*n* is the number of cross-sections into the evaluated beam's section. It depends directly to the meshing established (in our case: *n*=1000/10=100, i.e. 100 cross-sections into 1 m beam with element length of 10 mm.),

*m* is the number of parts in which the web's cross-section is divided (web partitions similar to the experimental sectioning method, also depending on the mesh).

*p* is the number of parts in which the flange's cross-section is divided (web partitions similar to the experimental sectioning method, also depending on the mesh).

*Sweb* is the residual stress of each web's partition.

*Sflange* is the residual stress of each flange's partition.

For example, in Figure 117 the residual stresses curves for the evaluated web's cross-sections for individual number 1 of generation 2 are displayed. The blue curve represents the mean value of all curves and the red curve represents the same mean value but in absolute value. Then, the area under the red curve corresponds to $\frac{1}{n}\sum_{k=1}^{n}\left(\sum_{h=1}^{m}\left|Sweb_{kh}\right|\right)$. In the same way, Figure 118 displays the residual stresses curves for the evaluated flange's cross-sections for the same individual, and therefore the area under the red curve represents

$\frac{1}{n}\sum_{k=1}^{n}(\sum_{u=1}^{p}|Sflange_{ku}|)$. The sum of both areas divided by *m* and *k*, respectively, corresponds to the goal function ($J_i$). The lower the goal function, the better the solution.

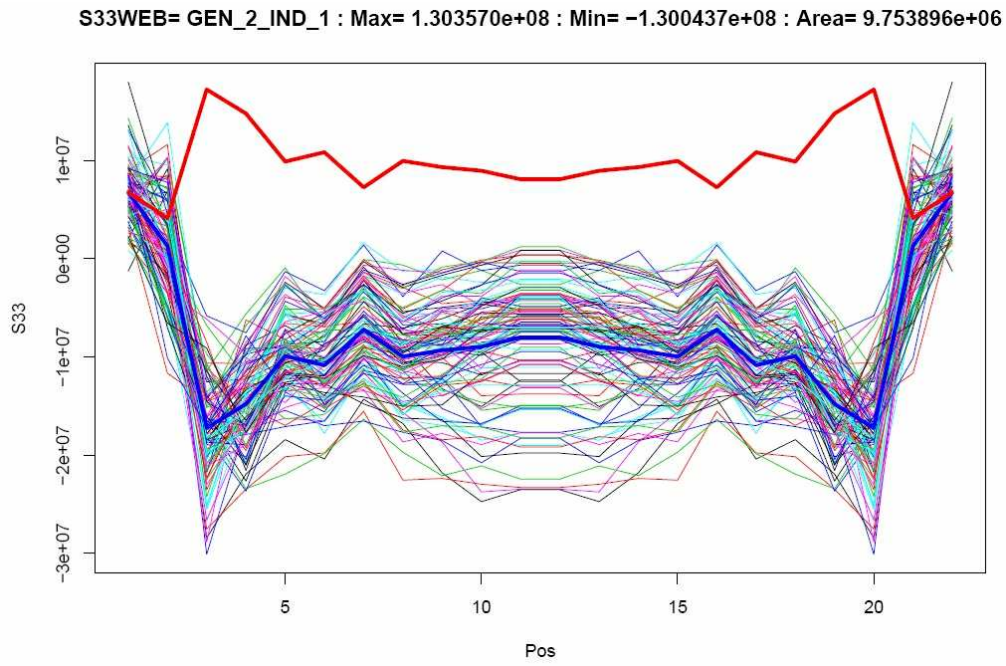


*Figure 117. Residual stresses curves in the 100 (n) central web's cross-sections for individual 1 of generation 2.*

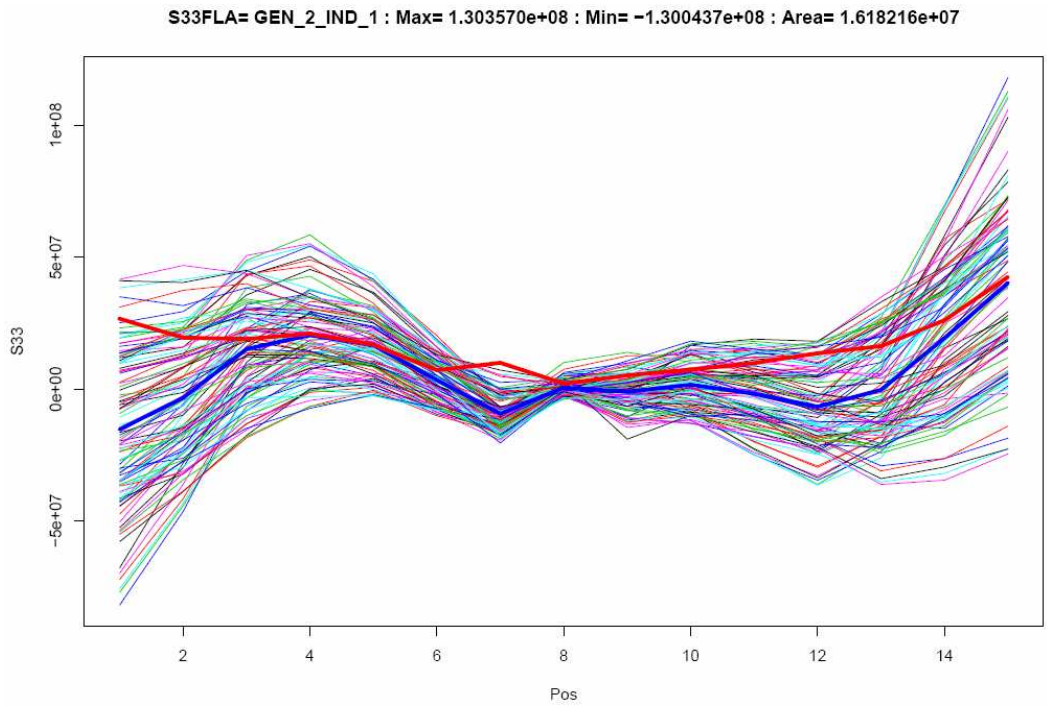


*Figure 118. Residual stresses curves in the 100 (n) central flange's cross-sections for individual 1 of generation 2.*

5. Two restriction were necessary to fulfill to select a case as an acceptable solution:

    a. The beam had has to reach the plastic behavior in several times during the process.

    b. The beam's curvature had to be lower than a predefined value (according to industry tolerances).

6. The first restriction (a) was verified by the number of times the von Mises of a predefined element set crosses over the steel's yield stress value. The elements set was composed by the eight upper and lower elements of the web's center section. The choice of the element set was made in such a way because its members suffer the lower plastic deformation during the process. Then if these elements behave plastically it means that plastic deformation in the rest of the beam is guaranteed. Figure 119 displays the 16 *von Mises* curves for the predefined elements set of individual 1 of generation 2. In blue, the yield stress value. In this case, the yield stress limit have been crossed 66 times (Num=66). The number of times the yield stress limit has to be crossed for a case to be selected as a good one was set in 20. But this value can be changed according to experimental criteria.

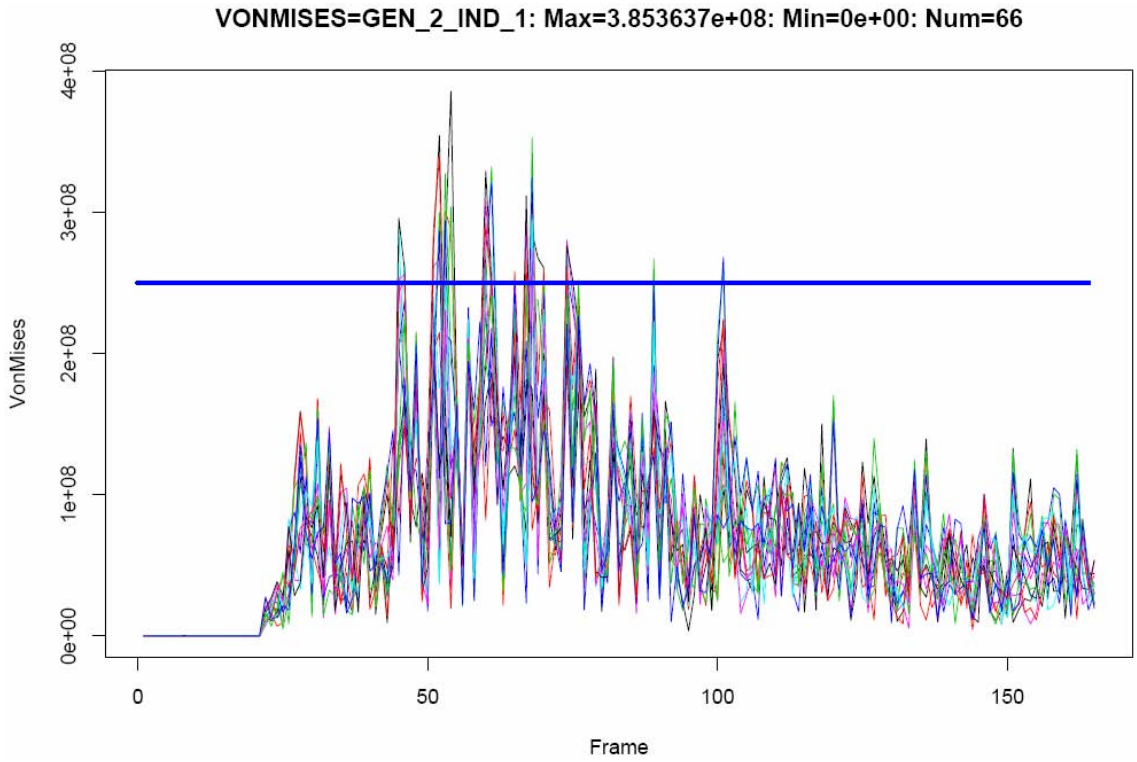


*Figure 119. Von Mises curves for the 16 elements of the web's center for individual 1 of generation 2. In blue the yield stress value.*

7. The second restriction (b) was verified by measuring the beam's sag at the straightening process output. When the sag was lower than a predefined value (set in this case in 2 mm) the case was set as an acceptable case, waiting for restriction (a) to be fulfilled.

8. If one of the restrictions is not fulfill then the goal function is set as infinity.

9. Once all goal functions were calculated, the five best individuals were chosen as parents to create the next generation (generation 1).

10. The 20 individuals of the next generation was created in the following way:

    a. 25% of the generation was composed by the 5 best individuals of previous generation.

    b. 60% was composed by cross-over of the 5 parents. The cross-over process was executed by changing several digits in the chromosomes (roller's positions) between two parents. The position and the number of digits to change were randomly achieved. Fist the method randomly decides if a roller's position is changed or not. If the answer is affirmative, then a position (Pos) between 1 and 4 and a length (L) also between 1 and 4 are randomly obtained. For example, Figure 120 shows the cross-over of two parents with shifts in the position of rollers 3, 5 and 9, changing 3 digits from place 2, 1 digit from place 4, and 2 digits from place 1 respectively. The restriction related to the decreasing order of the values for the rollers' position was always reviewed.

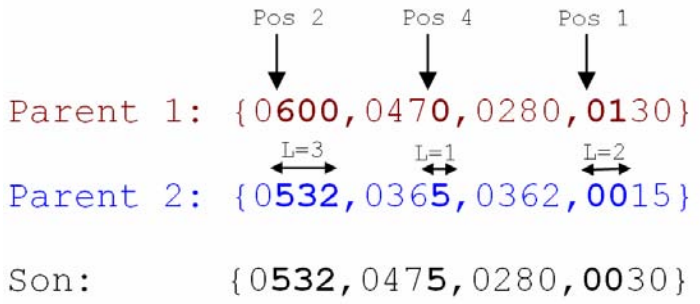


*Figure 120. Cross-over example: shifts in rollers' position 3, 5 and 9, changing 3 digits from place 2, 1 digit from place 4, and 2 digits from place 1 respectively.*

    c. The remaining 15% was obtained by mutation, randomly creating new rollers' positions. In this way was possible to find new solutions in searching areas not explored before.

11. At the end of each generation the method determines the five best individuals to create the next generation, following the guidelines set in the previous point.

After the simulation of several generations, the value of the goal function for the best individual of each generation will converge to a stable value. *The final solution will correspond to the best individual of the last generation*.

### 6.2.2 RESULTS

Table 14 show part of the results for generation 6 and 7 respectively. Only 10 of the 20 individuals of each generation are displayed.

In the tables it is possible to observe the values proposed by the methodology for rollers 3, 5, 7 and 9 (under the 'RollPosYN' label). Also the goal function value is presented (under 'Target value' label). The server number (under the 'Server' label) that solves the case and the date (under the 'Date-Time' label) for the end of the simulation are also provided.

*Table 13. Results values from generation 6.*

| File Name (INP) | Server | RollPosY3 | RollPosY5 | RollPosY7 | RollPosY9 | Target Value | Date-Time |
|---|---|---|---|---|---|---|---|
| GEN_6_IND_1.inp | **Completed** | 6.55 | 4.44 | 2.48 | 0.48 | 10,749,853 | ---------- |
| GEN_6_IND_2.inp | **Completed** | 7.28 | 3.84 | 0.89 | -2.23 | 12,534,279 | ---------- |
| GEN_6_IND_3.inp | **Completed** | 8.45 | 4.74 | 1.98 | -1.76 | 12,818,568 | ---------- |
| GEN_6_IND_4.inp | **Completed** | 7.80 | 3.83 | 1.91 | -2.21 | 12,844,355 | ---------- |
| GEN_6_IND_5.inp | **Completed** | 8.45 | 4.74 | 2.56 | -3.06 | 12,968,028 | ---------- |
| GEN_6_IND_6.inp | **Completed X06** | 7.28 | 4.44 | -0.41 | -7.23 | 19,211,535 | dom oct 29 11:40:56 CET 2006 |
| GEN_6_IND_7.inp | **Completed X16** | 8.45 | 4.74 | 1.91 | -2.26 | 14,701,766 | dom oct 29 11:44:43 CET 2006 |
| GEN_6_IND_8.inp | **Completed X07** | 7.80 | 4.45 | 2.48 | -6.94 | 12,797,452 | dom oct 29 11:49:39 CET 2006 |
| GEN_6_IND_9.inp | **Completed X17** | 7.28 | 3.84 | 1.39 | -3.06 | 13,714,022 | dom oct 29 11:54:21 CET 2006 |
| GEN_6_IND_10.inp | **Completed X08** | 8.45 | 4.74 | 2.58 | -2.76 | 17,978,844 | dom oct 29 11:58:16 CET 2006 |

With this methodology it was possible to obtain 'improved' rollers' positions from the original values provided by BFI: {6.00, 4.70, 2.80 and 1.30} (all in mm). The best solution obtained was: {6.55, 4.44, 2.48, 0.48}.

*Table 14. Results values from the last generation, generation 7.*

**Best Solution**

| File Name (INP) | Server | RollPosY3 | RollPosY5 | RollPosY7 | RollPosY9 | Target Value | Date-Time |
|---|---|---|---|---|---|---|---|
| GEN_7_IND_1.inp | **Completed** | 6.55 | 4.44 | 2.48 | 0.48 | 10,749,853 | ---------- |
| GEN_7_IND_2.inp | **Completed** | 8.45 | 4.69 | 1.96 | -2.22 | 12,398,227 | ---------- |
| GEN_7_IND_3.inp | **Completed** | 8.45 | 4.74 | 2.58 | -1.76 | 12,501,071 | ---------- |
| GEN_7_IND_4.inp | **Completed** | 7.28 | 3.84 | 0.89 | -2.23 | 12,534,279 | ---------- |
| GEN_7_IND_5.inp | **Completed** | 7.80 | 4.45 | 2.48 | -6.94 | 12,797,452 | ---------- |
| GEN_7_IND_6.inp | **Completed X06** | 7.28 | 3.84 | 1.59 | -1.76 | 12,223,815 | jue nov 2 08:32:51 CET 2006 |
| GEN_7_IND_7.inp | **Completed X16** | 7.18 | 4.70 | 2.48 | 0.48 | 19,249,658 | jue nov 2 08:36:23 CET 2006 |
| GEN_7_IND_8.inp | **Completed X07** | 8.45 | 4.70 | 2.48 | -1.94 | 15,435,968 | jue nov 2 08:40:04 CET 2006 |
| GEN_7_IND_9.inp | **Completed X17** | 7.28 | 3.84 | 1.59 | -2.23 | 14,409,013 | jue nov 2 08:43:58 CET 2006 |
| GEN_7_IND_10.inp | **Completed X08** | 8.45 | 4.74 | 2.51 | -1.76 | 18,226,159 | jue nov 2 08:47:41 CET 2006 |

Logically, the proposed values have to be tested in the *HSM* pilot plan to be able to assure that they provide better results. With experimental tests the methodology could be reviewed and improved thinking on an industrial application.

In Figure 121 the evolution of the goal function for the 'best' and 'second best' individuals are displayed. The advantage of a methodology based in genetic algorithm is that the user can count with several 'good' solutions to test.

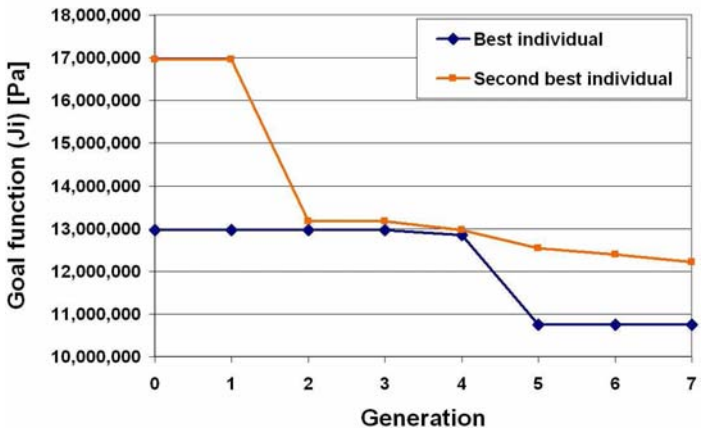


*Figure 121. Evolution of the goal function for the 'best' and 'second best' individuals throughout the optimization process.*

In the figure is possible to observe how the goal function of the best individual converges to a stable value after generation 5. The final goal function value for the best solution was 10.75 MPa. The 'best' solution provided a bending of 2 mm.

The residuals stresses at web and flange are displayed in Figure 122 and Figure 123.

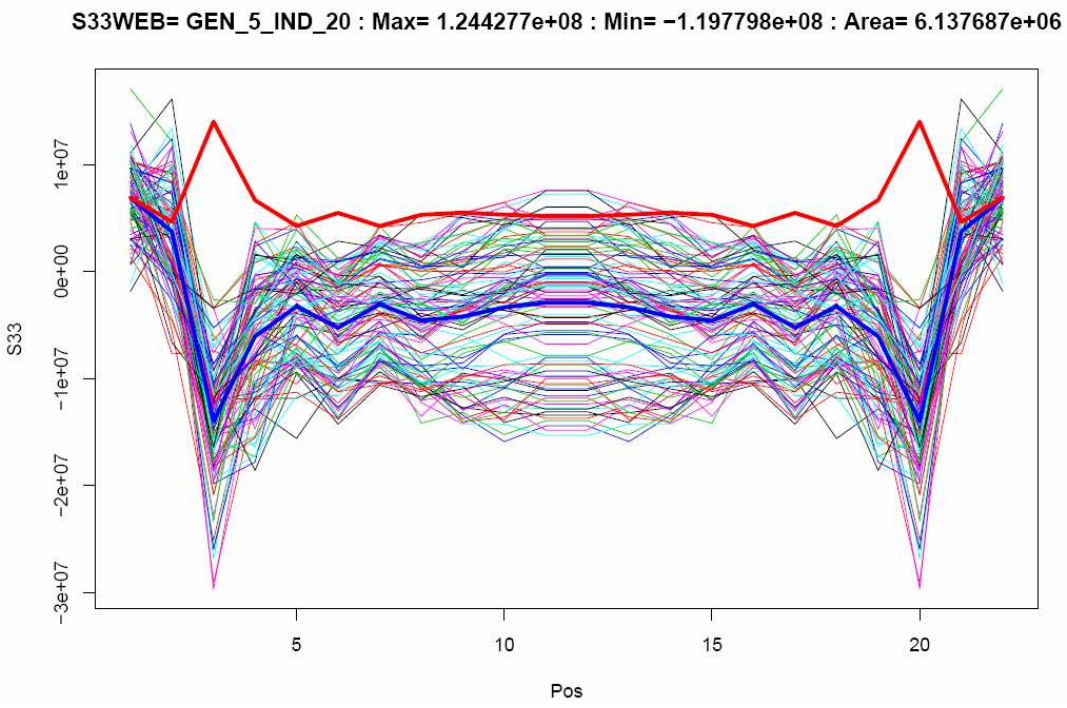


*Figure 122. Residual stresses curves in the 100 (*n*) central web's cross-sections for the 'best' solution (individual 20 of generation 5).*

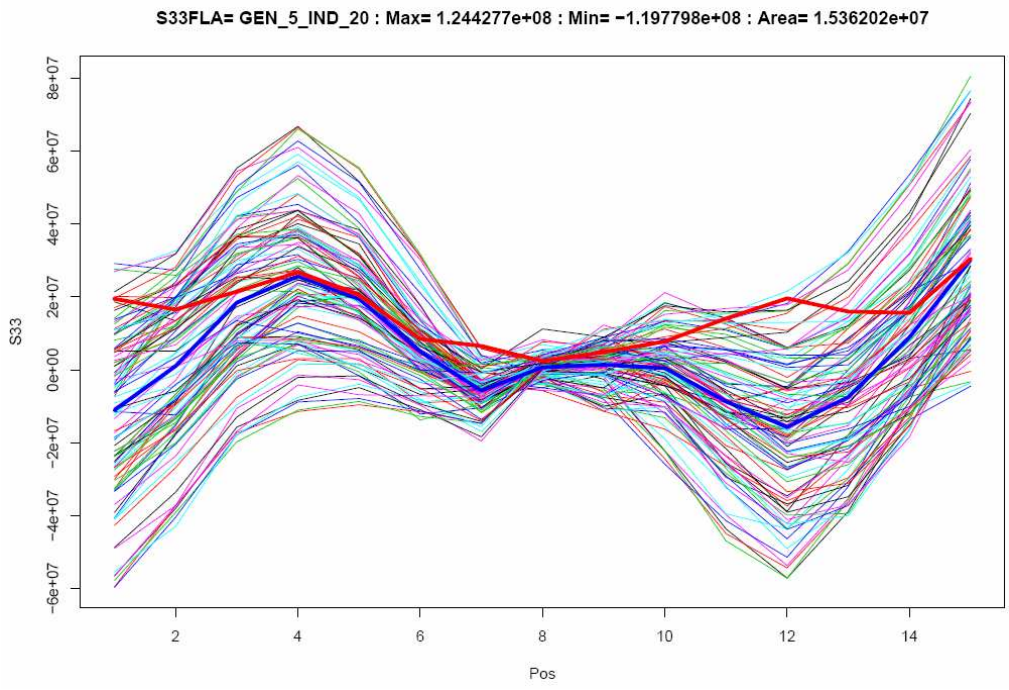


*Figure 123. Residual stresses curves in the 100 (*n*) central flange's cross-sections for the 'best' solution (individual 20 of generation 5).*

The 'best' solution provided lower residual stresses, represented by the goal function, than the original solution. The goal function for the original solution was 19.20 MPa against 10.75 MPa of the best solution. Therefore the improvement was of 44%.

The plastic behavior was assured because the yield stress limit was crossed 21 times (see Figure 124).

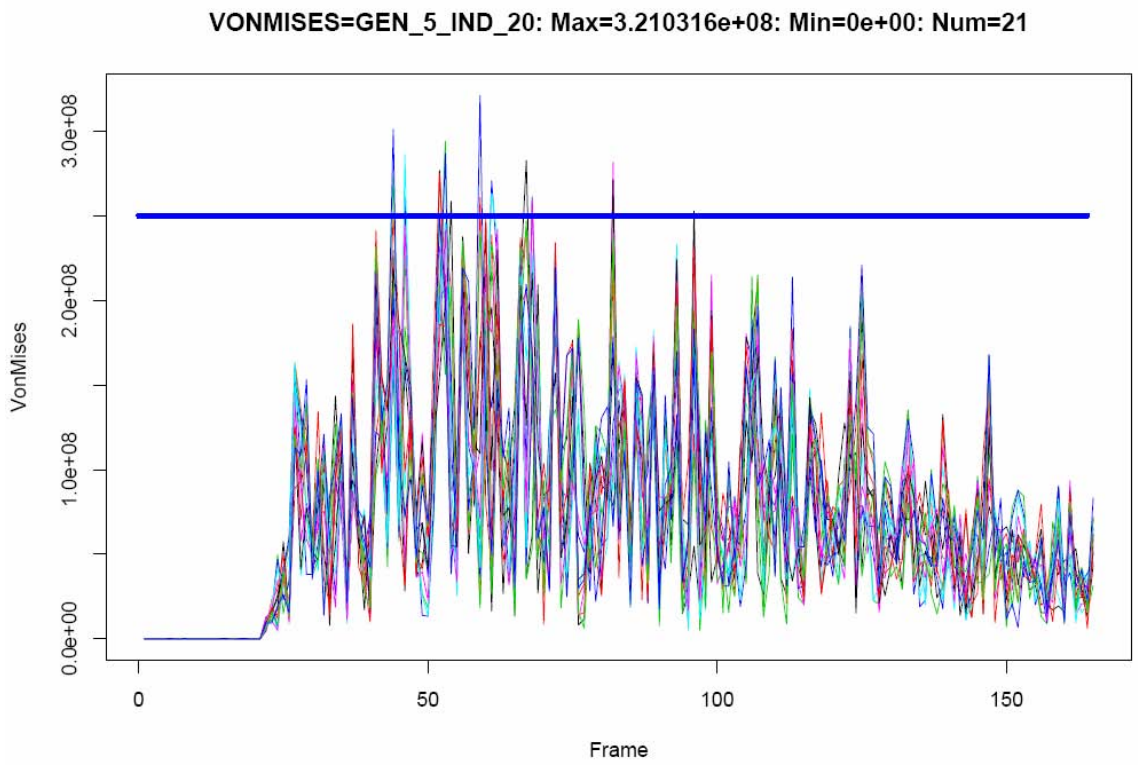


*Figure 124. Von Mises curves for the 16 elements of the web's center for the 'best' solution (individual 20 of generation 5). In blue the yield stress value.*

## 6.3 AN ON-LINE-TOOL TO MONITOR THE OPTIMIZATION PROCESS

To make possible the monitoring of the partial and total results obtained from the methodology exposed, an on-line tool based on PHP and R® have been created.

Through this tool the user can observe the evolution of the process for each generation, knowing which individuals have been already simulated by the servers and their results: rollers' positions, residual stresses graphics for web and flange, bending and von Misses values in a predefined cross-section. The user is also able to download the input file (.inp) and result file (.odb) of each individual.

The informatics tool is located and working in the follow address:

http://193.146.235.220/GENETICOS/leer.php?generacion=2

The user can choose which generation to analyze by putting the generation's number at the end of the address. For example, in the address above, the solutions for generation number 2 will be displayed (see also figure).

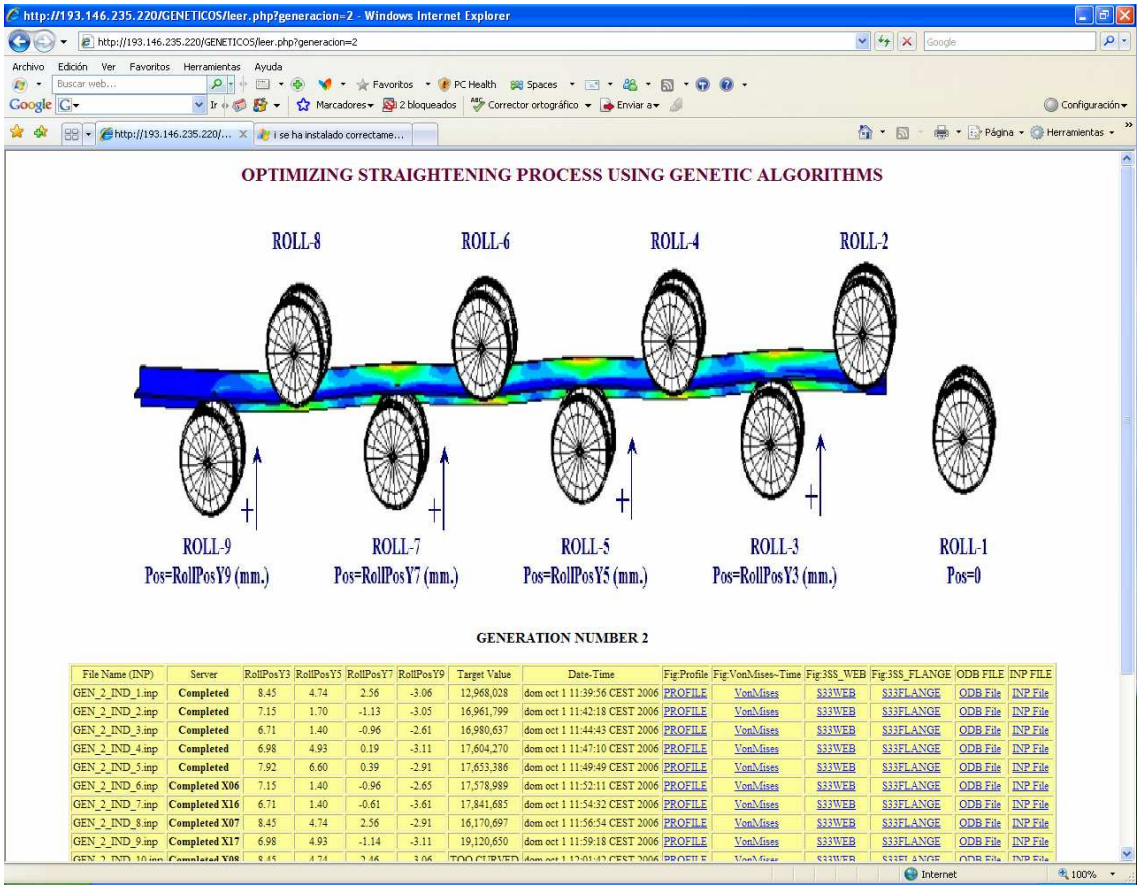


| File Name (INP) | Server | RollPosY3 | RollPosY5 | RollPosY7 | RollPosY9 | Target Value | Date-Time | Fig:Profile | Fig:VonMises-Time | Fig:3SS_WEB | Fig:3SS_FLANGE | ODB FILE | INP FILE |
|---|---|---|---|---|---|---|---|---|---|---|---|---|---|
| GEN_2_IND_1.inp | **Completed** | 8.45 | 4.74 | 2.56 | -3.06 | 12,968,028 | dom oct 1 11:39:56 CEST 2006 | PROFILE | VonMises | S33WEB | S33FLANGE | ODB File | INP File |
| GEN_2_IND_2.inp | **Completed** | 7.15 | 1.70 | -1.13 | -3.05 | 16,961,799 | dom oct 1 11:42:18 CEST 2006 | PROFILE | VonMises | S33WEB | S33FLANGE | ODB File | INP File |
| GEN_2_IND_3.inp | **Completed** | 6.71 | 1.40 | -0.96 | -2.61 | 16,980,637 | dom oct 1 11:44:43 CEST 2006 | PROFILE | VonMises | S33WEB | S33FLANGE | ODB File | INP File |
| GEN_2_IND_4.inp | **Completed** | 6.98 | 4.93 | 0.19 | -3.11 | 17,604,270 | dom oct 1 11:47:10 CEST 2006 | PROFILE | VonMises | S33WEB | S33FLANGE | ODB File | INP File |
| GEN_2_IND_5.inp | **Completed** | 7.92 | 6.60 | 0.39 | -2.91 | 17,653,386 | dom oct 1 11:49:49 CEST 2006 | PROFILE | VonMises | S33WEB | S33FLANGE | ODB File | INP File |
| GEN_2_IND_6.inp | **Completed X06** | 7.15 | 1.40 | -0.96 | -2.65 | 17,578,989 | dom oct 1 11:52:11 CEST 2006 | PROFILE | VonMises | S33WEB | S33FLANGE | ODB File | INP File |
| GEN_2_IND_7.inp | **Completed X16** | 6.71 | 1.40 | -0.61 | -3.61 | 17,841,685 | dom oct 1 11:54:32 CEST 2006 | PROFILE | VonMises | S33WEB | S33FLANGE | ODB File | INP File |
| GEN_2_IND_8.inp | **Completed X07** | 8.45 | 4.74 | 2.56 | -2.91 | 16,170,697 | dom oct 1 11:56:54 CEST 2006 | PROFILE | VonMises | S33WEB | S33FLANGE | ODB File | INP File |
| GEN_2_IND_9.inp | **Completed X17** | 6.98 | 4.93 | -1.14 | -3.11 | 19,120,650 | dom oct 1 11:59:18 CEST 2006 | PROFILE | VonMises | S33WEB | S33FLANGE | ODB File | INP File |

*Figure 125. One of the windows (for generation 2) of the informatics tool made for the on-line monitoring of the genetic algorithm optimization process.*

## 6.4 CONCLUSIONS

The methodology has proved to work properly, finding a solution, in theory, better than the original proposal. Nevertheless, it is important to validate these results by experimental tests on the pilot plant. Furthermore, the straightening model has to be improved in the sense of the meshing, mass scaling factor and plastic-model parameters, in order to obtain more realistic results in the simulation of the cases. In addition, it is important to discus the approach with the experts of the industries involved to adapt the methodology to their particular necessities. Beside, the methodology could be improved by means of clusters parallelization.

# RESUMEN DEL CAPÍTULO 7

## CONCLUSIONES

En el presente trabajo fueron desarrollados los modelos basados en elementos finitos (EF) de dos procesos secuenciales de fabricación de perfiles de acero. Los procesos modelados fueron el enfriamiento y el enderezamiento, para una viga 'H' (HEM500) y un rail ranurado (Ri60). Los resultados de las simulaciones fueron comparados con gran cantidad de datos experimentales y con las observaciones en planta, mostrando una concordancia aceptable.

El proceso de enfriamiento fue simulado tratando de incorporar las condiciones reales de la planta. Para poder contar con estos valores fue necesario realizar mediciones de campo de las condiciones ambientales. Ambas mesas de enfriamiento estudiadas (la del perfil 'H' y la del rail Ri60) fueron modeladas utilizando FLUENT® y ABAQUS®. Los modelos EF pudieron explicar la evolución de las temperaturas, tensiones y curvaturas durante el enfriamiento. Gracias al empleo de FLUENT® no fue necesario especificar el coeficiente de película o los factores de forma, ya que este software es capaz de calcularlos a partir de las propiedades de los perfiles (geometría, propiedades del material y temperatura) y las condiciones de contorno especificadas. Esto hizo que los modelos desarrollados tuvieran un carácter más realista que los presentados hasta ahora en la literatura consultada. Sin embargo, esta solución nos obligó a comunicar ambos softwares mediante un programa de conversión de resultados que denominamos *conv_flu_aba.sh*.

Los procesos de enderezamiento para los perfiles IPE100, HEM500 y Ri60 también fueron modelados. En particular, los procesos de enfriamiento y enderezamiento fueron acoplados para los perfiles 'H' y Ri60. De esta manera, fue posible modelar el proceso de enderezamiento incluyendo como condiciones iniciales del perfil la temperatura, tensiones y curvatura producto del proceso de enfriamiento. Esto representa una distinción respecto de la bibliografía consultada, donde lo común es simular ambos modelos por separado. Los modelos del proceso de enderezamiento fueron desarrollados utilizando ABAQUS®. Las simulaciones de estos modelos fueron comparadas con los datos experimentales disponibles, observándose gran similitud. Sin embargo, está clara la necesidad de mejorar y completar los parámetros del modelo plástico, que además deberían ser dependientes de la temperatura.

Por medio de los modelo EF fue posible observar lo que ocurre dentro de los perfiles estudiados tanto en el enfriamiento como en el enderezamiento, ofreciendo información adicional a las temperaturas superficiales y tensiones residuales conseguidas experimentalmente.

Con estos modelos se pretende proporcionar a los investigadores e ingenieros de procesos de una herramienta flexible para el estudio integrado de estos procesos y de esta manera poder diseñar estrategias que reduzcan las tensiones residuales y curvatura en el producto final.

Otro aporte interesante fue la propuesta de una metodología basada en algoritmos genéticos para mejorar de manera automática el proceso de enderezamiento. Esta metodología se centra en encontrar las deflexiones adecuadas de los rodillos que proporcionen un producto con tensiones residuales mínimas a la vez que una curvatura también mínima. Además, la metodología fue totalmente desarrollada utilizando software libre, de forma que pudiera ser implementada por cualquier usuario interesado.

CHAPTER 7

# CONCLUSIONS AND FURTHER RESEARCH LINES

## 7.1 CONCLUSIONS

1. In this dissertation, the Finite Element (FE) models for the cooling process and straightening process for the manufacturing of two important steel long products, the 'H' and Ri60 profiles, have been developed. Both models were tested successfully comparing them to experimental values and observations from the real plants.

2. The cooling process has been simulated according to real plant conditions. To attain this was necessary to carry out field measurements of the ambient conditions. Both cooling beds (the one for the 'H' section and the one for the rail) were modeled using FLUENT® and ABAQUS® software. Thank to the use of FLUENT® there was no need to specify the film heat transfer coefficient or view factors, as FLUENT® calculates them from the profile's properties (geometry, material and temperature) and the surrounding conditions. This made the models developed been more realistic than the models presented in the consulted literature.

3. In this way the FE models could explain the evolutions of the temperatures and stresses during the cooling process. In particularly, it was interesting to observe the evolution of the stresses in the interior parts of the sections, and how these stresses produce the resulting curvature. Moreover, the simulations demonstrated the residual stresses formation showing the critical moments (changes of stresses signs) along the cooling process. This knowledge can allow the researchers and plant engineers the development of cooling strategies to improve the residual stresses and final bending.

4. Two cooling configurations were simulated and compared in the cooling of the grooved rail: cooling in a vertical position and cooling in a lie-down position. There were some differences in the residual stresses obtained and the tendency seems to indicate that, in general, the configuration giving higher residual stress values was the lie-down position.

5. The straightening process for several profiles: IPE100, HEM500 and Ri60, have been also developed. The simulation results have been compared successfully with the experimental data available. The FE models could explain the evolution of not only the surface stresses but the inner one, while the product was cyclically bended by the rollers. To achieve a realistic model was necessary to made multiples adjustments in the ABAQUS' control parameters until reach acceptable results and computing times. It was critical the meshing of the sections, the set of the mass scaling factor and the plastic model. The best option to the plastic model was the nonlinear isotropic/kinematic hardening model (which is the Chaboche model with only considering the first coefficient).

6. In general, the material properties for the range of the studied temperature were very difficult to find. Nevertheless, the elastic behavior and the thermal properties were successfully found. However, the parameters of the plastic model were not located in any literature consulted. Therefore, the parameters were calibrated from the available experimental results obtained for only ambient temperature. In order to make possible the further study of the straightening process for several initial temperatures it is necessary to count with these parameters for the range of temperatures analyzed. The FE models developed for the straightening processes are ready to receive these parameters, without any modification, as they have been developed considering this fact.

7. In addition the coupling of both processes has been carried out, completing the modelling of these sequential processes. In this way was possible to observe the influence of the finishing state of the sections from the cooling process on the straightening process in the sense of final temperature, residual stresses and bending. The usual proceeding to model the straightening process observed in the literature is to not consider the residual stresses, temperature profile and final bending obtained after cooling process. The coupling of the processes allows the track of the residual stresses from their very beginning to their final state after the straightening process. All this allow the researchers and engineers to develop global strategies integrating both processes.

8. Through the coupling of the cooling process and the straightening process was possible to observe how the residual stresses are reduced and homogenized after the straightening process.

9. The FE-thermal and stress/displacement straightening models developed allow the simulation of the straightening process taking into account several initial conditions in the sense of temperature, residual stresses and bending coming

form the cooling process. Also the rollers' deflections can be easily changed. In this way is possible to study the process for different configurations and initial conditions in a deeper manner. Nevertheless, suited plastic model parameters ($C$ and $\gamma$) for the material behaviour in the range of interesting temperatures are still required.

10. A methodology based on genetic algorithms to automatically improve the straightening process in the sense of roller deflections has been developed. The programming was based totally on free software in order to be easily implemented for any user. The methodology was tested with the data and model of the IPE100-straightening process (BFI's pilot plant *HSM*). Starting with the suggested roller deflections the methodology performed properly and found a solution, in theory, with better characteristics than the original scheme. However, it is clear that these results have to be validated by experimental tests on the pilot plant. Furthermore, the straightening model has to be improved in the sense of the meshing, mass scaling factor and plastic model parameters, in order to obtain more realistic results in the simulation of the cases. In addition, it is important to discuss the approach with the plant engineers to improve the methodology according to their particular necessities.

## 7.2 FURTHER RESEARCH LINES

1. With the cooling process FE models it would be possible to test different strategies to reduce the residual stresses formation, as is in this part of the manufacturing process where the residual stresses start to develop. Some strategies as to put a plate over the beam to homogenize the temperature profile or to inject water in the root zones during the initial stage of the cooling are been tested currently.

2. Another interesting research line would be the incorporation in the cooling process models of the accelerated cooling system in the way of water showers. Most of the industries count on this type of systems to speed up the cooling of the profiles when the production rate demands it.

3. Model and simulate the behaviour of the beams when using especial disc in the straightening process as the Flange Supported disc (or FS disc, patented by BFI). Comparison of the results with both discs, conventional and FS, will be interesting. Also is considered interesting to simulate the roller axis titling.

4. A deeper study of the residual stresses behaviour after straightening is also considered interesting for further research. The oscillations and time decreasing of the residuals stresses must be analysed.

5. It is considered very important to continue the research on the plastic-model parameters, for the interesting range of temperatures. In this way, several laboratories for the required experimental test have been consulted. These values are fundamental to know how the temperature of the long product influences the straightening process.

6. Improve the genetic-algorithm-based-methodology consulting the plant expert, and in this way adapting it to the industry necessities. Apply the genetic algorithm methodology to the 'H' and grooved rail profiles. Also test the methodology in the 'I' and 'H' profiles incorporating the Flange Supported disc.

7. Furthermore, it is considered important the development of a software to be able to configure and manage parallelization of the genetic algorithm computing.

8. The straightener FE models could be used as a tool to develop new strategies in order to improve the process, not only in the sense of roller's deflexions and adequate initial temperatures but to test new discs designs and configurations. For example it would be interesting to employ artificial intelligence tools (genetic algorithms, neural networks, etc.) for optimize the discs shapes designs.

# REFERENCES


ABAQUS Analysis User's Manual (2005), version 6.5.

Abouaf M., Chenot J. L., Marcelin J. L. (1983), "A two-dimensional finite element idealization for thermo-elastic deflection in beams", *Int. J. Numer. Meth. Eng.*, 19, pp. 1453-1465.

Alpsten Göran (1967), "Egenspänninggar i varmvalsade stålprofiler" (Residual stress in hot rolled steel profiles), Institutionen för Brobyggnad, Kungliga Tekniska Högskolan, Stockholm, Sweden.

Alpsten Göran (1970), "Egenspänninggar of Materialhällfasthet H Kallriktade Bredflänsprofiler" (Residual Stress and Mechanical Properties of Cold-Straightened H Shapes), Jernkont. Ann. 283-154, pp. 255-283.

Argyris J., Balmer H., Doltsinis J. and William K. (1971), *Finite element analysis of thermomechanical problems*, in: Proceedings 3rd Conference on Matrix Methods in Structural Mechanics, Wright-Patterson Air Force Base, Dayton, OH.

Basu J., Srimani S. L., Gupta D. S. (2004), "Rail behaviour during cooling after hot rolling", *Journal of Strain Analysis for Engineering Design*, v.39, no.1, pp. 15.

Besuner P. (1978), "Fracture mechanics analysis of rail with shell-initiated transverse crack", *Rail Steels-Developments, Processing and Use*, ASTM STP 644 (D.H. Stone and G.G. Knupp, eds.), pp. 303-329.

Boyadjiev I.I., Thomson P.F., Lam Y.C. (1996), "Computation of the diffusional of continuously cooled austenite for predicting the coefficient of thermal expansion in the numerical analysis of thermal stress", *ISIJ Int.*, v. 36, no. 11, pp. 1413–1419.

Boyadjiev I.I., Thomson P.F., Lam Y.C. (2004a), "Prediction of the deflection and residual stress in controlled cooling of hot-rolled steel beams including load and arbitrary support. Part I. Computational model", *Journal of Material Processing Technology*, 147, pp. 370-376.

Boyadjiev I.I., Thomson P.F., Lam Y.C. (2004b), "Prediction of the deflection and residual stress in controlled cooling of hot-rolled steel beams including load and arbitrary support. Part II. Experimental validation and application", *Journal of Material Processing Technology*, 147, pp. 268-275.

Brünig M. (1989), "Ein Finite-Element-Modell zur numerishen Simulation des Rollenrichtens von schweren Profilen (A finite-element-model for the simulation of the roller straightening of heavy profiles)", Mitteilung 89-5, Ruhr-Univensität Bochum, Germany.

Cannon D. (2003), Rail defect management, Final Report – Part B, Union Internationale des Chemins de fer World Excecutive Council, Join Research Project 1 (JRP1).

Comini G., Del Guidice S., Lewis R., Zienkiewicz O. (1974), "Finite element solution of non-linear heat conduction problems with special reference to phase change", *International Journal of Numerical Methods*, Engrg. 8, pp. 613-624.

Die Eisenbahnschiene (The railway rail) (1977), (F. Fastenrath ed), Verlag Wihelm Ernst & Sohn, Berlin-München-Düsseldorf, Germany, pp. 37-38.

ERRI Project D 156 Report 4 (1987), *Studies concerning the measurement and improvement of the level of residual stresses*, European Rail Research Institute (www.erri.nl), Utrecht, The Netherlands.

ERRI Project D 173 Report 4 (1993), *Residual stresses measurement on naturally hard and two head-hardened rails by neutron diffraction*, European Rail Research Institute (www.erri.nl), Utrecht, The Netherlands.

ESRF Project FaME38 (2002), *Residual Stresses in Railway Rails*. P.J. Webster, D.J. Hughes, G. Mills, G.B.M. Vaughan. Principal publication in: *Materials Science Forum,* pp. 404-407, 767-772.

European Convention for Constructional Steelwork (1976), *Manual on stability of steel structures*.

Fastenrath F. (ed.) (1977), Die Eisenbahnschiene (The railway rail), Verlag Wilhelm Ernst & Sohn, Berlin-München-Düsseldorf, Germany, pp. 37-38.

Ferguson B. and Freborg A. (2005), "Modeling heat treatment of steel parts", *Computational Materials Science*, v. 34, no. 3, pp. 274-281.

Finstermann G., Dieter F. F., Shan G., Schleinzer G. (1998), "Residual stresses in rail due to roll straightening", *Steel Research -Metal Working*, v. 69, no. 7, pp. 272-278.

Fischer F.D., Hinteregger E., Rammerstorfer F.G. (1991), *A computational study of the residual stress distribution in thermally loaded beams of cross-section on frictional support*, in: P. Wrigers, W. Wagner (Eds.), Non-linear Comp. Mechanics, State of the Art, Springer, Berlin, pp. 737–750.

Fischer F.D., Hinteregger E., Rammerstorfer F.G. (1992), *The influence of frictional forces on the longitudinal stress distribution of thermally induced residual stresses in beams*, in: H. Fujiwara, T. Abe, K. Tanaka (Eds), Proceedings of the Third International Conference on Residual Stresses, Tokushima-shi, Japan, 1991, Residual Stresses. III. Science and Technology, v. 2, Elsevier, New York, London, pp. 1-16.

FLUENT® User's Manual v6.0.

Fukumoto Y., Aoki T. and Kajita N. (1976), "Evaluation of column curves based on probabilistic concepts", in: Proceedings of the International Conference on Stability. Preliminary report.

Gittler P., Kickinger R., Pirker S., Fuhrmann E., Lehner J., Steins J. (2000), "Application of computational fluid dynamics in the development and improvement of steelmaking processes", *Scandinavian Journal of Metallurgy,* 29, Denmark, pp. 166–176.

Guericke W. (1994), "Modell zur Simulation elastisch-plastischer Biegeverformungen fur technologische Bearbeitungsprozesse (Model for the simulation of elasto-plastic bending of technological working processes), Technische Mechanik, v. 14, pp. 155-176.

Guericke W., Weiser J. and Haas W. (1994), *Eigenspannungen beim Rollenrichten von Eisenbahnschienen (Formation of residual stresses during the roller straightening of rails)*, Forschungsvorhaben des Institus für Maschinen für die Thyssen-Stahl AG, Duisburg. Otto-von-Guericke-Universität Magderburg, Germany.

Hauk V., Kockelmann H. (1994), Eigenspannungszustand der Laufflänche einer Eisenbahnschienen (Residual stresses state in the running surface of a rail), HTM-Härterei-technische Mitteilungen, v. 49, pp. 340-352.

Henderson S., Cook W. T., Woolard L., Richardson A. D., Wood M. J. (1998), "Control of straightening operations for optimization of product properties", Report EUR 18540 EN, Office for Official Publications of the European Commission.

Hinteregge E., Fischer F.D., Rammerstorfer F.G. (1992), The influence of frictional force on the longitudinal distribution of thermally induced residual stresses in beams, in: H. Fujiwara, T. Abe, K. Tanaka (Eds.), Residual Stresses—III Science and Technology, vol. 2, Elsevier, London, pp. 1278-1283.

Hodgson W.H. (1993), *Residual stresses in rail,* in: Kalker J. J., et al. (Eds), *Rail Quality and Maintenance for Modern Railway Operation*, Kluwer Academic Publishers, Dordrecht, The Netherlands, pp. 61-73.

Horger O.J. (1943), "Residual stresses and fatigue studies", Proc. SESA vol. 1, no. 1, pp. 8-10.

Kalker J. J., Cannon D. F. and Orringer O., eds. (1993), *Rail Quality and Maintenance for Modern Railway Operation*, International Conference on Rail Quality and Maintenance for Modern Railway Operation, Delft, June 1992, Kluwer Academic Publishers, Dordrecht, The Netherlands.

Kolmogorov S. V., Makarov Y.D., Mikhailov, O. N. (1987), "Formation of residual stresses in heat treatment hardened rails", Steel in the USSR 17, pp. 271-273.

Kusakabe T., Mihara Y. (1980), "Analysis of residual stresses in hot-rolled H shapes", *Trans. ISIJ*, v. 20, pp. 454-461.

Maximov J. T., Kuzmanov T. V., Anchev A. P., Ichkova M. D. "A finite element simulation of the spherical mandrelling process of holes with cracks", *Journal of Materials Processing Technology*, v. 171, n.3, pp. 459-466.

Nikitin I. and Altenberger I. (2007), "Comparison of the fatigue behavior and residual stress stability of laser-shock peened and deep rolled austenitic stainless steel AISI 304 in the temperature range 25–600 ºC", Material Science and Engineering A, (to appear).

Osgood W. and Campus F. (1954), *Residual Stresses in Metal and Metal Construction*, Reinhold Publishing, New York, pp. 305-329.

Olden V., Thaulow C., Jjerpetjonn H., Sorli K. and Osen V. (1998), "Numerical Simulation of temperature distribution and cooling rate in ship profiles during water spray cooling", Materials Science Forum, Vols. 284-286, Trans Tech Publications, Switzerland, pp. 385-392.

Orringer O., Paxont W., Gray D., Raj P. (1996), "Residual stress and its consequences on both sides of the wheel-rail interface", *An International Journal on the Science and Technology of Friction, Lubrication and Wear (WEAR)*, Elsevier, v191, pp. 25-34.

Orringer O., Orkisz J. and Swiderski Z., eds. (1992), Residual Stresses in Rails, Effects on Rail Itegrity and Railroad Economics, Vol I: Field Experience and Test Results, Kluwer Academic Publishers, Dordrecht, The Netherlands.

Orringer O., Orkisz J. and Swiderski Z., eds. (1992), Residual Stresses in Rails, Effects on Rail Itegrity and Railroad Economics, Vol II: Theoretical and Numerical Analyses, Kluwer Academic Publishers, Dordrecht, The Netherlands.

Orringer O. (1988), "Crack propagation life of detail fracture in rails", Volpe National Transportation System Center, report no. DOT/FRA/ORD-88/13, October.

Marcelin J. L., Abouaf M. and Chenot J. L. (1986), "Analysis of residual stress in hot-rolled complex beams", *Computer Methods in Applied Mechanical and Engineering*, v. 56, pp. 1-16.

Maximov J.T., Kuzmanov T.V., Anchev A.P. and Ichkova M.D. (2006), "A finite element simulation of the spherical mandrelling process of holes with cracks", Journal of Materials Processing Technology, v. 171, no. 3, pp. 459-466.

Meier H. (1936), Eigenspannungen in Eisenbahnschienen; Organ f. d. Fortschritte im Eisenbahnwesen, 91, pp. 320-329;

Nakata N., Yoshida H. (1995), Influence of cooling uniformity at run-out table on strip flatness, Recent advances in heat transfer and micro-structure modelling for metal processing, in: Proceedings of the 1995ASME International Engineering Congress and Exposition, San Francisco, USA, Society of Mechanical Engineers, Materials Division, ASME, MD, pp. 67-77.

Naumann N. (1998), Zum Richten von Langgut über die grosse Trägheitsachse (Straightening of long products about the first moment of are), Ph.D. Thesis, Montanuniversität Leoben, Austria.

Nedorezov I. V., Volegov I. F., Orlov B. Ya. And Zudov A. F. (1999), "Reduction of residual stresses in unhardened rails during straightening by the 'momentless' method", *Steel in Transaction*, v. 29, no. 9, pp. 74-78.

Prime MB (1999), "Residual stress measurement by successive extension of a slot: The crack compliance method", *Applied Mechanical Reviews*, v. 52, no. 2, pp. 75-96.

Ringsberg J. and Lindbäck T. (2003), "Rolling contact fatigue analysis of rails including numerical simulation of the rail manufacturing process and repeated wheel rail contact loads", *International Journal of Fatigue*, v. 25, pp. 547-558.

Rohloff H. and Neuschütz E. (1990). *Fliesspannung von Stählen bei Warmumformung (Yield Stress of Steels in Hot Work)*. Edited by Betriebsforschungsinstitut – VDEh-Institut für angewandte Forschung GmbH. ISBN 3-514-00439-0. Germany.

Rongbin T., Di T., Lieping X., Minliao J. (1998): "Application of the finite element method to determine the residual stresses of steel rails", Simulation of Materials Processing: Theory, Methods and Applications, (NUMIFORM 98) (Heutik, Baaijens eds.), The Netherlands, pp. 695-700.

Schleinzer Gerard (2000), *Residual Stress Formation During the Roller Straightening of Rails*, Fortschr.-Ber. VDI Reihe 18 nr. 251. Düsseldorf: VDI Verlag. ISBN 3-18-325118-3, printed in Germany.

Schleinzer G. and Fischer F. D. (2001), "Residual stress formation during the roller straightening of railway rails", *Int. Journal of Mechanical Sciences*, v. 43, pp. 2281-2295.

Siebert Dieter (1973), *Beitrag zur Frage der Eigenspannungen in warmgewalzten Breitflanschträgern* (Contribution to the question of internal stresses in hot-rolled wide-flang beams), Doktor-Ingenieur dissertation. Technischen Universität Hannover.

Srimani S., Pankaj A. and Basu J. (2005), "Analysis of end straightness of rail during manufacturing", International Journal of Mechanical Sciences, v. 47, pp. 1874-1884.

Strating J. and Vos H. (1973), "Computer simulation of the E.C.C.S. buckling curves using Monte-Carlo method" HERON, v. 19, no. 2., pp. 1-38.

Szalai J., and Papp F. (2005), "A new residual stress distribution for hot-rolled I-shaped sections", Journal of Constructional Steel Research, v. 61, pp. 845-861.

Szalai J. (2003), *Overall sensitivity analysis if hot-rolled beam-columns*, in: Jármai K., Farkas J., editors. Metal structures: design, fabrication, economy. Rotterdam: Millpress.

Szelazek, J. (1992): Ultrasonic measurement of thermal stresses in continuously welded rails, Non Destructive testing & Evaluation 25, pp. 77-85.

Takashi K., Nose J., Yoshida T., Wakimoto N. (1973), "Residual Stress in hot-rolled H-section steel", *Nippon Kokan Technical Report*, Overseas.

Totten G., Howes M., Inoue T. (2002), *Handbook of residual stress and deformation of steel*. ASM International.

Urashima C., Sugino K. (1992), "Generation mechanism of residual stresses in rails", in Proc. International Conference en Residual Stresses ICRS 3, (H. Fujiwara, T. Abe, K. Tanaka, eds) 2, pp. 1489-1493.

Varney B. E., Farris T. N. (1998), "Mechanics of rollers straightening", *in Proc. 39th Mechanical Working and Steel Processing Conference*, Iron & Steel Soc. Of AIME, Warrendale, PA, USA, v. 35, pp. 1111-1121.

www.stahldat.de. Steel Data Base, Stahl-Zentrum. Germany.

Webster P.J., Wang X. and Mills G. (1992), in P*roc. NATO Advanced Research Workshop on Measurement of Residual Stress using Neutron Diffraction*, Oxford, Kluwer Academic Publishers, pp. 517-524.

Webster P. J., Mills G., Wang X., Xang W. P. (1993), "Residual stress measurements in rails by neutron diffraction", *Rail Quality and Maintenance for Modern Railway Operation* (J. J. Kalker, et al. eds.), Kluwer Academic Publishers, Dordrecht, The Netherlands, pp. 307-314.

Weiser J. (1997), Analyses der Eigenspannungsentstehung beim Rollenrichten von Schienen (Analysis of the formation of residual stresses during the roller straightening of rails), Ph.D. Thesis, Otto-von-Guericke-Universität Magderburg, Germany.

Wineman S. J., McClintock F. A. (1992), "Residual stress and web fracture in roller-straightened rail", Residual stress in Rails 2, (O. Orringer, J. Orkisz, Z. Swiderski, Eds), Kluwer Academic Publishers, Dordrecht, The Netherlands, pp. 1-22.

Yang Y. Y., Linkens D. A., Talamantes-Silva J. and Howard I. C. (2003), "Roll Force and Torque Prediction Using Neural Network and Finite Element Modelling", (IMMPETUS Department of Automatic Control University of Sheffield, United Kingdom), *ISIJ International*, v. 43, no. 12, pp. 1957-1966.

Yoshida H., Kataok K., Sasaki T., Tanaka T. (1982), "Analysis of deflection during cooling in rolled U-type sheet piles", Technology Laboratory Report, Kawasaki Iron Industry Pty. Ltd., 30 July.

Yoshida H. (1984a), "Analysis of residual stress in hot rolled H-beam", *Trans. ISIJ*, v. 24, pp. 401-407.

Yoshida H. (1984b), "Reduction of residual stress in hot rolled H-beam", *Trans. ISIJ*, v. 24, pp. 471–477.

Yoshida H. (1984c), "Analysis of flatness of hot rolled steel strip after cooling", *Trans. ISIJ*, v. 24, pp. 212–220.

Young B. W. (1972), *Residual Stresses in hot-rolled members*, in: IABSE international colloquium on column strength.

Zhou Z., Thomson P., Lam YCh., Yuen D.W. (2003), "Numerical analysis of residual stress in hot-rolled steel strip on the run-out table", *Journal of Materials Processing Technology*, v. 132, pp. 184-197.

Zienkiewicz o., Valliapan S., King I. (1969), "Elasto-plastic solutions of engineering problems. Initial stress finite element approach", *International Journal of Numerical Methods*, Engrg. 1, pp. 75-100.